University of Ghana http://ugspace.ug.edu.gh

UNIVERSITY OF GHANA

COLLEGE OF BASIC AND APPLIED SCIENCES

CHARACTERIZATION OF FAULT SYSTEMS USING GEOPHYSICS IN THE SOUTHWESTERN PARTS OF THE AKUAPEM – TOGO RANGE, SOUTHEAST GHANA

BY

KOFI DUKU

10279112

THIS THESIS IS SUBMITTED TO UNIVERSITY OF GHANA, LEGON, IN PARTIAL FULFILMENT OF THE REQUIREMENT FOR THE AWARD OF MPHIL GEOLOGY DEGREE

JUNE, 2015

University of Ghana http://ugspace.ug.edu.gh

DECLARATION

This thesis is the result of research work undertaken by Duku Kofi in the Department of Earth Science, University of Ghana, under the supervision of Dr. Thomas Armah and Dr. Paulina E. Amponsah in partial fulfillment for the award of a Master of Philosophy of Science in Geology.

..... Date:……

DUKU KOFI

STUDENT

…… Date:……

DR. THOMAS ARMAH

SUPERVISOR

..... Date:……

DR. PAULINA E. AMPONSAH

SUPERVISOR

University of Ghana http://ugspace.ug.edu.gh

ABSTRACT

The Akwapim Fault zone is one of the two major fault zones in the southeastern part of Ghana. Its junction with the Coastal Boundary Fault happens to be epicenter for most of the earthquakes that occur in Ghana. The earliest work done in this region was by the Gold Coast Geological Survey on a regional scale in mapping the area to determine the geological structures. With most of geological deformational features being inferred, it is prudent to carry out more research to identify more features to substantiate or disprove the inferences that have been made through different modes of investigation. In this study, regional resolution magnetic data, time and frequency domain electromagnetic data and gravity data are some geophysical data that are used to help define the structural setting of the Akwapim fault zone. Ground geophysical survey in addition to geological field mapping is carried out in the area to augment the information given by the aero geophysical data. The electrical resistivity methods comprising the Square array, the Schlumberger vertical electrical sounding and the Wenner azimuthal sounding were the geophysical survey methods used. The data obtained from the surveys were processed and interpreted. The data from the geological field mapping is plotted and analyzed to identify the attitudes of the geological structures associated with deformational terrain. From the aero geophysical data processed, grids are made to distinguish features relating to the deformation occurring within the study area and also identify a relation between the results of the surveys carried out. The occurrence of relatively high amounts of uranium from the radiometric concentration grid produced indicates the occurrence of tectonism within the area. The various results obtained from the ground geophysical survey were compared to see which array or combination of arrays best describes the subsurface. Plots from the various geo-electric arrays produced results to indicate a consistent layer of very low apparent resistivity for all the survey points. The Square array and the azimuthal array

University of Ghana http://ugspace.ug.edu.gh

were used to identify fractures and their properties while the Square array and the Schlumberger array were used to locate the bedrock at the various sample point. The square array had a higher penetration effect than the schlumberger array. Data from the azimuthal array was used to plot possible fault lines on a geological map of the area indicating that the faulting is not limited to just one geological domain. The square array tends to require less space than the two other arrays used and as such can be singularly used to do both depth soundings and azimuthal surveys to locate fractures at depth.

University of Ghana http://ugspace.ug.edu.gh

DEDICATION

To God, for giving me Rose Ackah and Dr. Moses H. Duku

University of Ghana http://ugspace.ug.edu.gh

ACKNOWLEDGEMENTS

My unreserved gratitude goes to my mum for all the encouragement and advice in starting this academic pursuit. My appreciation also goes to Dr. Thomas Armah and Dr. Paulina Amponsah for the guidance, help and encouragement throughout the period of writing this thesis.

I would want to appreciate Prof. Prosper M. Nude for the initial advice on the topic of the thesis. I express profound gratitude to Mr. Sampson Renner, Mr. Patrick Banahene and Mr. Emmanuel Haruna for their technical inputs and support in the writing of this thesis. Also to be acknowledged are Mr. Obeng, Mr. Prosper Apedo, Mr. Moses Mensah, Mr. Opuni Antwi-Bosiako, Mr. Ben Aidoo, Mr. Sampson Ebiasah, Team Chez, Team Tapes and Hammers and Team Four-Geos.

My indebtedness goes to the Geological Survey Department of Ghana for assisting me with secondary

Aerogeophysics data and to the University of Ghana for allowing me the opportunity to undertake a master's degree program

University of Ghana http://ugspace.ug.edu.gh

TABLE OF CONTENTS

University of Ghana http://ugspace.ug.edu.gh

University of Ghana http://ugspace.ug.edu.gh

University of Ghana http://ugspace.ug.edu.gh

LIST OF TABLES

University of Ghana http://ugspace.ug.edu.gh

LIST OF FIGURES

University of Ghana http://ugspace.ug.edu.gh

University of Ghana http://ugspace.ug.edu.gh

LIST OF APPENDIXES

University of Ghana http://ugspace.ug.edu.gh

CHAPTER ONE

1.1 Introduction

The Akwapim Fault is one of the two major fault zones in the southeastern part of Ghana. Its junction with the Coastal Boundary Fault happens to be epicenter for most of the earthquakes that occur in Ghana (Bacon and Quaah, 1981)

The earliest work done in this region was by the Gold Coast Geological Survey on a regional scale in mapping the area to determine the geological structures in the area (Amponsah et al., 2002). They recognized various structures that gave the indication of a fault occurring in this region.

Until recently, geophysical methods have not been used in the study area due to the fact that most of the geophysical investigations have been targeted at mineral exploration in other areas. Geological field mapping as well as geochemical methods have been carried out to identify the occurrence certain feature associated with deformation. With no exact knowledge of the subsurface, inferences made from these previous study have been accepted as the best description of the subsurface character in the study area.

Regional resolution magnetic data, time and frequency domain electromagnetic data and gravity data are some geophysical data that can be used to help define the structural setting of the Akwapim fault zone. Further analysis can be done to further define and delineate the structures associated with the main fault as well as the minor faults. This can be done using softwares such as ArcGIS, MapInfo and Oasis Montaj. Regional field data of the area with emphasis on the geological structures will be a boost in the development of a good interpretation of the nature of the Fault zone.

University of Ghana http://ugspace.ug.edu.gh

1.2 Objective

The main objectives of the study are to:

- identify and characterise the Western Boundary Fault and its associated minor faults in the Akwapim Fault zone in Southeast Ghana;
- determine the influence of the Akwapim Fault zone on the seismicity in the study area and
- determine which geophysical method best characterizes the fault structures in the subsurface, data from which will be used to support the geological data already known.

1.3 Study Area

1.3.1 Location and size

The Akwapim-Togo Range is a narrow belt of ridges and hills in Ghana. It extends in a southwest-northeast line for about 320 km from the mouth of the Densu River (near Accra) on the Atlantic coast to the boundary with Togo. Averaging 460 m in height, the hills continue eastward to the Niger River as the Togo Mountains in Togo and as the Atakora Mountains in Benin, and they contain isolated peaks near the Togo border. The study area (figures 1 and 6) falls within the Ga South Municipal area and the Awutu Senya East District.

University of Ghana http://ugspace.ug.edu.gh

1.3.2 Accessibility

The study area is mainly accessible by a first class road (Accra to Winneba road), second class roads (Kasoa main town to Nyanyano) as well as feeder roads (Weija Toll Booth Junction to Tuba, Kokrobite and Langma and surrounding towns).

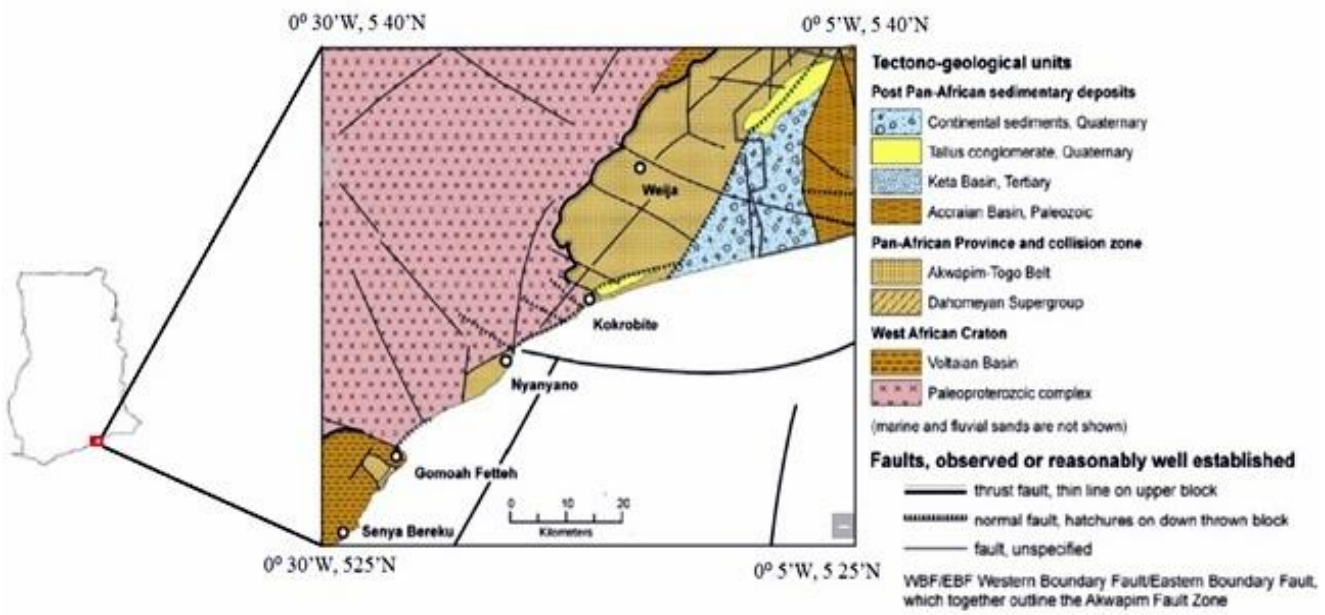

Figure 1: Geological Map of the Study Area (After Geological Survey Department Of Ghana, 2010)

1.3.3 Physiography

Three major rivers that drain the area are Densu, Nsaki and Onyasana rivers. The largest of the three, the Densu drains down from the Eastern Region through the western part of the Municipality to Weija where it enters the sea. The land area consists of gentle slopes interspersed with plains in most parts and generally undulating at less than 76 m above sea level. The slopes are mostly formed over the clay soils of the Dahomeyan gneiss with alluvial areas surrounding the coastal lagoons generally flat.

The Akwapim range and the Weija hills rise steeply above the western edge. The crest of the Akwapim range lies generally at 300 m elevation southwards. This line of hills

University of Ghana http://ugspace.ug.edu.gh

continues through to the Weija hills with the highest point reaching 192 m near Weija. There are three major rivers namely; the Densu, Nsaki and Ponpon River that drain the district. The largest of the three is the Densu which drains down from the Eastern Region through the western portions of the district to Weija where it enters the sea. It is the main source of water supply to over half the entire population of the Accra Metropolis. Other water bodies mostly tributaries of the Densu are the Adaiso, Doblo, Ntafafa and the Ponpon River.

Most parts of the study area are well drained although there are vast lowland areas present. There are two major hills with the south-western portion of the Akwapim-Togo range also present in the area. The south-western part of the Weija Lake occurs in the northeastern part of the area and in addition to that the Weija estuary is also present at the south-western part of the area.

The study area lies wholly in the coastal savannah agro-ecological zone. The rainfall pattern is bi-modal with an annual mean varying between 790 mm on the coast to about 1270 mm in the extreme north. The annual average temperature ranges between 25.1°C in August and 28.4°C in February and March. Humidity is generally high during the year. Average humidity figures are about 94% and 69% and 15:00 hours respectively (Ministry of Local Government and Rural Development, 2006). The Municipal lies wholly in the coastal savanna agro-ecological zone. The land area is underlain by shallow rocky soils and are extensively developed on the steep slopes of the Akwapim range and the Weija hills as well as the basic gneiss inselbergs. On the Akwapim range the soils are mainly pale and sandy with brushy quartzite occurring to the surface in most places. The abundant sandstone and limestone present in the area are good source of material for the construction industry (Muff and Efa, 2006).

University of Ghana http://ugspace.ug.edu.gh

They are typically loamy in texture near the surface becoming more clay below. The red soils are porous and well drained and support road development and also provide ample moisture storage at depth for deep-rooting plants. Nutrients supplies are concentrated in the humus top-soil.

1.4 Geological Setting

About two thirds of the land surface of Ghana is covered by the Birimian rocks of the Paleoproterozoic age (Ahmed et al., 1977). The Birimian rocks form the eastern end of the West African Craton which has remained stable since 1.7Ga. The Birimian rocks are made up of the Volcanic Belts and the Sedimentary Basins. The rocks of the Dahomeyide and the Voltaian lie in the eastern portions of Ghana. The Dahomeyide is made up of the Dahomeyan, Togo and Buem structural units (Ahmed et el, 1977, Muff and Efa, 2006). The study area falls in the area of the Togo rock units.

The Togo rock formation is generally made up of quartzites, quartz-schists, sericite schists and phillites (Junner and Service, 1936). The sedimentary rocks of the Togo form a prominent northeast-southwest trending mountain range known as the Akwapim-Togo range. The Togo structural unit is characterized by structures such as foliation, folds, faults and joints caused by the Pan African Orogeny (Ahmed et al., 1977). The Pan African Orogeny resulted in the intense folding and faulting of the supracrustal sedimentary rocks in the Togo. The mountain range is bounded to the east by the Dahomeyan rocks and to the west by the Cape Coast granitoid complex, the Voltaian and the Buem Structural Units. Two major thrust faults bound the Akwapim-Togo range. The fault on the east is at the contact with the Dahomeyan while the other fault also known as the Western Boundary fault is at the contact with the Cape Coast granitoid complex, the Voltaian and the Buem (Ahmed et al., 1977).

University of Ghana http://ugspace.ug.edu.gh

The Togo Structural unit is of the late Proterozoic age. It consists of siliciclastic sediments that have been subjected to a low- to intermediate grade type of metamorphism. The Togo Structural unit forms the greatest part of the north-north-east trending Akwapim Range and the Weija Mountains (Ahmed et al., 1977). In the work done by Muff and Efa (2006) the Togo Structural has been subdivided into three main units which reflect their lithological properties. These units are:

a) Phyllite/Phyllonite Unit
b) Quartz-Schist Unit
c) Quartzite Unit

(a) Phyllite/Phyllonite Unit

This unit consists mainly of phyllite and phyllonite, which are often talcy. Phyllonites make up a large part of this unit. Phyllonites are phyllitic rocks of mylonitic origin and they belong to the group of rocks called fault rocks. The phyllonites show thin, stretched out lenses of grey or white quartz in a very fine grained foliated matrix. Sometimes thin, planar layers exhibit clear signs of mylonisation (Ahmed et al., 1977). The phyllonites often possess a cherty aspect and sometimes they have a soapy feeling to the touch. The terms cherty phyllite, quartz-phyllite or finely-laminated quartzite describe their texture and composition best.

Phyllonites underlie large parts of the eastern part of the Akwapim Range and they form the low-lying country rock in the Achimota area. Phyllonite has been found in many excavation pits along the Togo Structural unit/Dahomeyan System contact to the northeast of the Ghana Atomic Energy Commission offices and fragments of phyllonites are often found in the top of shallow elevations where red soil formed over mica schists of the

University of Ghana http://ugspace.ug.edu.gh

Dahomeyan System. The fragments are relics of phyllonite layers which now have been eroded.

Mapping done by Efa and Muff (2006) in the coastal area showed that phyllonites are exposed southwest of Gomoa Fetteh, where they are associated with augen schists of the Dahomeyan Structural unit at a thrust fault. Phyllonite also occurs in a track leading to the top of a hill immediately west of Gomoa Fetteh, and it outcrops over several tens of meters in a ditch in the dirt road leading from Gomoa Fetteh to Petuduase and Senya Beraku (Ahmed et al., 1977).

The occurrence of phyllonite and fragments of phyllonites in soil over Dahomeyan rocks indicates that much of the Dahomeyan terrane was formerly overlain by the Togo Structural. The phyllonites are interpreted as products of the thrust of the Togo Structural unit over the Dahomeyan Formation along a thrust fault. The rocks belonging to the Togo Structural which are exposed in the area to the east of the Akwapim Range are interpreted as infolded or infaultet klippen of the Togo Series (Kesse, 1985).

(b) Quartz-Schist Unit

This unit encompasses mainly sericitic quartz-schist and chlorite-schist and contains layers of quartzite, phyllite or chlorite schist. The sequence is well bedded and strongly jointed. The thickness of argillitic layers is several millimeters to some centimeters, the arenaceous layers are some centimeters to a few meters thick. Schistosity is well developed and parallel to bedding (Ahmed et al., 1977). Quartz-schist may also have been formed by mylonisation. This type of quartz-schist possesses a strong slip cleavage and it consists of planar recrystallized quartzite layers of 0.5 to 2 centimeters thickness which alter with 1

University of Ghana http://ugspace.ug.edu.gh

to 3 millimeters thick layers of phyllosilicates which are often green or grey. The planar surfaces are sometimes thrown into small crinkles, called crenulation folds. The wavelengths and amplitudes of the crinkles are measured in millimeters (Effah and Muff, 2006).

(c) Quartzite Unit

This unit comprises mainly quartzite and the amount of quartz-schist and phyllite is very variable. In some places, the quartzite possesses aspects of vaguely banded chert. Quartzite may occur as massive layers of up to 2 m width, or it may be laminated and with increasing lamination it may grade into phyllonite (Muff and Efa, 2006).

Three types of quartzite are recognized. These are:

a) Metaquartzite
b) Micaceous quartzite
c) Cherty quartzite

Metaquartzite: It is very hard, exhibits splintery fracturing and is medium- to thick-bedded with interlayers of phyllite. Fresh surfaces have glassy luster and are grey or dark grey. Rounded or stretched out quartz grains are visible.

Micaceous quartzite: It is very-thin to thin-bedded and contains very thin layers of phyllite between quartzitic layers. In some places it is cherty. When fresh it is grey. Weathered surfaces are often white.

Cherty quartzite: It is grey to white, sometimes with faint dark bands. It forms lenses which are 1 to 2 m thick and 10 to 20 m long which are parallel to the bedding. The

University of Ghana http://ugspace.ug.edu.gh

cherty quartzite is interpreted as flinty crush rock, which is a fault rock often associated with dynamic metamorphism.

The Togo Structural unit has been intensely tectonically stressed and strongly brecciated (Ahmed et al., 1977). The rocks which make up the Akwapim Range represent the lowermost portion of a once much more thick sequence, of which the top part has been eroded away. The strata generally dip towards the east-south-east and the intercalations of erosion resistant quartzites and quartz-schists with soft phyllites cause an asymmetric topography of steep cliff-slopes facing the west-northwest, and gentle dip-slopes facing the east-southeast.

Because the bottom of the scree has not been exposed by creeks, the eastern contact between Togo Series and the Dahomeyan System has to be inferred from exposures some hundred meters apart. Fractured rocks of the Quartzite and Quartz-Schist Unit are very permeable for groundwater. The Phyllite/Phyllonite Unit is very prone to erosion when slopes are graded or cleared at construction sites.

The only location, where Togo Structural unit overlies the granitoids is at the northwest side of the mountainous block south of the Weija Lake. The “V-type” pattern of the granitoid/Togo Structural unit contact in valley incisions indicates a gentle southeast dip of the contact at the regional scale (Muff and Efa, 2006). The contact itself is exposed in the ditch south of the major road which leads to Winneba and beyond. The Togo Structural unit consists of contorted quartz and chlorite schists, and the underlying granitic rocks are strongly sheared. Although the contact at this specific location dips approximately 10 degrees to the northeast, a generally low southeast dip is inferred from the outcrop pattern.

Kesse (1985), indicate that the contact between Togo Structural unit and Dahomeyan Structural unit can best be studied at low tide along the coast between Gomoa Fetteh and

University of Ghana http://ugspace.ug.edu.gh

Nyanyano. Augen schist, sericitic quartz-schists, chloritic and amphibolitic rocks belonging to the Dahomeyan Structural units are tightly folded and overlain by fine-laminated, light-colored cherty phyllonites. The amplitudes and wavelengths of the folds measure several decimeters, and they are overturned so that their axial planes dip shallowly to the east-south-east. The small folds are interpreted as drag folds which indicate that the overlying strata have been pushed towards the west-north-west direction. At some locations along the beach from Kokrobite to Nyannyano, garnet porphyroblasts are found in the Augen gneisses as well as in sericitic quartz-schist and phyllonites of the Togo Structural unit (Muff and Efa, 2006).

The economic importance of the Togo structural unit is not just limited to the mining of the laminated sericite-quartz-schists in many places to be used as decorative floor and wall tiles and paving but also brecciated quartzites are important as crushed aggregate material for road and housing foundations.

University of Ghana http://ugspace.ug.edu.gh

CHAPTER TWO

LITERATURE REVIEW

2.1 Geology

Birimian rocks of the Paleoproterozoic age cover about two-thirds of the land surface of Ghana. The Birimian rocks form the eastern end of the West African Craton which has remained stable since 1.7 Ga (Ahmed et al., 1977). The Birimian rocks are made up of the Volcanic Belts and the Sedimentary Basins. The rocks of the Dahomeyide and the Voltaian lie in the eastern portions of Ghana. The Dahomeyide is made up of the Dahomeyan, Togo and Buem structural units. The study area falls in the area of the Togo rock units. The Dahomeyide resulted from the Pan African Event. The term Pan-African is used to describe tectonic, magmatic, and metamorphic activity of Neoproterozoic to earliest Palaeozoic age, especially for crust that was once Part of Gondwana. Because of its tremendous geographical and temporal extent, the Pan-African cannot be a single orogeny but must be a protracted orogenic cycle reflecting the opening and closing of large oceanic realms as well as accretion and collision of buoyant crustal blocks (Attoh and Ekwueme, 1997). Pan-African events culminated in the formation of the Late Neoproterozoic supercontinent Gondwana.

The Romanche transform margin, offshore Ghana (as shown in Figure 3) is an oblique transect of the boundary between the West African Craton (WAC), underlain by Paleoproterozoic (Birimian) rocks, and the Pan-African orogenic belt (Attoh and Ekwueme, 1997). Along this transect the principal tectonic elements of the onshore geology include prominent structures such as:

(i) the Pan-African front (PF), representing the western limit of deformation in the external zone, and

University of Ghana http://ugspace.ug.edu.gh

(ii) the Pan-African suture (PS) represented by a ductile shear zone at the base of high-pressure (HP) mafic granulites which mark the eastern edge of WAC (Attoh et al., 1997).

The Romanche Fracture Zone (RFZ) intersects the coastline east of the suture zone and projects into the Pan-African dextral shear zone (TSS). To the west of the Pan-African front, the WAC is underlain by Birimian granitoids and greenstone belts.

2.1.1 The Pan-African cross section

A schematic geological cross-section of the southern segment of the Pan-African Dahomeyide Orogeny (Figures 2 and 3) allows comparison of structures in the seismic sections with those inferred from onshore geology (Attoh et al., 1997). It shows the boundary between the WAC, to the west, and the Dahomeyide orogeny east of the Pan-African front (PF). The Pan-African external zone comprises of west-verging Atacora nappes composed of quartzites and quartz schists locally imbricated with low-strain mylonites derived from granitoids of the deformed margin of the 2.1 Ga West African Craton. To the east of the Pan-African suture zone (PS) are the Neoproterozoic rocks that comprise the accreted (Attoh et al, 1997).

University of Ghana http://ugspace.ug.edu.gh

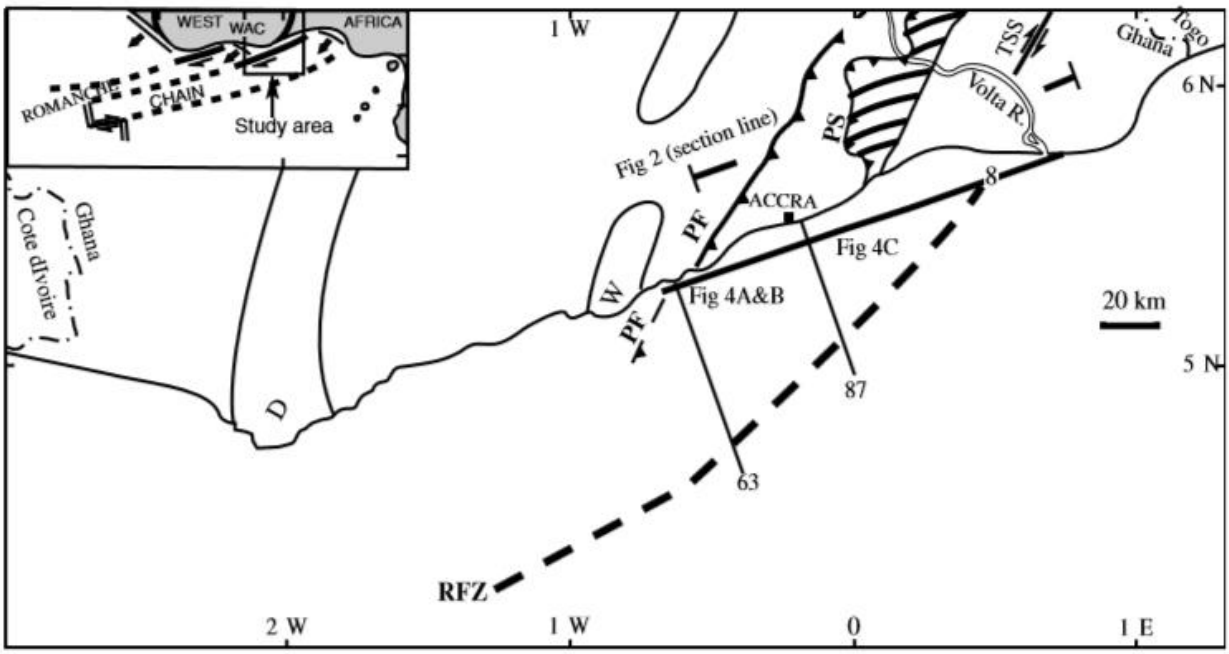

Figure 2: The Romanche transform margin, offshore Ghana showing the major tectonic elements of onshore geology and offshore seismic lines referred to in this study: PF = Pan-African Front, PS = Pan-African Suture zone (suture zone gneiss shown in striped pattern)

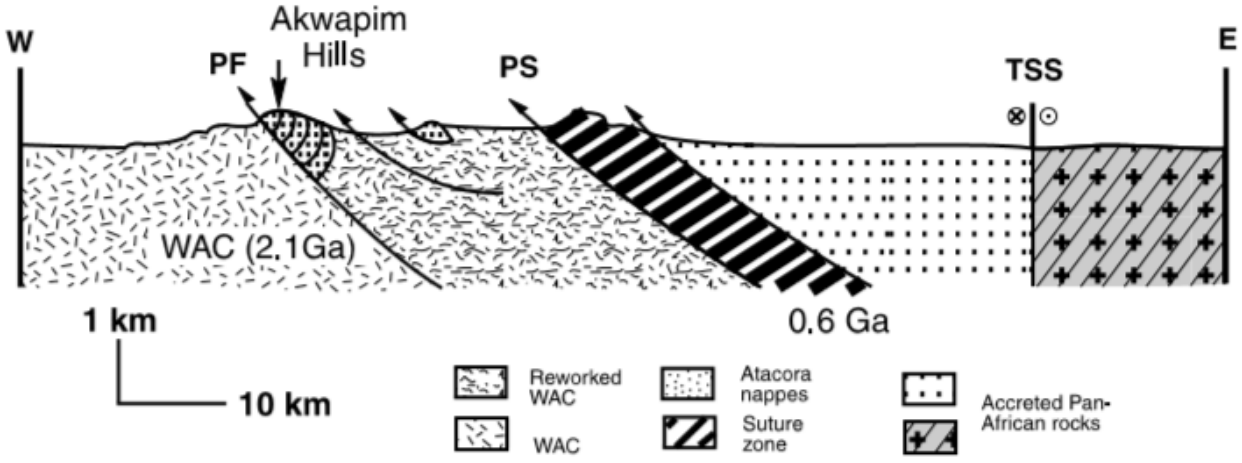

Figure 3: Schematic cross section of the Pan-African Dahomeyide orogeny and the eastern margin of the WAC in southeastern Ghana. Symbols and abbreviations as in Fig. 3 after Attoh et al, 2005

University of Ghana http://ugspace.ug.edu.gh

Although Ghana is remote from the major earthquake zones, it is moderately active seismically, with a history of earthquakes damaging the capital, Accra. Seismic recording done during 1977 to 1980 has been used to develop a crustal velocity model and locate epicenters. Work done by Bacon and Quaah (1981) indicate that most of the earthquakes occur in an area to the west of Accra around the junction of two major fault systems, the east-west trending Coastal Boundary fault and the NNE trending Akwapim fault zone. Fault plane solutions suggest a mixture of normal faulting on the Akwapim fault zone (in agreement with geological evidence) and strike-slip faulting, in response to a regional ESE tensional stress perhaps caused by strike-slip movement along the Romanche fracture zone. The Akwapim Fault is one of the two major fault zones in the southeastern part of Ghana. Its junction with the Coastal Boundary Fault happens to be epicenter for most of the earthquakes that occur in Ghana.

The Akwapim Fault Zone (AFZ) is made up of a northeast–southwest trending system of faults outlined by the Western Boundary Fault (WBF) on the western side and the Eastern Boundary Fault (EBF) on the eastern side as described by Ahmed et al., (1977). Both faults are overthrusts of Neo- Proterozoic age. Edwards et al., (1997) suggest that the fault contact of the West African Craton with the Pan-African Province can be extrapolated beneath the continental shelf although the bathymetric maps do not show a continuation of the Akwapim Range out into the shelf area. Recent large-scale mapping exercises in the southern part of the Akwapim fault zone (Muff and Efa, 2006) shows that at a later stage, the Akwapim Togo Belt has been subjected to a block-tectonic style of deformation and that many normal faults of local extension have developed in recent times.

Coastal Boundary Fault (CBF) Seismic studies established the occurrence of sedimentary basins and crustal blocks separated by normal faults in the Ghana shelf area (Blundell and Banson, 1975). They named the most prominent normal fault in the shelf area coastal

University of Ghana http://ugspace.ug.edu.gh

boundary fault. It strikes northeast at a distance of 3–5 km from the coast and downthrows the block south of it for several 1000 m. Sedimentation contemporaneous with and subsequent to the down-throw leveled the horizontal displacement. The coastal boundary fault is the northern boundary of a basin filled with sediments of Upper Jurassic to recent age. The fault was probably active throughout the entire time of deposition. West of Accra it bends to strike E-W and intersects the AFZ. Blundell (1976) suggest that the coastal boundary fault forms the northern margin of the Keta Basin.

The basin geometry and sediment fill is dominated by the NE–SW striking Fenyi-Yakoe and Adina Faults (Akpati, 1978). Cyclic deposition commenced in the Cretaceous and continued until Holocene times, indicating that the Fenyi-Yakoe and Adina Faults may still be tectonically active (Akpati, 1978). Akpati (1978) interprets the Fenyi-Yakoe Fault as the extension of the Romanche Fracture Zone, while Blundell (1976) suggests that the Fenyi-Yakoe Fault is the eastern extension of the coastal boundary fault. The Romanche Fracture Zone (RFZ) represents an offshore fault system related to the opening of the Atlantic Ocean. The fracture zone is 6–11 km wide and runs approximately parallel to the coast. It represents an inactive transform fault of the Mid-Atlantic Ridge which separates continental from oceanic crust (Deltail et al., 1974; Mascle and Sibuet, 1974; Edwards et al., 1997; Attoh and Brown, 2008). Transform motion at the Romanche Fracture Zone (RFZ) off- shore Ghana ended after West Africa had migrated along and beyond the spreading center lying at the opposite side of the transform fault and the oceanic lithosphere south of the Romanche Fracture Zone. The continental lithosphere to the north of it assumed the same sense of movement. Necessarily, the forces related to the Atlantic spreading are ruled out as a source for the present day seismic activities. The eastward projection of the Romanche Fracture Zone has been speculated in many studies without arriving at a consensus (Akpati, 1978; Blundell and Banson, 1975; Bacon and Quaah,

University of Ghana http://ugspace.ug.edu.gh

1981; Attoh et al., 1997, 2005). This dividedness on the eastward continuation of the Romanche Fracture Zone was mainly caused by the fact that previous investigators treated the entire transform domain as a generally straight single segment. Recent interpretation of multichannel seismic reflections (Antobreh et al., 2009) shows that the Romanche Fracture Zone is composed of several segments which developed under distinct conditions. Antobreh et al. (2009) provide evidence that the Romanche Fracture Zone does not make landfall in south-east Ghana as previously thought and they are of the opinion that the AFZ are splays of the Romanche Fracture Zone instead of continental extensions.

2.1.2 The Western Boundary Fault

This separates unmetamorphosed siliciclastic rocks of the Voltaian Structural unit from metamorphosed sedimentary rocks of the Togo Structural unit in the northern part of the study area. The fault itself cannot be observed but its existence is inferred on the grounds that unmetamorphosed rocks are juxtaposed to dynamically metamorphosed rocks. Deformation in the rocks adjoining the Western Boundary Fault is present as tilting of strata and brittle brecciation. The fault appears to be restricted to a relatively narrow zone and the straight fault line favors a steep to mediocre dip of the fault. The location of unmetamorphosed sedimentary rocks next to metamorphic rocks suggests that the eastern bloc of the fault moved upwards (Muff and Efa, 2006). Also, the general regime of a compressive tectonic style calls for a reverse or thrust fault. Extensive mylonisation in a wide zone, comparable to that observed in the Eastern Boundary Fault, has not been observed and is suggestive of an entirely different faulting style.

To the north of the Weija Lake, the western scarp of the Akwapim Range is considered an erosion scarp. The occurrence of a steeply dipping dip-fault located at the foot of the scarp

University of Ghana http://ugspace.ug.edu.gh

is ruled out, as the cliff slope represents only the present stage of a receding scarp caused by ongoing lateral erosion of the Densu River drainage system. Field evidence at the foot of the western scarp delivers no evidence of major tectonic processes, such as intense deformation or brecciation. The outcrop pattern follows the rule of V's and indicates a planar contact dipping shallowly to the southeast (Muff and Efa, 2006).

At the western side of the mountain block between the Weija Lake and Kokrobite, no rocks belonging to the Voltaian System have been found to fringe the Togo Series. As Voltaian rocks are found again further to the southwest along the coast, they have possibly been eroded. To the south of the Weija Lake, the continuation of the Western Boundary Fault which north of the lake separates Togo and Voltaian rocks, possibly runs some distance away from the scarp in the granitoid rocks, possibly in the topographic depression linking Galilea (immediately south of Weija Lake), Gidan-Tuba and Nyanyano, from where it extends into the ocean. In the accompanying map, it is shown as an inferred fault.

Here it appears appropriate to look at the nomenclature which in the past has been used when describing faults in the Akwapim Range. The term "Akwapim Fault Zone" has been applied in the past by various authors with varying meanings. Some refer to it as a compound name for all faults occurring in the Akwapim Range, for others it is a synonym for either the Eastern Boundary Fault, the Western Boundary Fault, or a thrust fault which has not been properly described and defined.

2.1.3 Faults Parallel or Subparallel To the Coast

They are tectonically important, because some of them cause major displacements in such a way, that the south block was displaced downward. This can be seen in the Kokrobite and Langma area, where shattered quartzites and quartzschists of the Togo Series came to

University of Ghana http://ugspace.ug.edu.gh

lie adjacently to granitoids along the coast. The downthrow is at least 100 m, because close to the coast deeply weathered granitoid rocks are exposed on top of a 100 m high Langma Hill, while along the beach, and a few meters above sea level, rocks of the Togo Series are exposed.

In the littoral zone in front of the Kako Lagoon near Gomoa Fetteh a fault is inferred, because sandstones of the Voltaian System form two large rocks which are exposed during low tide (Muff and Efa, 2006).

The faults described above are parallel to a major off-shore fault which has been termed Great Boundary Fault, and later Coastal Boundary Fault:

Seismic studies (Blundell & Banson, 1975; Blundell, 1976) established the presence of the Coastal Boundary Fault. It runs approximately parallel to the west-north-west extending coast at a distance of 3 to 5 km. South of Accra it curves to an east-west direction and intersects with the coastal area near the village of Nyanyano. The Coastal Boundary Fault separates a sedimentary basin filled with Jurassic and younger sediments on the seaward side from Devonian to Carboniferous and older rocks on the continental side Subsidence along this fault continues to the present time. Blundell & Banson (1975) state that the downthrow of the southern side of the Coastal Boundary Fault since Jurassic times is some several thousand meters.

Edwards et al. (1997) suggest that the contact of the West African Craton with the Pan-African Belt can be extrapolated beneath the continental shelf. The bathymetric maps do not show a continuation of the Akwapim Range out into the shelf area and it is likely that the mountain range has been downthrown along the coast and is being buried by recent sediments.

University of Ghana http://ugspace.ug.edu.gh

2.1.4 Transverse Faults

Efa and Muff (2006) acknowledged the presence of transverse faults in the area with an orientation that may vary from east-west to north-northwesterly directions. High-angle normal and reverse faults were observed in the areas of Kokrobite, Gomoa Fetteh, Nyanyano, and Weija, south of the Accra - Winneba road.

In the Akwapim Range, their occurrence has been inferred from topographical features or erosion patterns. When erosional valleys are developed on both slope sides of a strike ridge in such a way that the valleys cut across the ridge, the occurrence of a fault is inferred because such a feature develops preferably when a weakened rock zone transects the strike ridge giving way to the formation of erosional valleys on both sides of the ridge. This topographic feature has been used to map several short inferred faults which cross the ridges of the range (Ahmed et al, 1997).

Some major roads follow valleys formed by transform faults. The road leading from Accra to Ablekuma, the railway and main road to Amasaman, and the road from Kwabenya to Mayera are such examples. Also, the Winneba road seems to follow a transverse fault on the stretch that crosses the ridge of the range near the Weija Lake (Muff and Efa, 2006). Transverse faults result in block tectonics in the Togo Series and the individual blocks appear to have been lightly tilted. This is indicated by slightly varying attitudes of the contacts, either observed or trigonometrically calculated, between the Togo Series and the granitoid basement rocks. The transverse faults are considered to be tear-faults related to the formation of the longitudinal faults. They are probably due to inhomogeneous simple shear and formed to accommodate differential movement of tectonic blocks which formed by the breaking of the brittle metasedimentary and sedimentary rocks.

University of Ghana http://ugspace.ug.edu.gh

Work done by Efa and Muff (2006) indicate the presence of a notable fault which is transverse to the Akwapim Fault Zone and is known as the Weija Fault. It strikes west-north-west and cuts across the Akwapim Range at the Weija Dam were it marks a deep gorge in strongly indurated quartz-schists. It is buried by recent sands and continental deposits and appears to connect to faults which have been mapped in the Accraian Series. Ahmed et al., (1977) quote two reasons for inferring this fault, although no direct observation exists.

These two reasons are:

(1) the Densu River turns sharply to the east and cuts a deep gorge into the highly indurated Togo rocks to cross the mountain range, and

(2) Seismic activity along this inferred fault is conspicuous.

2.1.5 Fault Patterns in the Akwapim Range and Related Earthquakes

Southern Ghana is an earthquake-prone area and for this reason it appears appropriate to elaborate on the tectonic structure in the area and the possible causes of the earthquakes (Blundell, 1976). Amponsah (2002) points out that seismic activity in southern Ghana is concentrated in the junction area of the Akwapim Fault and Coastal Boundary Fault.

Active tectonic movement at the foot of the Akwapim Range was observed during the earthquake in 1939 when a nearly 10 km long fissure opened immediately west of the hills south of the Weija Lake. The geodynamic forces which strain this fault zone are speculated about, but consensus converges on the idea that the forces are related to the Romanche Fracture Zone (Muff and Efa, 2006).

University of Ghana http://ugspace.ug.edu.gh

The Coastal Boundary Fault, which runs approximately parallel to the coast at a distance of 3 km and south of Accra turns towards west-northeast to continue inshore at the village of Nyanyano, has been shown to be active by Blundell and Banson (1975) and Blundell (1976). They suggest a connection between the Coastal Boundary Fault and the Romanche Fracture Zone.

The Romanche Fracture Zone and its continuation, the Côte d'Ivoire – Ghana Transform Margin, have often been cited as sources of earthquakes in southern Ghana. Deltail et al. (1974); Mascle and Sibuet, (1974); Edwards et al. (1997) observed that the fracture zone is at a distance of approximately 65 km from the coast of Accra. They state that it is 6 to 11 km wide and runs approximately parallel to the coast. From their study, they indicate that the Romanche Fracture Zone represents a transform fault of the Mid-Atlantic Ridge which separates continental from oceanic crust. The development of this fault started with active transform motion when Africa and South America separated. After the spreading center had migrated along and beyond the fault, movement along this fault ceased. The forces related to the Atlantic spreading which formed the Romanche Fracture Zone, are also ruled out as a source for the present day seismic activities (Muff and Efa, 2006).

Pickett and Allerton (1998) note another tectonic episode at the Côte d'Ivoire – Ghana Transform Margin during the Eocene. Following the Eocene, the transform margin subsided to its present depth. Pickett and Allerton (1998) relate the subsidence with a change from uncoupled to coupled linkage at the continental-oceanic contact.

Geological investigations in the coastal Keta Basin, some 80 km to the east of the investigation area, reveal a sedimentary succession from Devonian to Pliocene Holocene, interrupted by several unconformities (Akpati, 1978). Akpati (1978) relates the basin

University of Ghana http://ugspace.ug.edu.gh

development and sedimentary accumulation with the development of a graben related to the Romanche Fracture Zone.

The foregoing discussion on the geo-dynamic situation in the region shows that seismic activities are concentrated along the Coastal Boundary Fault and the Pan African structures of the Akwapim Fault Zone. The forces responsible for seismic activity along the Coastal Boundary Fault could possibly be related to isostatic equilibration along the Côte d'Ivoire – Ghana Transform Margin, while no answer is available as to which forces cause the present day seismic activities related to the Pan-African structural elements.

2.2 Geological Structures

2.2.1 Joints

Joints are the commonest kind of fractures in rocks and they are of utmost importance in promoting erosion and thus shaping the topography. The surface configuration of mountain slopes and summits, drainage patterns, elbow turns in rivers and coastal cliffs are strongly governed by rock fractures (Muff and Efa, 2006).

The formation of joints is the result of stress on a rock mass and for this reason, joints show typical patterns, that is, they occur in distinctive sets.

The density or intensity of joints, expressed in number of joints per meter normal to the joint surface, depends mainly on the rock type. Brittle rocks like quartzite, quartzitic sandstone and granite, show a higher joint density than softer rocks which have been exposed to the same stress. Strength and permeability of a rock mass depends strongly on the presence and nature of fractures. When loads are normal to a joint set, deformation increases in proportion to joint density (Muff and Efa, 2006).

University of Ghana http://ugspace.ug.edu.gh

Quartzites and quartz-schists of the Togo Structural unit, quartz sandstones of the Voltaian Structural unit, and granites display most joints in the study area. The joints are open and have not been cemented by mobilized secondary minerals (Muff and Efa, 2006)

The joints observed in quarries or excavations in the study area often occur as sets of one or more directions. They occur as straight, continuous, parallel joints. Non-systematic fractures that form irregular patterns occur in addition to the systematic fractures present.

Muff and Efa, (2006) show that joint orientations are widely scattered and very variable (Figure 4). A stereographic plot of 73 joints evenly distributed in the Togo Series in the area of investigation reveals that several clusters occur. Joints are generally steeply dipping, their strike directions vary widely. One set possesses strike directions ranging from east to north, and another direction strikes to the north-northwest. Near-horizontal sheet joints are rare.

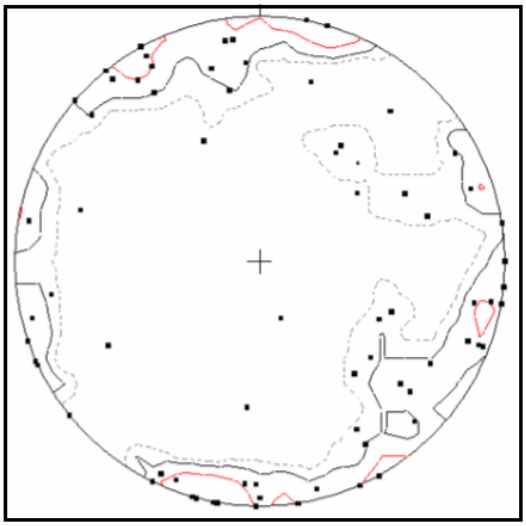

Figure 4: Stereographic polar diagram of joints in Togo Series, plotted on equal area net, lower Hemisphere. Contour intervals: 2, 4, 8 %. Max.: 13.7 % (after Efa and Muff, 2006).

University of Ghana http://ugspace.ug.edu.gh

The wide spread of values is may be due to the fact that the plotted joints were sampled in a large area. The clear distinction of definite joint sets gets lost because of tilting or translation of tectonic blocks and possible rotation of certain areas due to later tectonic processes.

2.2.2 Folds

Muff and Efa (2006) state that folds do not play an important part as a structural element in the tectonic development of the brittle rock units. They appear to be related to local tectonic processes and faulting. Folds in the Togo Structural unit are exposed in several places. They are open or closed folds, they often show axial plane cleavage, and their amplitude is often between one to a few meters. Monoclines related to faults also occur. Phyllites and quartzschists often show small crenulation folds.

In the Dahomeyan Structural unit, recumbent drag folds at the tectonic contact between Dahomeyan schists and overlying phyllonites of the Togo Series are exposed along the beach southwest of Gomoa Fetteh. They indicate shearing along a thrust fault (Ahmed, 1977 and Muff and Efa, 2006).

2.3 Geophysical Investigation Methods

The advancement of science has resulted in the use of faster and more efficient methods in solving problems. A limitation in geological field mapping is now solved by the use of geophysical investigation methods. These include: seismic, electromagnetic, magnetic and electrical resistivity methods. Electrical resistivity methods tend to be cheaper and easier to access hence its popularity.

University of Ghana http://ugspace.ug.edu.gh

Electrical resistivity methods is made up of a number of arrays which are mainly differentiated by the position of the electrodes. Some of the popular electrical resistivity arrays include the schlumberger, wenner, dipole-dipole, pole-dipole and the gradient array. Optimized forms of some of the popular arrays are the square array (from the wenner), the azimuthal resistivity array (made up of the wenner azimuthal, the equatorial dipole array and the arrow array) (Schmutz et al., 2006).

Habberjam, (1979) proposed nonconventional arrays such as the square array which could also be used for azimuthal resistivity measurements. The square array and its modified version (Habberjam, 1979) have also proven to be very effective in the investigation of ground inhomogeneity and anisotropy, (Habberjam, 1967, 1975). The use of square arrays also provides a fourth parameter, the ‘‘anisotropic non-compatibility ratio’’ (Habberjam, 1979), which is an indication of whether the subsurface is anisotropic or if fracturing or other in-homogeneities prevail. The Square array method was originally developed as an alternative to Wenner or Schlumberger arrays for work on dipping subsurface, bedding or foliation planes. It is used to detect fractures within the earth. The square array resistivity sounding method is more sensitive to a given rock anisotropy than the more usually used Schlumberger and Wenner arrays. An advantage of the square array over the other arrays is that it requires just about 65 percent less land area than the equivalent survey using Schlumberger or Wenner array.

For field techniques, three conventional methods are used for resistivity analysis of the subsurface. They are the vertical electric sounding (VES), the constant separation method (CST) and the combined procedures which utilize characteristics of both VES and CST (Cardimona, 2002). The vertical electric sounding (VES) employs collinear arrays that are configured to produce a 1-D vertical apparent resistivity versus depth model at the points of investigation. The induced current passes through progressively deeper layers at

University of Ghana http://ugspace.ug.edu.gh

greater electrode spacing and as such a series of potential differences are acquired at successively greater electrode spacing while maintaining a fixed central reference point. For the VES, Schlumberger array or Wenner array can be used. The measured potential differences are directly proportional to the changes with depth (Cardimona, 2002). The Square-array method (Habberjam and Watkins, 1967) was used to determine the presence and azimuth of subsurface fracture zones in the volcanic tuff.

Over the years azimuthal apparent resistivity has been advanced as a methodology for measuring fracture orientation of sub-vertical fracture sets. Fractures usually occur in preferred orientation that induces anisotropic physical properties on the rock mass. If the measurements are repeated over a period of time, any variations indicate an alteration of the physical properties of the rock mass, one of which would be changes in dilatancy within the fracture network.

The theoretical development of the response of a homogeneous, but anisotropic, rock mass to a collinear apparent-resistivity measurement has been covered by Taylor and Fleming (1988). Lane et al., (1995) extended the analysis to a non-linear square array. The apparent resistivity for any one electrode spacing, obtained by expanding the electrode array along each azimuth, are plotted against azimuth in a polar diagram (Figure 5). If this is circular then either there are no measurable fracture sets or the volume of rock investigated was insufficient (because the electrode-array spacing was too small) for the rock to behave anisotropically. If a distinct ellipse results then the major axis of the ellipse is coincident with the strike of the fractures. This is true, regardless of whether the fracture-fill is more, or less, resistive than the host rock (Nunn, et al., 1983), because the resistivity along strike is the arithmetic mean and is always higher than the resistivity across strike, which is the harmonic mean. Due to the paradox of anisotropy (Keller and Frischknecht 1966,), the

University of Ghana http://ugspace.ug.edu.gh

measured apparent resistivity normal to the fractures is equal to the true resistivity parallel to the fractures.

The coefficient of anisotropy l is defined by Habberjam and Watkins, (1967) as

$$\lambda = \sqrt{\frac{\rho_y}{\rho_x}} = \frac{\rho_{x_{app}}}{\rho_{y_{app}}} \quad (1)$$

Where

ρ_y is the true resistivity normal to the fractures,

ρ_x is the true resistivity parallel to the fractures,

ρ_{xapp} is the apparent resistivity parallel to the fractures and

ρ_{yapp} is the apparent resistivity normal to the fractures.

The measured apparent resistivity values for the various points are then subjected to a filtering technique to highlight the isotropic and anisotropic characters of the subsurface. Lilian and Niels (1994) indicate that the filtering is done by subtracting the function:

$$\frac{\rho a_{min} - 1}{10(\rho a_{max} - \rho a_{min})} \quad (2)$$

The results are plotted against angular axes to generate a resultant anisotropic Figure. Using radar charts, the data is plotted from minimum to maximum values on the outer radial axis. If a multiple-peaked pattern is observed then the azimuth of the peaks indicates the strike of more than one fracture set. Since the degree of anisotropy is usually small, a datum value is commonly removed from the data before plotting in order to emphasize the anisotropy.

University of Ghana http://ugspace.ug.edu.gh

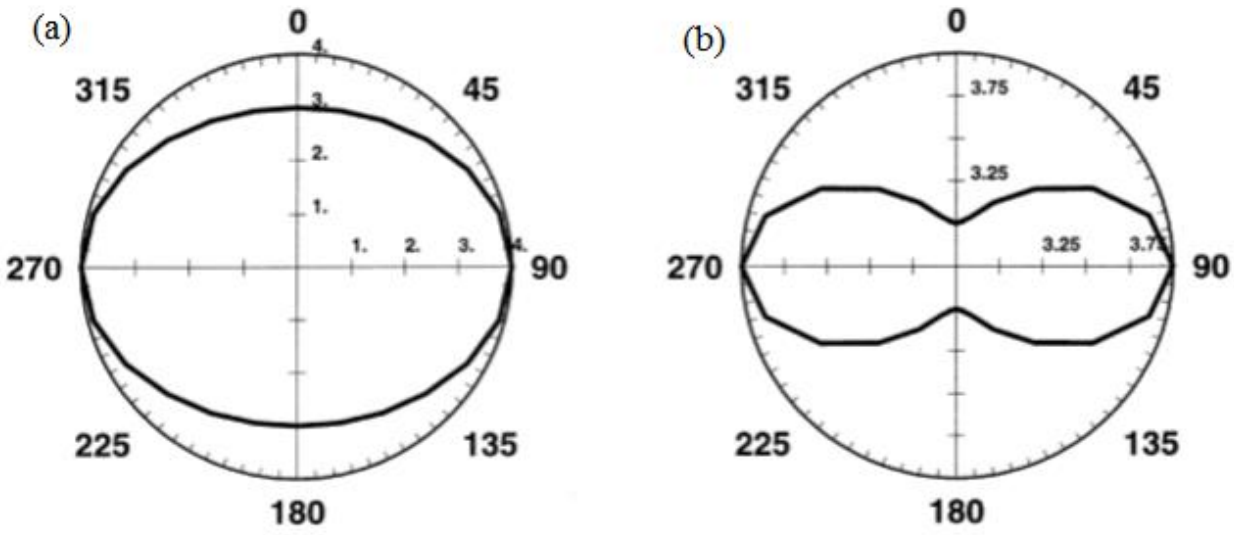

Figure 5: (a) Theoretical azimuthal apparent-resistivity ellipse plotted as a polar diagram. (b) After removal of a datum value the ellipse takes on a characteristic double-lobed form. (After Busby, 2000)

From the polar plots, circular plots indicate no measurable fracture sets or that the volume of the rock investigated were insufficient because the structure and material sampled were, to the limit of the measurement, isotropic. Elliptical plots show a defined principal fracture set. Habberjam and Watkins (1967) write that for collinear arrays, the major axis of the ellipse coincides with the strike of the fractures whereas for non-collinear arrays such as square array, the minor axis of the ellipse is parallel to the strike fracture.

Two situations that need to be distinguished are firstly, the apparent resistivity varying with electrode array orientation but independent of coordinates (Bolshakov et al, 1997) and secondly apparent resistivity dependent on both coordinates and orientation of electrodes. As a result of the paradox of anisotropy (Keller and Frischknecht, 1996), the measured apparent resistivity of normal to the fractures is equal to the true resistivity parallel to the fracture. A fractured layer is electrically anisotropic thus resistivities in any of the three orthogonal directions can be different from each other (Iddirisu and Armah, 1997). The variation in

University of Ghana http://ugspace.ug.edu.gh

the horizontal permeability within the subsurface generate electrical anisotropy characteristics in surface electrical resistivity. Taylor and Flemming (1988) and Lillian and Niels (1994) show that, for a given set of vertical fractures, the potential distribution in the horizontal plane is given by the expression by Taylor and Flemming, (1988) as:

$$V = \frac{I\rho_m}{2\pi r\sqrt{(cos^2\vartheta + \lambda^2 sin^2\vartheta}} \quad (3)$$

Where V is the potential at a point defined by M = (x, y, ϑ) with polar coordinates (r, ϑ, 0),

ρ_m is the mean bulk resistivity,

I is the magnitude of the input current and

λ is the coefficient of anisotropy which is greater than unity (Keller and Frischknecht, 1966).

For situations where anisotropy is due to the fracturing, the fracture orientation is directly observed from the data. Single lobbed ellipses indicate only one primary fracture set that is parallel to the minor axis of the fitted ellipses (Lane, 1995). Double lobbed ellipses show two fracture set orientations based on visual inspection of the polar plots.

The minimum axes which indicate the direction of high resistivity in the anisotropic medium within the subsurface rocks also represents the direction of subsurface conductive features having a high probability of very good porosity and permeability (Iddirisu and Armah, 1997). Keller and Frischknecht (1996) tag this occurrence as the paradox of anisotropy.

University of Ghana http://ugspace.ug.edu.gh

CHAPTER THREE

METHOLOGY

3.1 Introduction

The project was carried out in three stages, namely desk study, field and laboratory work and data analysis. The methods employed in each stage are described out in details below.

3.2 Desk Study

The project consisted of a preliminary desktop study and processing of the regional geophysical data to help target areas for subsequent field work. Good regional resolution magnetic and radiometric data was assembled and assessed to constrain the structures for the field work.

3.3 Aero – Geophysical Data: Acquisition and Processing

Over the years, the methods of geophysical survey have improved with time. The advent of airborne geophysical survey has been a major step in the improvement of geophysical surveys as a whole. Presently the use of airborne geophysics helps in the survey and mapping of areas that may be inaccessible by ground or having unfavorable conditions for ground geophysics.

Airborne geophysical survey was carried out in the southern parts of Ghana within November 1999 and 2000 by High Sense Geophysics Incorporated of Canada. The survey comprised magnetic, radiometric and VLF surveys of four selected areas.

University of Ghana http://ugspace.ug.edu.gh

3.3.1 Magnetic Data

The following steps were carried out prior to levelling:

1. Base-station correction to account for diurnal variations in the geomagnetic field.
2. Lag correction to correct for positioning error between the GPS and mag-sensor.
3. Heading correction to correct for errors caused by the aircraft's position relative to the geomagnetic field.
4. IGRF correction. Subtraction of the IGRF-field in the area.

Levelling was made in two steps:

1. Standard tie line leveling.
2. "Micro- Levelling" as described by Geosoft (Geosoft levelling system, Tutorial and user guide, Chapter 6, p. 53-54).

The micro- levelling was made according to the Geosoft procedure, except that a limit was set to the correction allowed. This was made to minimize the effect on anomalies of geological origin. Typically a maximum correction of +/- 3 nT was accepted.

3.3.1.1 Processing and Integration

The initially processed airborne geophysical data was further processed to suit the objectives of the study. Under this, various principles were applied to the data in order to produce the expected graphical map representation. The various principles used in the processing of the data are discussed as follows:

University of Ghana http://ugspace.ug.edu.gh

3.3.1.2 Microlevelling

Working with complex datasets such as airborne magnetic or radiometric data requires one key processing objective that is to eliminate levelling problems which were not removed during the regular processing (such as lag correction, tie line levelling and base level correction (Reeves, 2005). In the study, although the airborne magnetic data set had already been microlevelled, the microlevelling was carried out on the data to cross check for any errors in the first microlevelling process. This was to increase the confidence level of the data by minimizing all levelling errors as much as possible. This was done using Geosoft's Oasis Montaj software.

3.3.1.4 Butterworth Filter

The Butterworth filter is good for applying straight forward high-pass and low-pass filters to data due to the fact that the degree of filter roll-off can be controlled leaving the central wave number fixed. It is the simplified alternative of the Cosine filter (COSN). For the butterworth filter, the mathematical principle used is defined by Reeves, (2005) as:

$$\mathrm{L}(k) = \frac{1}{[1+\left(\frac{k}{ko}\right)^{n}]} \qquad (4)$$

Where: k_o is the central wave number of the filter

n is the degree of the Butterworth filter function (By default = 8)

0/1 is used to flag the pass required. It specifies if a residual (0) high pass or a regional (1) low pass is required. By default, a regional filter is applied

University of Ghana http://ugspace.ug.edu.gh

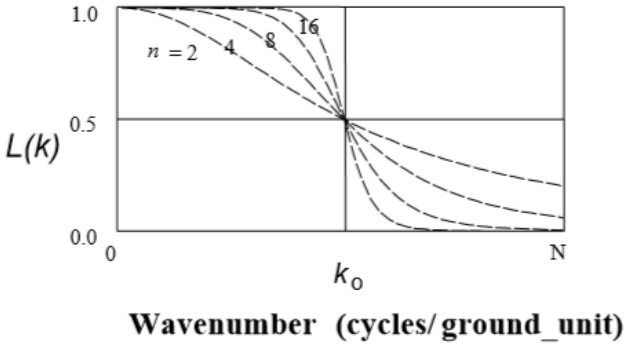

The total magnetic intensity map was produced by gridding the magnetic anomaly channel of the magnetic geodatabase using the minimum curvature gridding method at a chosen grid cell size of 100 m. The grid cell size is normally set to be ½ to ¼ the nominal line spacing; in this case, ¼ of the sample interval (400 m) was used (Reeves, 2005). A minimum curvature surface is the smoothest possible surface that will fit the given data values. This process serves as the basic processing method that can be performed on a magnetic dataset (Reeves, 2005). However, the disadvantage of applying this method in gridding the data is that the minimum curvature does not entirely account for or remove noise. As a result, a smoothening technique (butterworth filter) had to be adopted to correct for these error using the parameters as shown in table below:

Table 1: A table showing the parameters used for the butterworth filtering process.

Butterworth Filter	
Cut Off Wavelength	400 m
Filter Order	8
High / low Pass	Low

University of Ghana http://ugspace.ug.edu.gh

3.3.1.5 First Vertical Derivative

The vertical derivative is commonly applied to total magnetic field data to enhance the shallowest geologic sources and suppress deeper sources in the data. It computes the vertical rate of change in the magnetic field and suppresses the long wavelengths. It is defined by multiplying the amplitude spectra of a field by a factor of a form

$$\frac{1}{n}\{(u^2 + v^2)^{\frac{1}{2}}\}^n \quad (5)$$

where n is the order of differentiation of the vertical derivative, μ is the rate of change of the magnetic field in the "x" plane and ν is the rate of change of the magnetic field in the "y" plane with the "x" plane and the "y" plane perpendicular to each other (Reeves, 2005).

The order of differentiation defines the high wavenumber components to enhance; increasing the order will enhance higher wavenumber components of the spectrum. The first vertical derivative is theoretically equivalent to the measurement of the magnetic field at two points perpendicularly above each order; subtracting the data and dividing the outcome by the vertical spatial separation of the measurement points. (Milligan and Gunn, 1997).

3.3.1.6 International Geomagnetic Reference Field (IGRF)

The magnitude of the magnetic field F generally varies between 20,000 and 70,000 nT on the Earth's surface (Telford et al., 1990; Reeves, 2005). It does also have local variations of several hundred nT (sometimes, but less often, several thousand nT) imposed on it by the effects of the magnetization of the crustal geology (Telford et al., 1990). Anomalies produced usually indicate a magnitude about two orders smaller than the original total field value.

University of Ghana http://ugspace.ug.edu.gh

The IGRF provides the means of subtracting on a rational basis the expected variation in the main field to leave anomalies that may be compared from one survey to another, even when surveys are conducted several decades apart and when, as a consequence, the main field may have been subject to considerable secular variation (Telford et al., 1990). Its removal thus involves subtracting of close to 99% of the measured value and will require a precise definition if an accuracy of the residual is to be retained. The IGRF channel routine in Oasis Montaj was applied to calculate the inclination and declination of the study area related to the period with which the data was acquired. The IGRF model year which is calculated every 5 years, was set to the most recent year

2005. After these parameters were used the calculated declination (D) and inclination (I) values were obtained to be –4.5° and -15.5° respectively.

3.3.1.7 Analytic Signal

The analytic signal is another quantitative method developed for interpretation of potential field data and combines the horizontal and vertical derivatives of the anomaly (Bilim and Ates, 2003). The analytical signal can be useful for locating the edges of remanently magnetized bodies and for centering anomalies over their causative bodies in areas of low magnetic latitudes (MacLeod et al., 1993). It is defined as the square root of the sum of squares of the derivatives in the x, y, and z directions.

$$(A|x,y|) = (\{\left(\frac{\partial m^2}{\partial x}\right)^2 + \left(\frac{\partial m^2}{\partial y}\right)^2 + (\frac{\partial m^2}{\partial z})^2\})^{1/2} \quad (6)$$

(A|x, y|) is the amplitude of the analytical signal at a given point (x,y) and m is the observed magnetic field at (x, y) while z is the depth of that point.

University of Ghana http://ugspace.ug.edu.gh

The analytical signal is not a measurable quantity and is not dependent on the direction of magnetization and the direction of the earth's magnetic field. All bodies with the same geometry have the same analytical signal (Milligan and Gunn, 1997) only differing in the contrast of their susceptibilities.

The distortion caused by a body's magnetization remains in the analytical signal but produces a better result in terms of amplitudinal signatures if the analytical signal is applied to a reduced to pole anomaly (Bilim and Ates, 2003). The amplitude of the analytical signal of the total magnetic field produces a maxima over magnetic bodies regardless of the direction of magnetization (MacLeod et al., 1993). This is due to the fact that the strength of the magnetization of rocks is inversely related to the amplitude of their analytical signals

3.3.1.8 Upward and Downward Continuation

The upward continuation filtering technique is considered a "clean filter" because it produces almost no side effects that may require the application of other filters or processes to correct and is thus frequently used to minimize or clean shallow source and noise effects in grids.

Unlike many other filtering processes, upward continued data may be interpreted numerically and with modelling programs. Because it has a smooth shape and does not alter the energy spectrum below the start of roll off, it is usually used for simple low-pass operations.

Gunn (1997) described the filter as having a frequency response of

$$e^{-h}(u^2 + v^2)^{1/2} \qquad (7)$$

University of Ghana http://ugspace.ug.edu.gh

where u and v are the changes in magnetic field in the “x’ and “y” planes respectively and “h”, the elevation. This implies that upward continuation smoothens out high frequency anomalies relative to lower frequency ones and can thus be used for suppressing the effect of shallow anomalies when emphasis is to be placed on deeper anomalies (Gunn, 1997). The downward continuation process is similar but enhances shallower features which are of interest.

3.3.2 Radiometric Data

The occurrence of naturally occurring gamma radiation serves as a tool which can be used in the study of faults and fractures within the earth (Nsiah-Akoto et al, 2013). It is believed that these radioactive gases emanate from within the earth and get to the surface through gaps and crevices mostly generated by the break in continuity of the underlying rocks (Nsiah-Akoto et al, 2013). This serves as a good tool to track shear zones, faulted zones and other unconformities that result in the break in the continuity of the underlying rocks. There are more than fifty naturally occurring existing radioactive isotopes though only a few such as Uranium (^{238}U), Thorium (^{232}Th) and Potassium (^{40}K) emit significant amounts of gamma radiation. The abundance of these gases is dependent on the geology, soils, regolith and surface cover. The purpose of radiometrics is to determine either the relative or absolute values of U, Th, or K in surface rocks and soils (Graham, 2013). Regionally, gamma ray spectrometry can be used to delineate geologic provinces, fold belts, sedimentary basins and tectonic and structural detail of shear zones (Graham, 2013).

The information contained in the aero geophysical data includes the coordinate system, and the mode of measurements of the radioelements.

University of Ghana http://ugspace.ug.edu.gh

The radioelements (uranium, thorium and potassium were gridded using Geosoft's minimum curvature gridding technique to produce separate maps that showed individual radioactive signatures in the study area. The grids produced were then correlated with the geological units, patterns and trends from which analysis were made.

3.4 Geological Structural Mapping

Geological structural mapping was carried out at areas with rock exposures within the study area. The rocks in the study are predominantly made up of the rocks of the Togo structural unit bounded to the west by the cape coast granitoids and to the east by the Dahomeyan structural unit.

The structural features that were targeted are joints, foliation, folds and faults. With most parts of the area falling within the lowland areas, the number of exposures seen are few. Also, the high rate of urban settlement development within the area in addition to other anthropogenic activities have left the area with few outcrop exposures although they are representative of the area. The prominent geological structures present are the foliation and joints. The structural measurements were done in concordance with the right-hand-rule using a Konustar compass. Repetitive measurements were taken at each point to ensure a high level of accuracy.

3.5 Ground Geophysical Surveys

3.5.1 Geophysical Resistivity Methods

The study involved the use of various electrical resistivity techniques to acquire data. These methods included the Square Array Method, the Schlumberger Sounding method

University of Ghana http://ugspace.ug.edu.gh

and the Azimuthal Sounding method. These resistivity investigation methods were selected because of their effectiveness in fracture and fault zones mapping. The points for the geophysical survey were selected based on the maps generated from the aeromagnetic and radiometric data. The points were selected to fall within the fault and fracture zone and are representative of the whole study area.

Resistivity is a measure of a materials resistance to the flow of electrical current. Field measurement result in apparent resistivity (ρ_a) values that are generally related to the rock type and water content, which are often related to grain-size distribution as finer grained materials usually have a lower water content than coarse grained materials and consolidated rock (Cardimona, 2002) The values are also affected by the location and spacing of the electrode arrays. The larger the spacing of the electrode array, the larger the sample volume covered and as such the deeper depth reached. The variation of electrical properties of material with direction (anisotropy) also affects the resistivity measured based on the direction of measurement (Habberjam, 1975). Horizontally stratified rocks have their plane of anisotropy generally parallel to the surface unlike dipping layered rock units which have their plane of anisotropy being dependent on the orientation. The plane of anisotropy of fractured rock units such as those in the study area follows the same principle as that of dipping layered rock units. The instrument used is the Scintrex Automated Resistivity Imaging System (SARIS). This was used together with electrical cables, alligator clips, banana plugs and electrodes. The electrode positioning was varied based on the geophysical electrical resistivity array being carried out. For every sample point (as shown in Figure 6), the Square array, Schlumberger soundings and Wenner Azimuthal Soundings were carried out.

University of Ghana http://ugspace.ug.edu.gh

For this survey, electrical resistivity methods were chosen because:

i. They are relatively rapid to carry out and are flexible. The field time increases with the intended depth of reach.
ii. Minimal expenses are made in this kind of survey other than on personnel.
iii. The equipment used are relatively light and portable.
iv. There is a relatively better response to different material properties than other geophysical survey methods.
v. Qualitative interpretation of the data is straightforward.

University of Ghana http://ugspace.ug.edu.gh

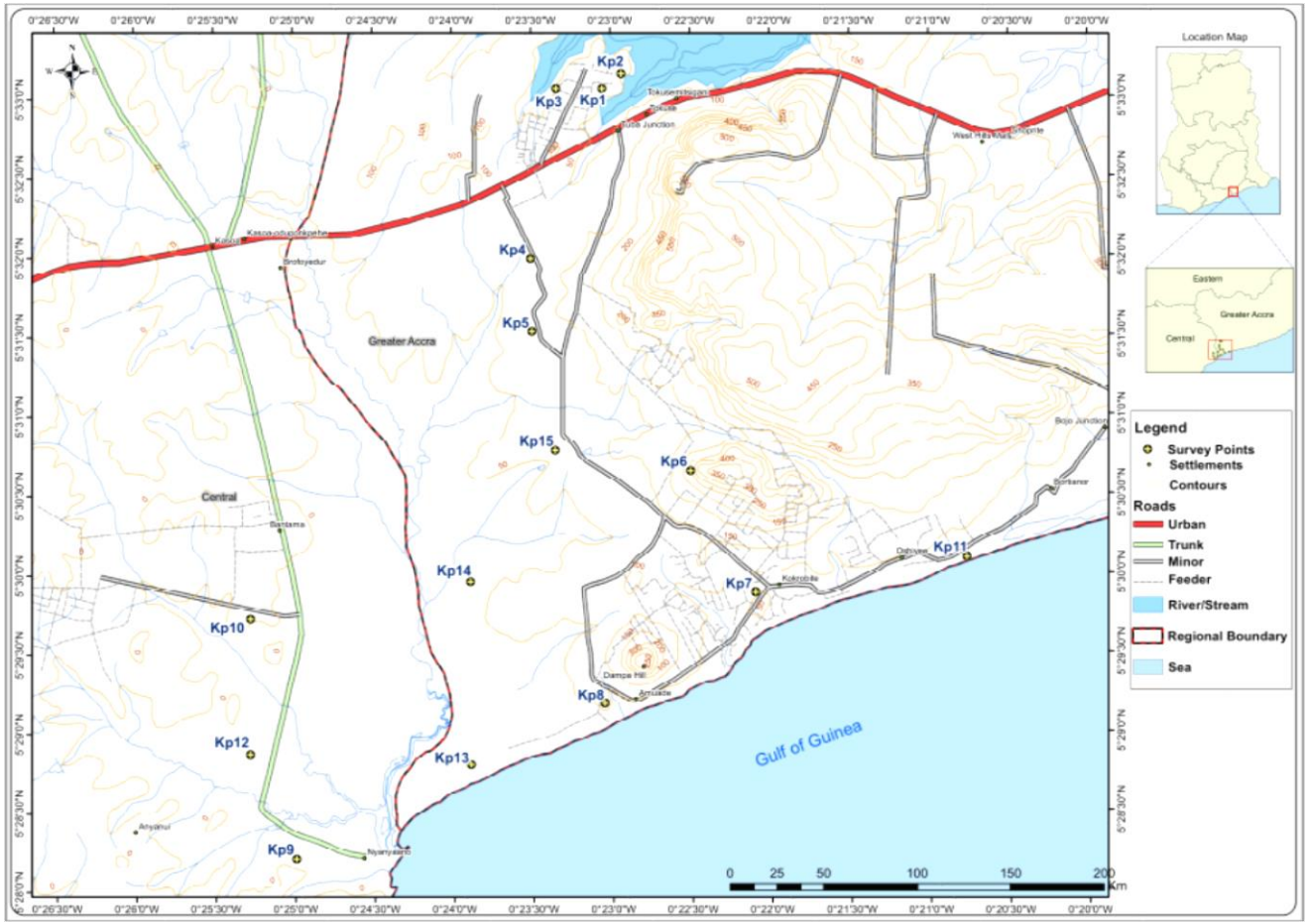

Figure 6: Map of the study area showing the survey points

University of Ghana http://ugspace.ug.edu.gh

3.5.2 Square Array

For this study, the interpreted results of the Square Array method is supported by Azimuthal Wenner Array Sounding data and Schlumberger Sounding data.

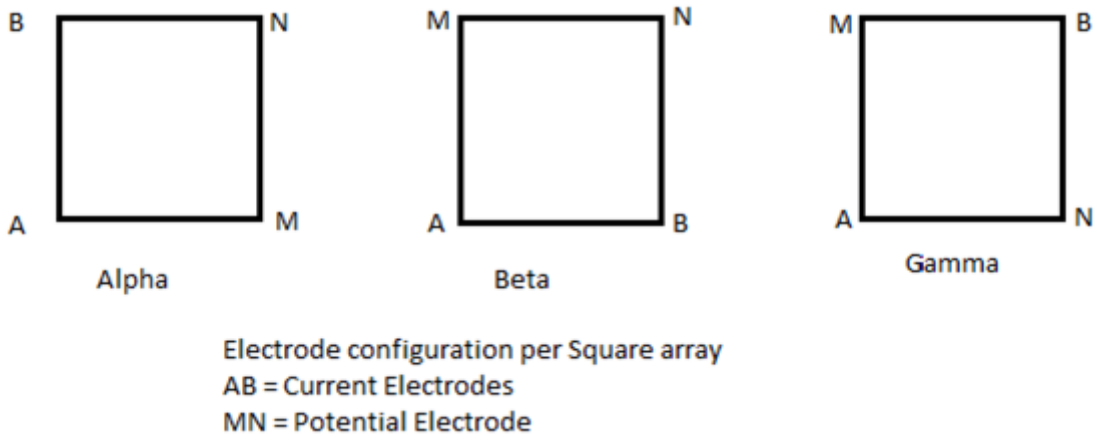

Figure 7: Electrode positions for Square Array measurements

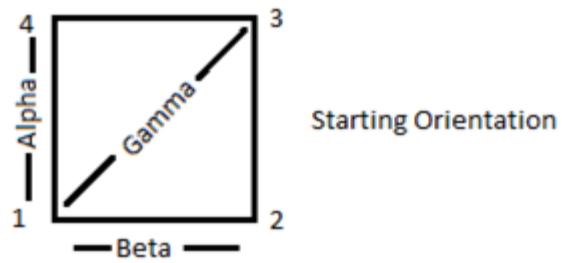

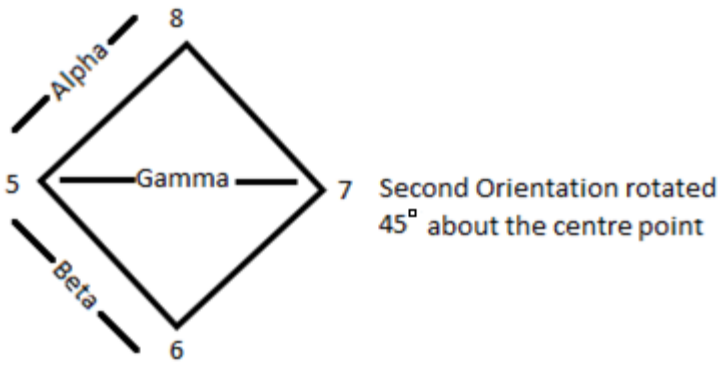

Figure 8: Electrode positions for the first and second orientation of the Square array

Current electrode configuration for Crossed Square Array

University of Ghana http://ugspace.ug.edu.gh

Alpha 1 – 4 = ρ_{a1}

Alpha' 5 – 8 = ρ_{a2}

Beta 1 – 2 = ρ_{a3}

Beta' 5 – 6 = p_{a4}

Gamma 1 – 3

Gamma' 5 – 7

Using the Square-array method, the azimuth of the existing structures is generally indicated by a decrease in resistivity along a particular azimuth relative to the other azimuths.

The direct- current survey using the Square-array method is conducted in a similar manner as the traditional collinear arrays. In this study, the positioning is similar to the traditional Wenner method. The position of the measurement is assigned to the center point of the square (figure 8). The array size, defined by the symbol "A", is the length of the side of the square. Expansions of the square are made symmetrically about the center point in increments of A $(2)^{1/2}$ (Habberjam and Watkins, 1967), so that the soundings can be interpreted as a function of depth. The electrode positions are connected to the Resistivity meter such that electrodes A and B are the transmitter electrodes or the current electrodes while the electrodes M and N are the receiver electrodes or the potential electrodes. The depth of investigation is generally considered to be approximately equal to the side of the square but varies with resistivity (Habberjam, 1975).

For each square, two perpendicular measurements (alpha, α and beta, β) were taken in addition to one diagonal measurement (gamma, γ) as indicated in Figure 8. The diagonal

University of Ghana http://ugspace.ug.edu.gh

(gamma) measurement provides a check on the accuracy of the two perpendicular (alpha and beta) measurements.

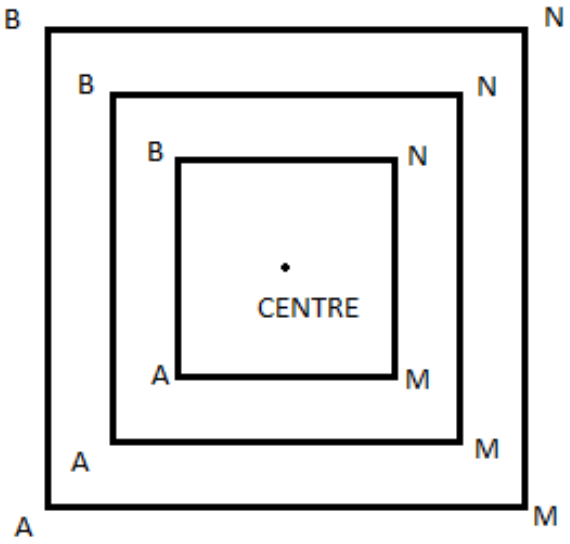

Figure 9: Symmetrical Expansion of the square about the center point.

In an isotropic medium,

Gamma, $\gamma\rho_a = 0$, therefore, $\alpha\rho_a = \beta\rho_a$ and

In a homogenous anisotropic medium,

$$\gamma\rho_a = \alpha\rho_a - \beta\rho_a. \quad (9)$$

The array is expanded symmetrically about the center of the square (as shown in Figure 9) after all three measurements have been made.

The apparent resistivity values are obtained from the following relation:

$$\rho_a = \frac{K\Delta V}{I} \quad (10)$$

Where: ρ_a = the apparent resistivity, in ohm – meter;

University of Ghana http://ugspace.ug.edu.gh

K = the geometric factor for the array;

ΔV is the change in potential difference

I = the applied current, in amperes.

For the square array, the geometric factor is given by Habberjam and Watkins, 1967 as

$$K = \frac{2\pi A}{2-\sqrt{2}}, \quad (11)$$

Where "A" is the square array side length, in meters.

The square is collapsed after the measurement of the largest square and a 45^0 rotation is made after which the square is expanded again just like before.

3.5.3 Schlumberger Array

The Schlumberger method carried out in the field followed the traditional collinear Schlumberger electrode positioning. The current cables were connected to the terminals C_1 and C_2 and the potential terminals connected to their terminals P_1 and P_2 respectively as shown in Figure 10.

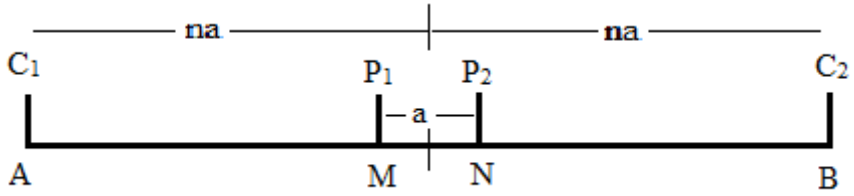

Figure 10: A schematic representation of the Schlumberger array Configuration

For the Schlumberger array, the apparent resistivity is given by the equation

ρ_a = KR, where K is the geometric factor given by

University of Ghana http://ugspace.ug.edu.gh

$$K = \frac{\pi a^2}{na}\left[1 - \frac{na^2}{4a^2}\right] \quad (12)$$

and

$$R = \frac{\Delta V}{I} \quad (13)$$

The Schlumberger sounding that was done started with a potential electrode spacing ($\frac{MN}{2}$) of 0.5m and a current electrode spacing ($\frac{AB}{2}$) of 1.58m expanding progressively to 158m (at eight readings per decade)

3.5.4 Wenner Azimuthal Array

The Wenner Azimuthal array was carried out as part of the geophysical methods to identify the fractures present in the area. The azimuthal electrical resistivity method is widely used in characterizing anisotropy in the subsurface. Generally, variations in horizontal permeability within the subsurface generate electrical anisotropy characteristics in surface electrical resistivity surveys.

Azimuthal apparent resistivity has been advanced as a methodology for measuring fracture orientations of sub-vertical fracture sets (e.g. Taylor and Fleming, 1988; Cohn and Rudman, 1995; Lane et al., 1995). Fractures often occur in sets with a preferred orientation that imposes anisotropic physical properties on the rock mass. Factors of anisotropy calculated from the measurements are to vary with time if the fractures are dilating and these could be utilized as indicators of cliff instability (Taylor and Flemming, 1988).

University of Ghana http://ugspace.ug.edu.gh

3.5.5 Azimuthal Apparent Resistivity Measurements

Azimuthal apparent resistivity measurements are made by taking resistivity measurements along a sufficient number of azimuths to define any variation of apparent resistivity with orientation (Taylor and Fleming, 1988). The apparent resistivity for each electrode spacing are plotted against azimuth in a polar diagram. If the plotted Figure is circular then either, there are no measurable fracture sets or the volume of rock investigated was insufficient because the structure and material sampled were, to the limit of measurement, isotropic. If an ellipse results then the azimuth of the principal fracture set can be defined. For a collinear array, the major axis of the ellipse is coincident with the strike of the fractures, but for non-linear arrays, such as the Square array (Habberjam and Watkins, 1967), the minor axis of the ellipse is parallel to the fracture strike.

For this study, the Wenner array was selected for use taking into consideration the limited space available as compared to the expected depth of coverage. The traditional collinear positioning of four electrodes at equal spacing as per the Wenner array configuration was done and readings taken. The array was expanded after each reading until maximum space limitation was reached. The array was then rotated through an angle of 10 degrees clockwise about the point of measurement. The measurements were taken at electrode spacing of 6m, 12m, 17m, 24m and 34m. This procedure was carried out to cover the entire azimuth. The rotation is done to cover 360 degrees and the plots of the apparent resistivities are each potential electrode spacing are plotted in a polar diagram using Microsoft Excel.

University of Ghana http://ugspace.ug.edu.gh

CHAPTER 4

RESULTS AND DISCUSSION

4.1 Aeromagnetic Data

As mentioned in the methodology, the total magnetic intensity data from the aeromagnetic data was processed using various filters and enhancers in the Oasis Montaj software. This processing was done stepwise and each grid produced was carefully analyzed to determine the next action to be taken on it.

4.1.1 Microlevelling

Microlevelling was carried out on the data to remove any form of unevenness in the data. Through this process, all levelling problems were eliminated and as such, a clean data was obtained to work with. A grid of the microlevelled data (Figure 11) gives an indication of certain trends in the northeast-southwest directions. As a result of the trends not being very distinct, there was the need to apply more filters and enhancement processes to the image to distinguish any occurring feature from the background. The butterworth filter is applied to the microlevelled data as the first image enhancement method to be used.

University of Ghana http://ugspace.ug.edu.gh

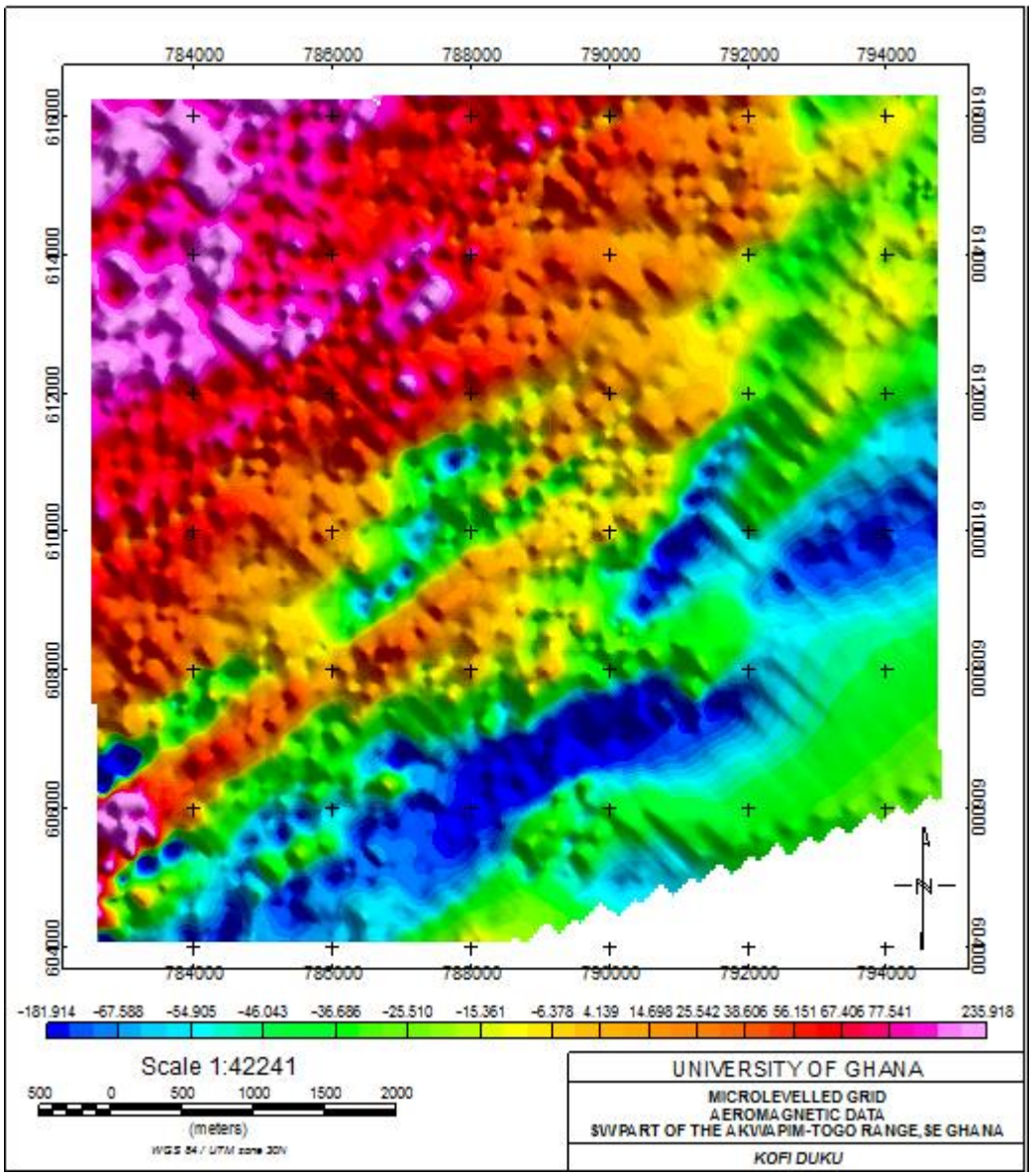

Figure 11: A map grid of the microlevelled total magnetic intensity (TMI) data of the study area.

University of Ghana http://ugspace.ug.edu.gh

4.1.2 Butterworth Filter

The butterworth filter is used to apply the low pass filter to the microlevelled grid (shown in Figure 11). With a cut-off wavelength parameter of 400 and a filter order of 8, this filter is used to enhance the microlevelled grid to produce a finer grid (Figure 12) with more distinct features and trends.

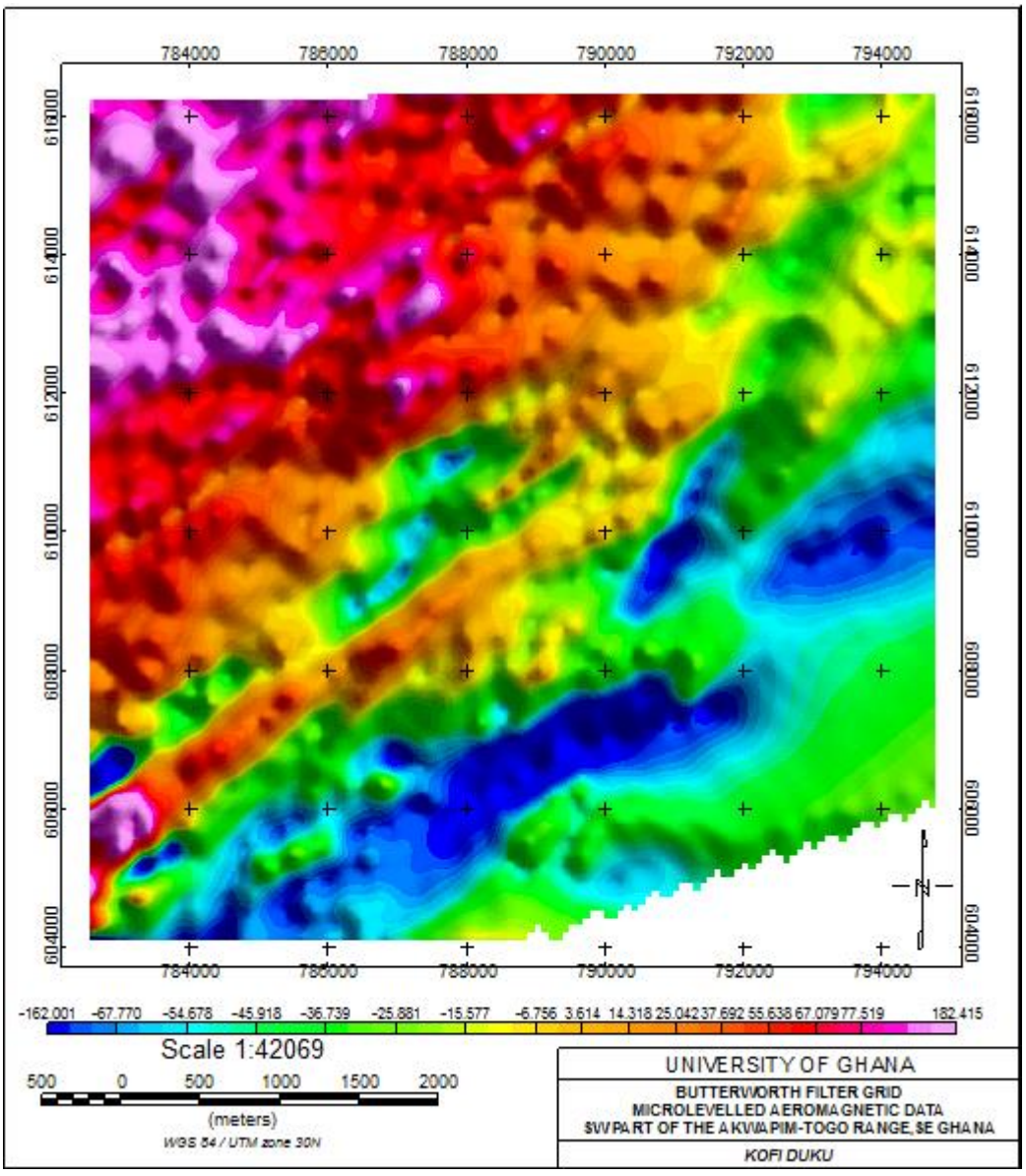

Figure 12: Butterworth filter grid of the total magnetic intensity (TMI) data of the study area.

The grid produced as shown in Figure 12 shows more distinct northeast-southwest trends with the blues representing the low magnetic values while the shades of red to pink

University of Ghana http://ugspace.ug.edu.gh

represent the high magnetic values. The first vertical derivative filter is then applied to highlight the shallow features within the ground.

4.1.3 First Vertical Derivative filter

The vertical derivative is applied to total magnetic field data to enhance the shallowest geologic sources and suppress deeper sources in the data. It computed the vertical rate of change in the magnetic field and suppresses the long wavelengths. With this filter, it is easier to notice the subsurface features as their signatures are brought to fore as shown in Figure 13.

This filter shows the trends of the structural features as well as buried objects or artefacts that are within a depth of 0 to about 50 meters within the earth (Milligan and Gunn, 1997). The same northeast-southwest trends, northwest-southeast trends as well as east-west trends are seen in figure 13 after this filter is applied. However it is better defined and delineated. This gives an indication that the surficial trends go a bit deep into the subsurface.

The reduced to magnetic equator filter is then applied to the grid to further enhance it.

University of Ghana http://ugspace.ug.edu.gh

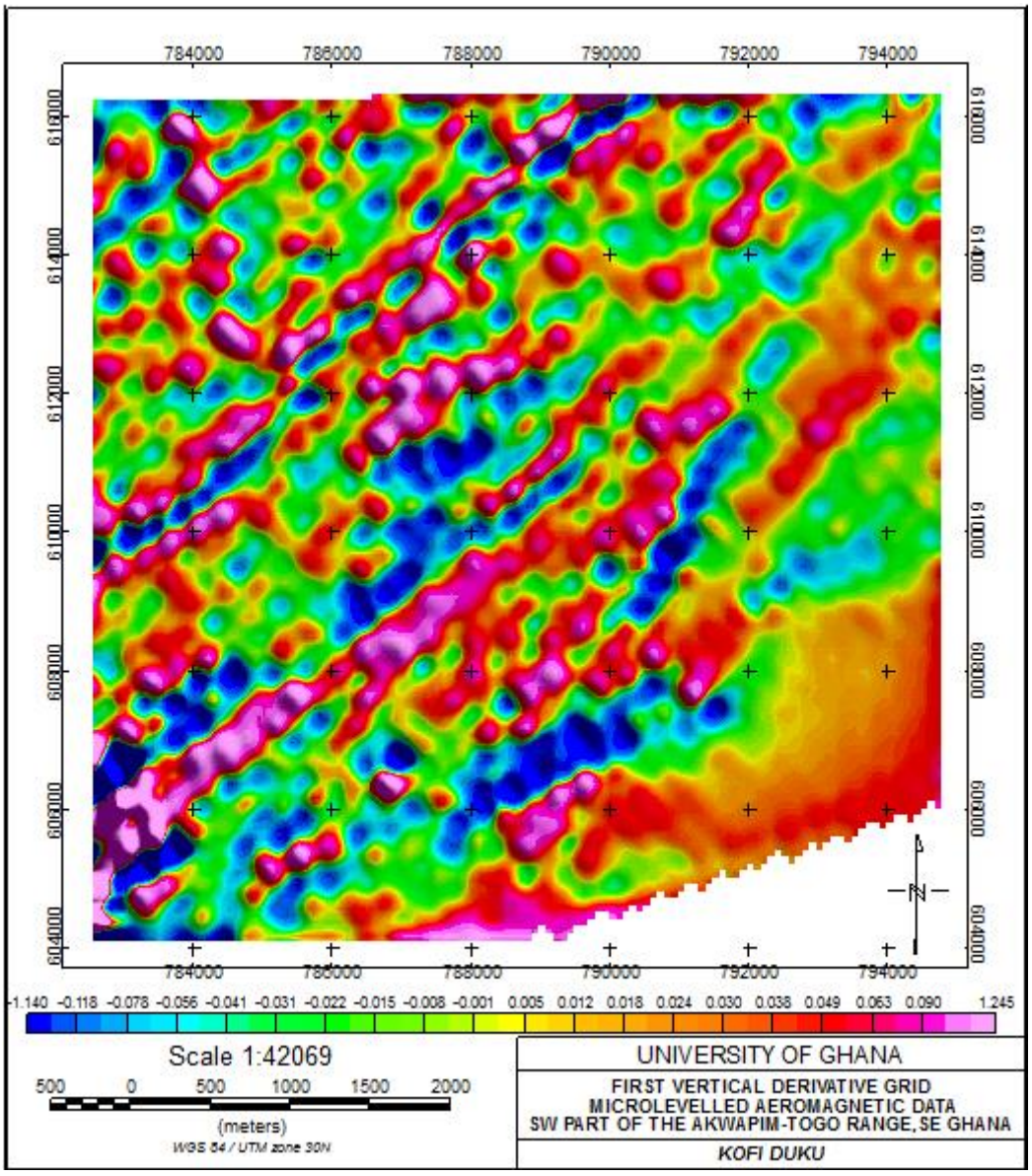

Figure 13: First Vertical Derivative grid of the total magnetic intensity (TMI) data of the study area.

4.1.4 Analytical Signal

The analytical signal filter was used to center the anomalies occurring in the study area over their causative bodies. From the grid produced (Figure14) prominent northeast-southwest rending anomalies were observed. This was concordant with the grid produced using the first vertical derivative filter.

University of Ghana http://ugspace.ug.edu.gh

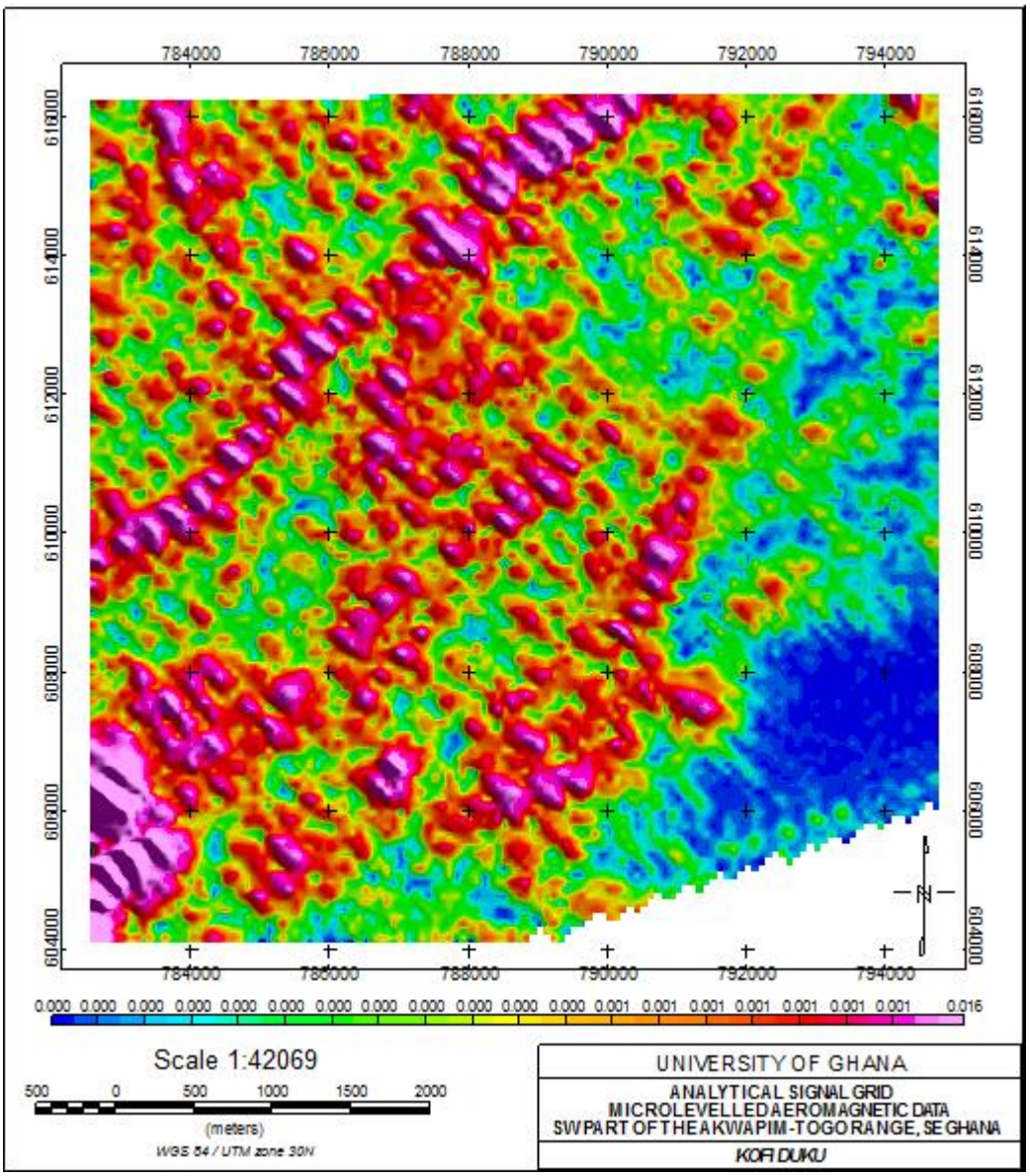

Figure 14: Analytical signal grid of the total magnetic intensity (TMI) data of the study area.

The grid produced from this filtering method further enhances the northeast-southwest trends, northwest-southeast trends as well as east-west trends are seen scattered in the grid. It also shows the breaks and continuation of the trends present.

University of Ghana http://ugspace.ug.edu.gh

4.1.5 Directional Cosine Filter

The directional cosine filter was used to process the grid produced from the analytical signal filter (Figure 14) to remove the northwest-southeast trends. The grid produced (Figure 15) highlights the northeast-southwest trends while suppressing the noise in the northwest-southeast direction. The grid produced was thereafter filtered using the downward continuation method and the upward continuation method.

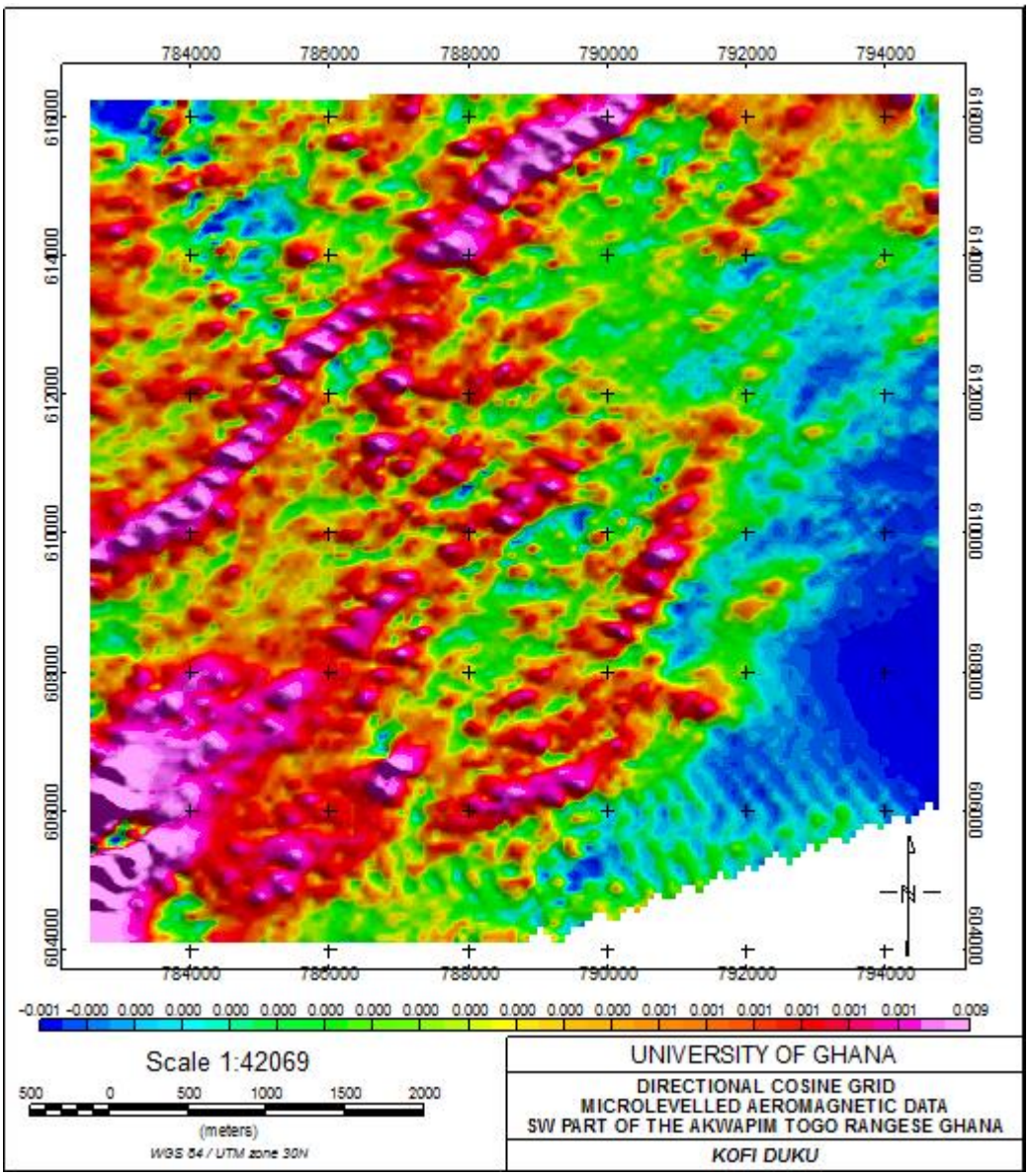

Figure 15: Directional cosine filter grid of the total magnetic intensity (TMI) data of the study area.

University of Ghana http://ugspace.ug.edu.gh

The downward continuation filter and the upward continuation filter are carried out separately on the grid produced from the reduced to magnetic equator grid after which the grids produced are compared.

4.1.6 Downward Continuation Filter

This filter is applied on the analytical signal grid to enhance the response from anomaly sources at shallow depths by bringing the plane of measurement further away from the source.

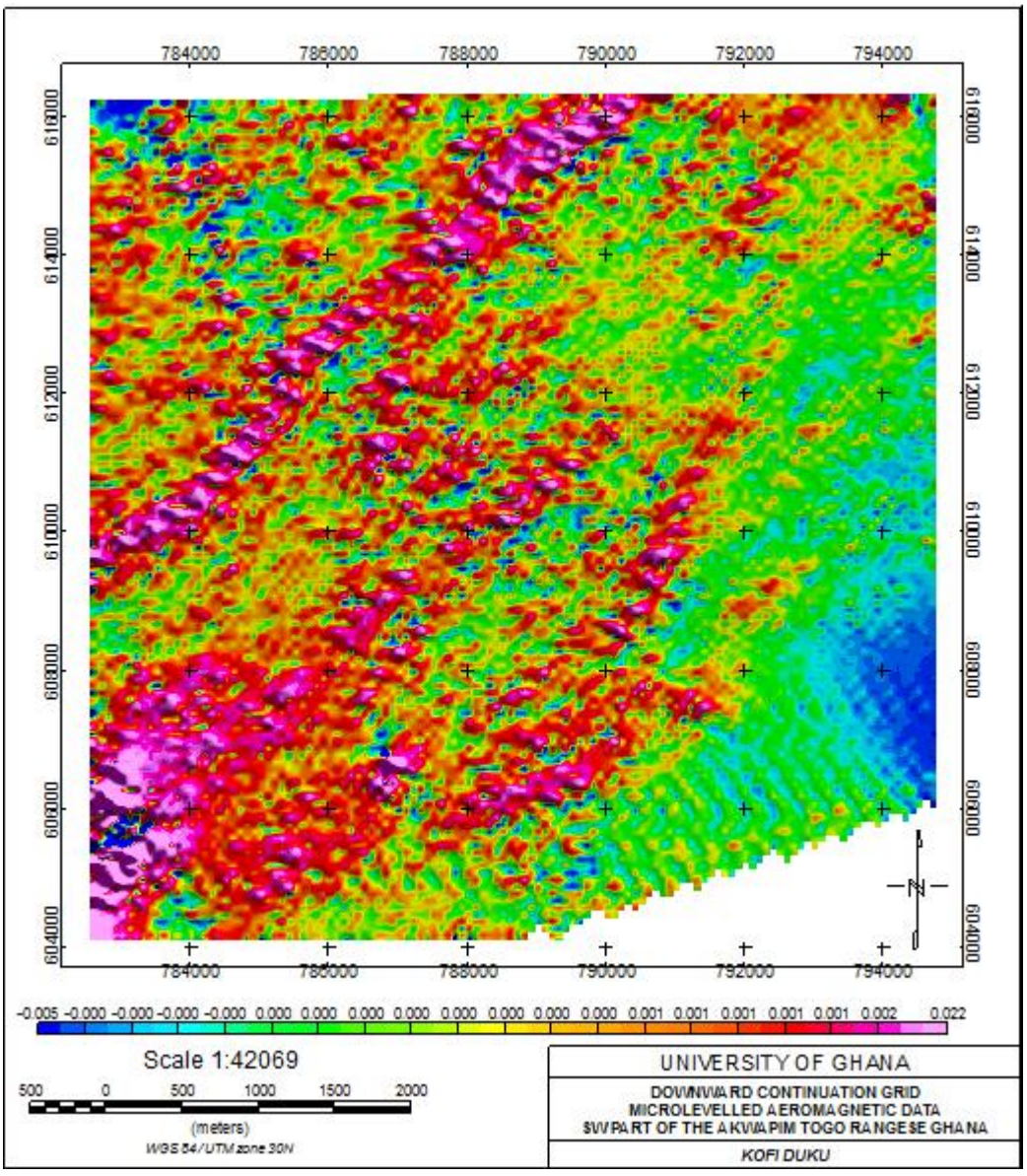

Figure 16: Downward Continuation grid of the total magnetic intensity (TMI) data of the study area.

University of Ghana http://ugspace.ug.edu.gh

It smoothens the low frequency anomalies relative to high frequency anomalies thus suppressing the effect of deep seated anomalies. The grid produced (Figure 16) confirms that the northeast-southwest trending features observed source from deep below the subsurface. Other prominent features showing northwest-southeast trends as well as east-west trends are seen scattered in the map.

4.1.6 Upward Continuation Filter

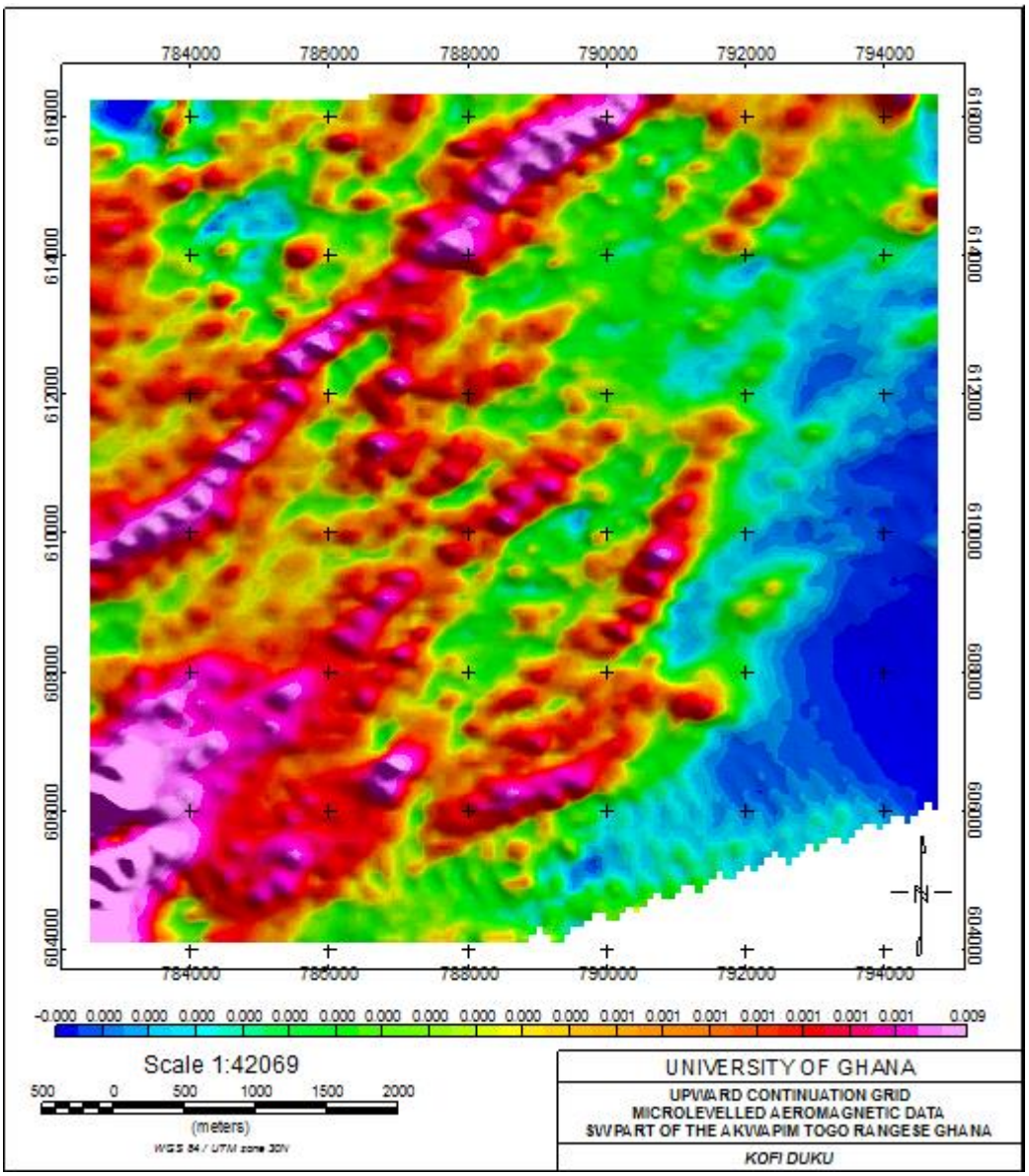

Figure 17: Upward Continuation grid of the total magnetic intensity (TMI) data of the study area.

University of Ghana http://ugspace.ug.edu.gh

The upward continuation filter is used to remove the effects of shallow sources or noise. This is done by moving the plane of measurement closer to the source thus suppressing the effects of shallow anomaly sources. The process results in a grid as shown in Figure 17 which highlights the northeast-southwest trending features that are seen in the previous grids produced.

4.1.7 Inferred Fault/ Fracture Lines

From the grids produced using the downward continuation filter (Figure 16) and the upward continuation filter (Figure 17), it can be deduced that the northeast-southwest trending features as well as the other prominent features in the grids showing slight deviations from the northeast-southwest directions are anomalies which have to be investigated on the ground.

The first vertical derivative filter shows the trends of the structural features as well as buried objects or artefacts that are within a depth of 0 to about 50 meters within the earth (Milligan and Gunn, 1997). These highlighted features as shown in Figure 18 are labelled as “inferred fault/fracture lines” on which the ground geophysical survey and the geological field mapping are carried on within the study area. The inferred fault/ fracture lines have a general concordant trend with the Akwapim-Togo range. The lines are mostly in close proximity with the areas with closely packed contours representing the highlands.

University of Ghana http://ugspace.ug.edu.gh

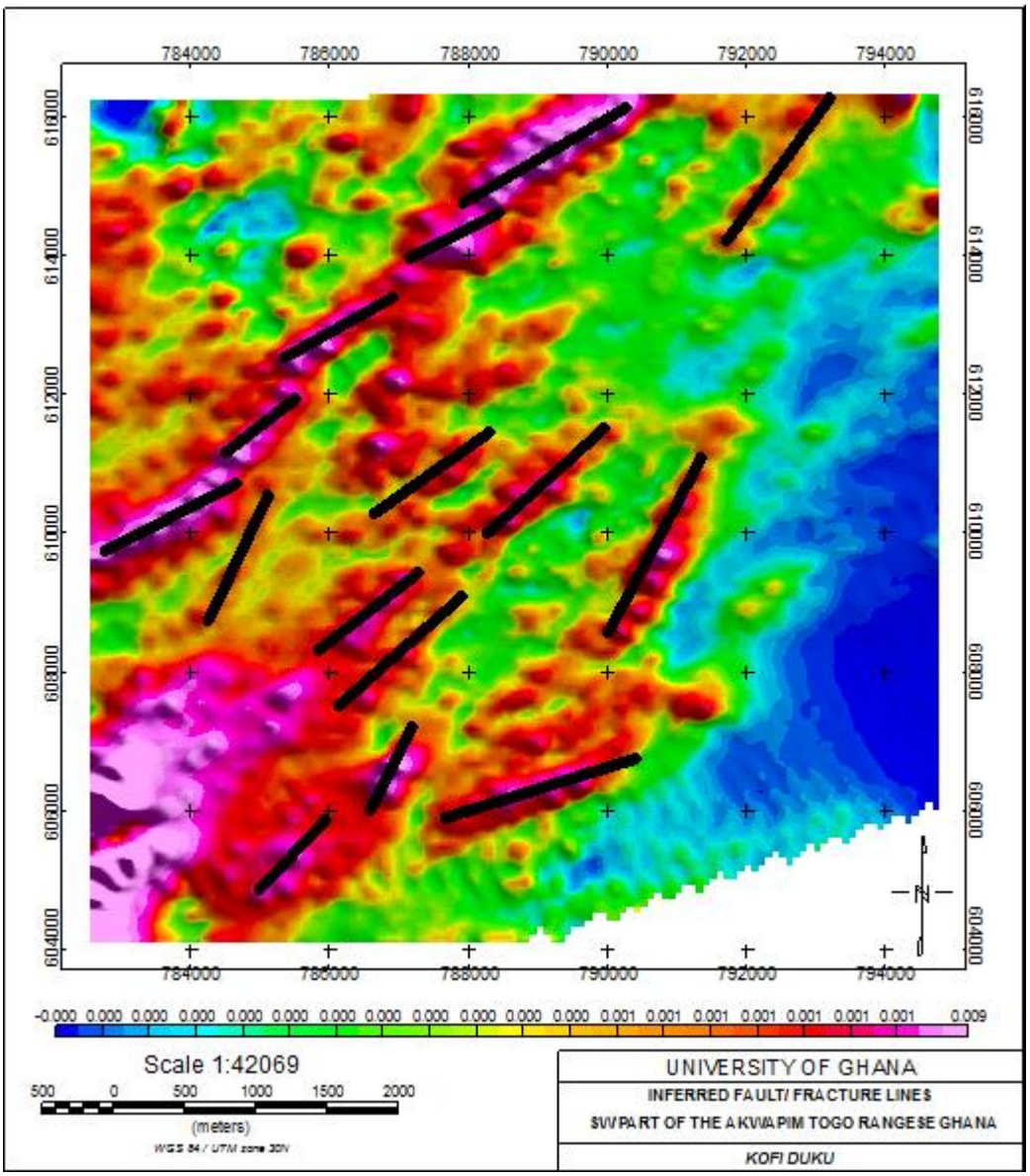

Figure 18: A grid of the aeromagnetic data of the area showing traces of possible fault/ fracture lines in the area

University of Ghana http://ugspace.ug.edu.gh

4.2 Radiometric Data

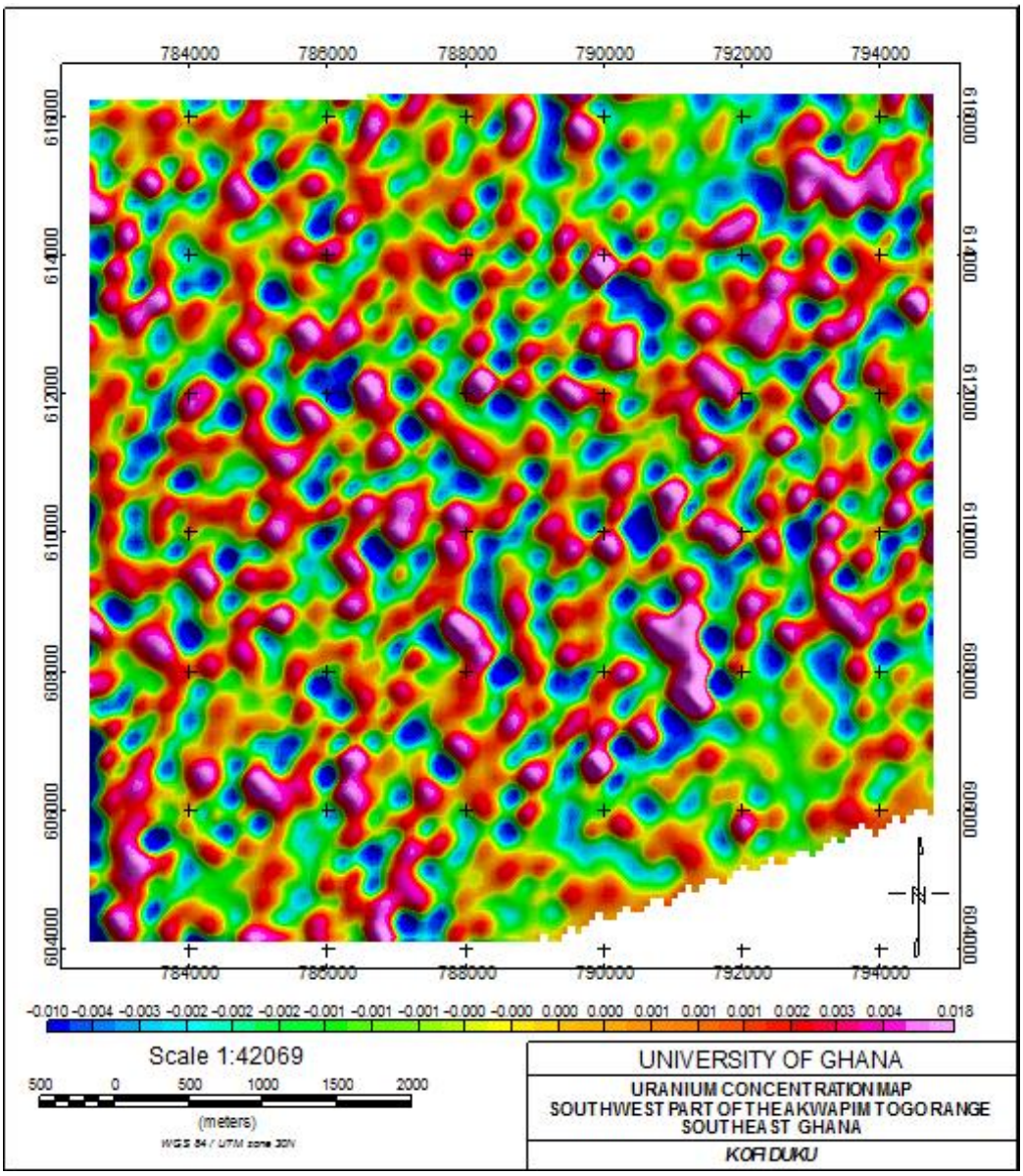

Figure 19: Uranium concentration map of the study area.

Radioactive gases occur within the earth. The occurrence of any break in continuity of the underlying rock bodies result in the occurrence of the radioactive gases being present at the earth surface as the gases tend to go through the pore spaces and the airspaces within the soil (Nsiah-Akoto et al., 2013). The radiometric data used of the data processing gives a measurement of the various concentrations of uranium within the study area. The grids

University of Ghana http://ugspace.ug.edu.gh

produced from the data show the occurrence of high amounts of uranium scattered within the area. Uranium occurrence is directly proportional to radon occurrence since the decay of uranium results in the formation of radon (Nsiah-Akoto et al., 2013). From the grid (Figure 19), high concentrations of radon are expected in the area as there are high concentrations of uranium scattered within the area. The occurrence of radioactive gases is linked to the presence of faults and fractures within the earth due to the fact that the break in continuity of the rocks allows the formation of channels and paths through which these radioactive gases escape to the top of the soil profile and eventually in to the atmosphere. Asumadu-Sakyi et al., (2011) attribute the differences in soil radon concentration as well as uranium concentration to the differences in the underlying bedrock and geology of the area. They further indicate that high anomaly are likely to be due to gaps and fissures falling on covered fault lines in the crust since radon gas concentration is taken as proportional to the fracture opening. Large sized fault lines tend to act as channels for soil radon gas to the surface. Although no directional pattern can be deduced from the grid, it can be deduced that the high concentrations of the uranium measured in the area is an indication of the extent of the tectonic activity that has occurred in the area resulting in numerous fractures within the subsurface.

4.3 LITHOLOGICAL DISTRIBUTION

Within the study area, the major rock exposures are quartzites and phyllites. These are prominent on the hill close to the Weija Lake and extents to the environs of Tuba. From the geological structural measurements taken from the field, it is observed that the rocks in the study area have general northeast- southwest trend direction. The average dip of the foliation surfaces of the rocks in the area is 12^0 with a northeast dip-direction. The average dip for the joints in the area is 64^0 with a southeast dip-direction as shown in figure 21.

University of Ghana http://ugspace.ug.edu.gh

From the field measurements done, it is observed that there are at least five different joint sets in the quartzites and phyllites from which the structural measurements were taken. Along the beach from Langma to Nyanyano, outcrops of the quartzites (as shown in Figure 20) were observed but however they were complexly jointed and as such difficult to map.

Figure 20: An outcrop of the quartzites along the beach from Langma to Nyanyano showing multiple joints

4.3.1 Foliation

A total of 79 measurements were taken for the foliation planes in the quartzites that outcropped within the study area. The stereographic plots of the dips and dip direction (Figures 21 and 22) indicate a mean resultant direction of $017^0/197^0$ in the northeast-southwest direction. It shows that there are two main foliation directions for the quartzites and they are the northeast-southwest and the northwest-southeast directions. An equal area plot of the dip and dip direction values (Figures 23 and 24) show a mean resultant plot of 012^0 with a calculated girdle of 88/171. From this, it can be deduced that the dips of the foliation surfaces are averagely steep with a small variance between them.

University of Ghana http://ugspace.ug.edu.gh

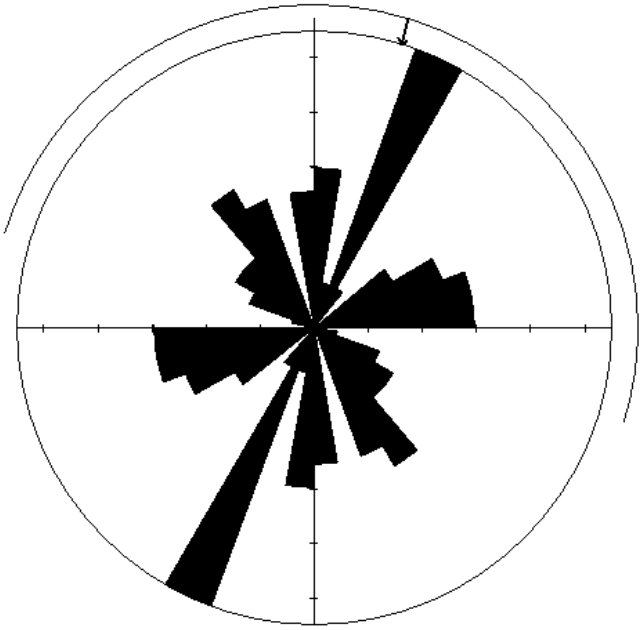

Axial (non-polar) data

No. of Data = 79

Sector angle = 10°

Scale: tick interval = 3% [2.4 data]

Maximum = 16.5% [13 data]

Mean Resultant direction = 017-197

[Approx. 95% Confidence interval = ±90.0°]

Figure 21: A stereographic plot to pole of the dips and dip direction of the foliation

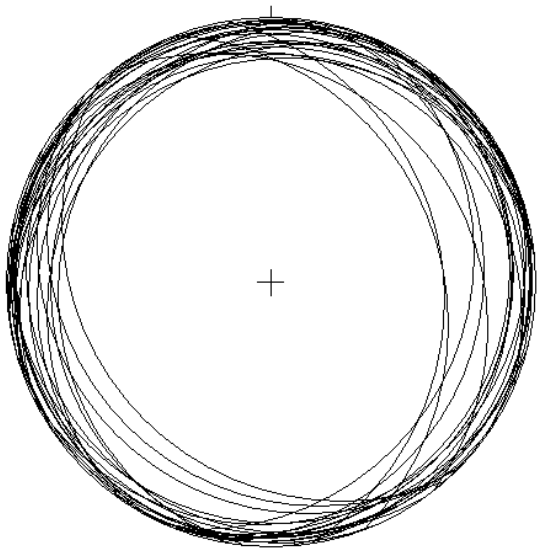

Axial (non-polar) data

No. of Data = 79

Sector angle = 10°

Scale: tick interval = 3% [2.4 data]

Maximum = 16.5% [13 data]

Mean Resultant direction = 017-197

[Approx. 95% Confidence interval = ±90.0°]

Figure 22: A stereographic plot of the dips and dip direction of the foliation in the quartzites.

University of Ghana http://ugspace.ug.edu.gh

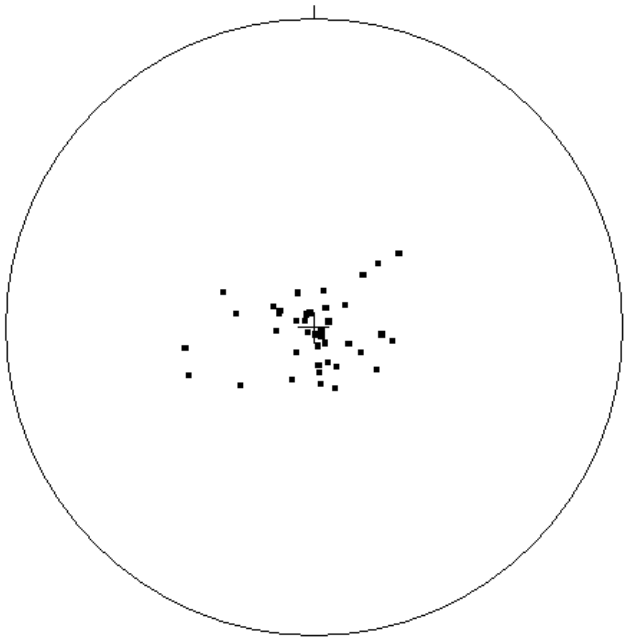

No. of Data = 79

Mean Principal Orientation = 3/012

Mean Resultant direction = 3-017

Mean Resultant length = 0.97

(Variance = 0.03)

Calculated girdle: 88/171

Figure 23: An equal area plot of the dips and dip directions of the foliations in the quartzites.

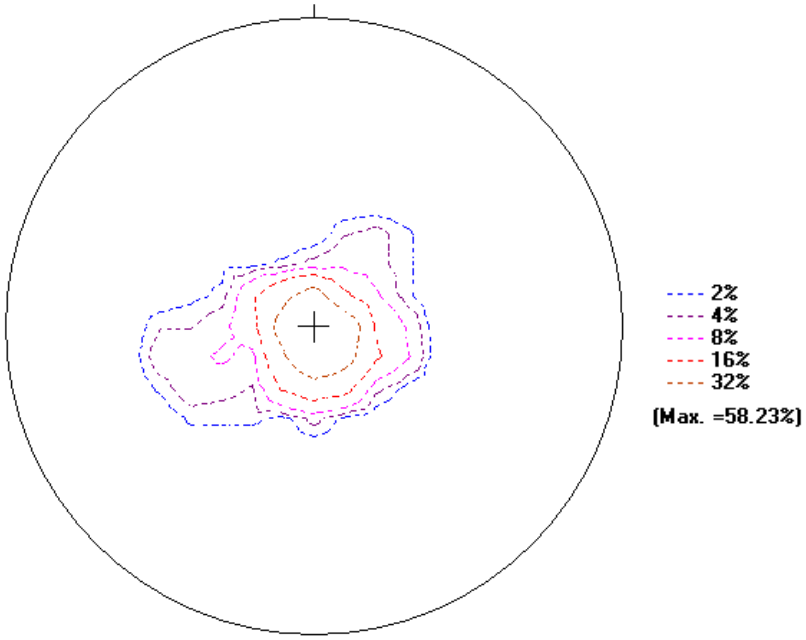

Figure 24: A contour plot of the dips and dip directions of the foliation of the quartzites.

University of Ghana http://ugspace.ug.edu.gh

4.3.2 Joints

A total of 150 measurements were taken for the joint planes in the quartzites and phyllites that outcropped within the study area as a result of the limited number of outcrop exposures. The rose diagram plots of the dips and dip direction (Figure 25) indicate a mean resultant direction of $017^0/197^0$ in the NE - SW direction. An equal area plot of the dip and dip direction values (as shown in Figure 25 and 26) show a mean resultant plot of 012^0 with a calculated girdle of 88/171. The mean resultant length of the plot is 0.97 with a variance of 0.03. This indicates that there are two major joints (master joints) occurring in the area alongside a number of minor joint sets. The two major joints are in the northeast-southwest and the northwest-southeast directions. The minor joint sets are in the north-south and the east-west directions.

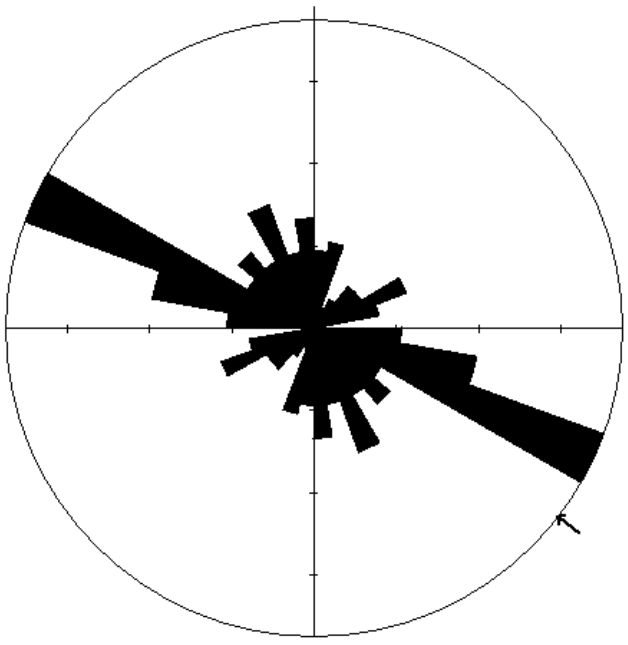

Axial (non-polar) data

No. of Data = 150

Sector angle = 10°

Scale: tick interval = 5% [7.5 data]

Maximum = 18.7% [28 data]

Mean Resultant Direction = 128-308

[Approx. 95% Confidence interval = ±25.0°]

(Valid only for unimodal data)

Figure 25: A rose plot of the dips and dip directions of the joints of the quartzites

University of Ghana http://ugspace.ug.edu.gh

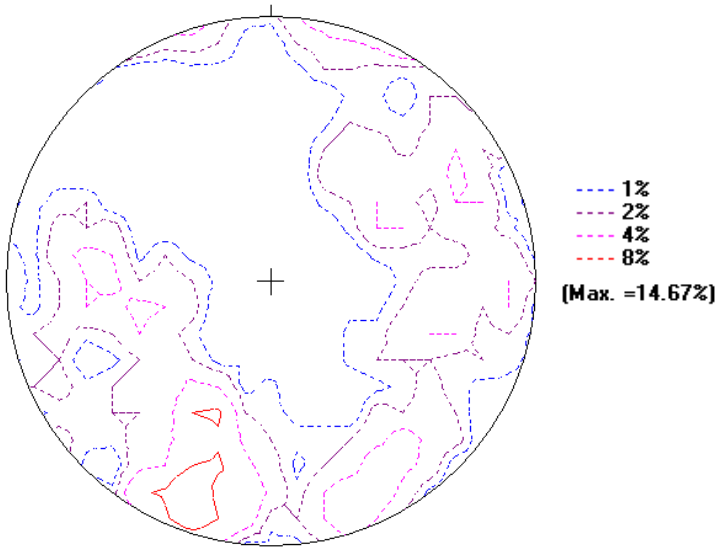

Figure 26: A contour plot of the dips and dip directions of the joints of the quartzites

4.4 GROUND GEOPHYSICAL SURVEY

A total of 15 survey points (KP1 to KP15) were covered in the study area as a result of heavy anthropogenic activities limiting the number of good survey points in the study area. For the geophysical survey, an average plain ground space of about 96 m^2 was required. This proved difficult to find because of the cluster of residential properties, farms and some commercial properties. The most common available spaces were undeveloped lands, school sports-fields and community meeting grounds/ parks that host social events held in the communities. However, the points surveyed are considered representative of the area and are evenly spread to cover the entire area.

University of Ghana http://ugspace.ug.edu.gh

4.4.1 Square Array Method

Three sets of data were collected from the square array survey. They are the two perpendicular readings; Alpha and Beta readings, and the diagonal readings; the gamma readings (as indicated in figure 8). The diagonal readings (gamma readings) serve as a check on the anisotropy of the ground (Habberjam and Watkins, 1967). A mean of the two perpendicular readings was calculated using:

$$\rho_m = \sqrt{(\rho_\alpha)(\rho_\beta)} \qquad (14)$$

The mean resistivity values from the various points ranged between 1 - 100 Ω.m except for the survey points close to the sea that recorded very high apparent resistivity values close to 1000 Ω.m.

For this study, the square array readings were taken in two orientations. The first orientation or position was done so that one side of the square lay parallel to the regional strike of the rocks in the area (between 30° to 40° northeast). The 30° regional strike is used for simplicity in ground positioning. The square configuration is rotated through a 45° clockwise angle to obtain the second square orientation. The second position is oriented to face the angles between 75° to 85° in the northeast direction. Table 2 is used to compare the data for both orientations to check for any significant differences.

Apparent resistivity measurements taken at point KP3 (table 2) indicate slight differences between α, β and γ readings for both positions. The apparent resistivity is relatively low for shallow depths but increases slightly with increase in the electrode spacing up to the 12 meter spacing and then drops toward the 67 meter spacing. The γ readings that serve as a check for the anisotropy of the subsurface are relatively low at shallow depths.

University of Ghana http://ugspace.ug.edu.gh

Table 2: Apparent resistivity measurements at point KP3

ELECTRODE SPACING (m)	α1	α2	β1	β2	γ1	γ2	γ1/γ2	ρm1	ρm2
3	4.48	3.89	3.99	4.50	0.49	0.75	0.65	4.23	4.18
4.3	4.73	4.03	4.72	4.03	0.16	0.47	0.34	4.72	4.03
6	5.04	4.88	5.12	4.70	0.40	0.80	0.49	5.08	4.79
8.5	4.91	6.51	6.28	5.62	0.95	0.93	1.03	5.55	6.05
12	7.64	7.91	9.49	6.88	1.56	2.44	0.64	8.52	7.38
17	6.83	11.30	10.62	10.91	0.34	1.26	0.27	8.52	11.10
24	5.83	4.30	11.50	9.05	0.14	1.39	0.10	8.19	6.24
34	2.11	4.74	8.38	8.67	0.14	4.38	0.03	4.20	6.41
48	1.70	4.94	5.35	15.54	1.26	2.03	0.62	3.01	8.76
67	2.80	6.76	6.10	23.72	2.18	4.77	0.46	4.14	12.67

Where: 1 = first position and
2 = second position
Apparent resistivity measurements are in **Ω**.m.

At the 12, 34 and 67 meter electrode spacing, high anisotropy is observed and this can be attributed to heterogeneity at the depths corresponding to those electrode spacing. The readings taken for the second position (45° rotation) are slightly higher than that of the first position although the differences are considered not too significant. Neighboring points KP1 and KP2 (appendix 2a) show similar trends although the datasets are different from the measurements from KP3.

Relatively high values for γ were recorded at the point KP5 (table 3). This indicates high anisotropy within the subsurface at this point as the γ readings taken are mostly above 1 **Ω**.m. The apparent resistivity for α and β readings varied significantly at the various electrode spacings. The apparent resistivity readings (α and β) for the first position tends to reduce with increasing electrode spacing whereas α and β values for the second position fluctuates with increasing electrode spacing.

The ratio of the γ measurements for both positions are generally less than one thus indicating high variation in the anisotropy measured in both positions. The datasets from

University of Ghana http://ugspace.ug.edu.gh

point KP4 (appendix 2a) show similar trends in the anisotropy and apparent resistivity measurements just as point KP10 (appendix 2a) as compared to the trends of the data from KP5.

Table 3: Apparent resistivity measurements taken at point KP5

ELECTRODE SPACING	α1	α2	β1	β2	γ1	γ2	γ1/γ2	ρm1	ρm2
3	13.65	14.90	7.28	10.23	4.55	11.42	0.40	9.97	12.35
4.3	9.61	7.69	5.75	3.71	3.52	4.71	0.75	7.43	5.34
6	11.27	9.90	5.87	4.83	4.01	5.17	0.77	8.14	6.91
8.5	11.42	10.24	7.51	1.98	2.05	7.33	0.28	9.26	4.51
12	9.10	15.81	6.46	4.29	0.44	5.57	0.08	7.67	8.24
17	6.16	19.13	4.03	3.08	0.46	2.52	0.18	4.98	7.68
24	4.09	23.27	3.62	4.75	0.11	1.05	0.11	3.85	10.51
34	4.57	23.82	4.37	1.39	0.28	0.85	0.33	4.47	5.76
48	4.39	6.57	3.71	3.78	0.20	3.60	0.06	4.04	3.73
67	4.41	15.47	3.78	3.28	0.24	0.72	0.34	4.08	7.12
96	3.90	12.59	3.51	3.50	0.97	0.90	1.08	3.70	6.64

Where: 1 = first position and
2 = second position
Apparent resistivity measurements are in Ω.m.

Table 4 shows the apparent resistivity values obtained from pint KP6. Relatively high apparent resistivity measurements are recorded at this station as compared to the data from points KP3 and KP5. The degree of anisotropy decreases with increasing electrode spacing while α and β values for both positions decrease with increasing electrode spacing as well. Significant differences are seen in the α and β for both positions with the α and β values in the position being relatively greater than the values for the first position. Point KP15 showed similar values and trends although the differences in the readings for both positions are minimal.

University of Ghana http://ugspace.ug.edu.gh

Table 4: Apparent resistivity measurements taken at point KP6

ELECTRODE SPACING	α1	α2	β1	β2	γ1	γ2	γ1/γ2	ρm1	ρm2
3	16.23	21.66	19.77	13.03	1.33	9.19	0.14	17.91	16.80
4.3	11.71	11.14	10.40	9.80	1.30	1.89	0.69	11.04	10.45
6	12.94	10.49	11.22	7.65	1.64	0.91	1.79	12.05	8.96
8.5	14.55	1.37	13.79	7.42	0.75	0.78	0.95	14.16	3.19
12	6.52	15.45	7.06	6.38	0.41	0.63	0.65	6.79	9.93
17	6.23	21.85	3.55	4.17	0.26	0.43	0.61	4.70	9.55
24	6.56	25.04	3.66	5.55	0.63	0.53	1.17	4.90	11.79
34	6.65	28.35	1.64	1.67	0.52	1.42	0.37	3.30	6.87
48	2.48	35.67	6.54	2.08	0.78	0.35	2.22	4.02	8.60
67	5.12	36.37	1.64	1.51	0.25	0.34	0.74	2.89	7.42
96	2.63	25.27	9.18	2.59	0.23	0.47	0.48	4.91	8.09
136	1.52	6.17	0.75	1.49	0.34	0.16	2.13	1.07	3.03

Where: 1 = first position and
2 = second position
Apparent resistivity measurements are in Ω.m.

Table 5: Apparent resistivity measurements from point KP7

ELECTRODE SPACING	α1	α2	β1	β2	γ1	γ2	γ1/γ2	ρm1	ρm2
3	2.25	3.18	5.06	3.58	2.54	0.35	7.22	3.37	3.37
4.3	2.67	3.66	5.36	3.73	2.97	0.16	18.94	3.79	3.70
6	3.00	4.16	5.36	4.56	2.51	0.28	8.98	4.01	4.35
8.5	3.58	5.28	5.54	4.56	3.91	0.14	27.74	4.45	4.91
12	3.33	5.24	8.09	5.74	4.14	0.32	12.92	5.19	5.48
17	4.44	7.54	9.76	6.36	5.58	0.01	398.86	6.58	6.92
24	5.45	7.94	11.69	9.72	5.59	0.68	8.18	7.98	8.79
34	8.66	11.15	15.73	9.80	9.11	1.66	5.50	11.67	10.46
48	9.19	14.99	21.40	17.97	12.37	2.07	5.97	14.02	16.41
67	12.15	16.65	27.79	22.33	17.97	2.04	8.81	18.38	19.28

Where: 1 = first position and
2 = second position
Apparent resistivity measurements are in Ω.m.

Relatively very low γ values were recorded for the second position at point KP7 (shown in Table 5) as compared to the values for the first position. Significant variation were seen in both the α and β values for both positions as well as in the γ values as indicated by the γ ratio for the first and second positions. Very low anisotropy is observed from the γ

University of Ghana http://ugspace.ug.edu.gh

readings in the second position and as such it can be deduced that the subsurface at this point is relatively homogenous. Appendix 2a shows the data sets for the points KP9 and KP12 which give similar trends to the data from KP7.

The degree of anisotropy deduced from the γ values recorded at point KP8 is relatively low for the first position than in the second position (45° rotation). Although the mean apparent resistivities for both positions are (Table 6) are close for some electrode spacing, others showed a large variation. The measured apparent resistivity (α and β) increases with increasing electrode spacing corresponding to higher depths similar to the data from point KP13 (Appendix 2a).

Table 6: Apparent resistivity measurements at point KP8

ELECTRODE SPACING	α1	α2	β1	β2	γ1	γ2	γ1/γ2	ρm1	ρm2
3	5.01	4.30	5.58	6.11	0.55	1.46	0.38	5.29	5.13
4.3	5.00	4.82	4.71	4.83	0.80	0.51	1.56	4.85	4.83
6	4.83	4.78	6.13	5.34	0.96	0.07	14.39	5.44	5.05
8.5	5.70	4.35	6.71	4.95	0.69	0.37	1.86	6.19	4.64
12	4.36	5.50	8.06	7.96	0.29	1.32	0.22	5.93	6.62
17	8.41	7.79	9.93	9.10	0.77	1.56	0.50	9.14	8.42
24	10.77	11.05	12.55	13.58	0.81	3.31	0.24	11.63	12.25
34	14.72	15.67	14.31	14.23	0.90	9.42	0.10	14.51	14.93
48	29.66	16.86	23.96	20.26	3.26	6.20	0.53	26.66	18.48
67	28.52	24.10	26.74	19.10	7.44	7.14	1.04	27.62	21.45
96	43.83	29.36	25.90	22.60	2.47	13.09	0.19	33.69	25.76

Where: 1 = first position and
2 = second position
Apparent resistivity measurements are in **Ω**.m.

University of Ghana http://ugspace.ug.edu.gh

Table 7: Apparent resistivity values taken at point KP11

ELECTRODE SPACING (m)	α1	α2	β1	β2	γ1	γ2	γ1/γ2	ρm1	ρm2
3	313.20	464.10	484.40	272.00	91.01	209.10	0.44	389.50	355.30
4.3	183.70	198.10	203.50	130.60	16.66	68.15	0.24	193.35	160.85
6	41.69	69.87	78.51	31.77	37.45	37.37	1.00	57.21	47.11
8.5	7.77	17.70	21.40	8.60	12.45	9.74	1.28	12.89	12.33
12	1.61	4.24	3.96	3.30	2.14	2.12	1.01	2.53	3.74
17	3.31	2.18	2.51	2.37	0.46	1.53	0.30	2.88	2.27
24	0.96	4.34	1.66	5.57	0.61	6.05	0.10	1.27	4.91
34	3.92	3.61	2.65	3.56	1.10	0.81	1.36	3.22	3.58
48	2.64	3.43	3.71	6.07	2.05	0.95	2.16	3.13	4.57
67	3.33	9.60	6.09	12.21	4.42	0.23	19.06	4.50	10.83

Where: 1 = first position and
2 = second position
Apparent resistivity measurements are in Ω.m

At the point KP11, located at the Kokrobite beach, the tabulated values of the apparent resistivity measures (Table 7) shows the sharp drop of the values for both α and β as well as with increasing apparent resistivity increasing with increasing electrode spacing for both the first and second position as shown in Figure 8. The gamma plot gives a similar trend indicating a decrease in anisotropy with increasing electrode spacing. Comparing the trend of the values with the corresponding depths of the current electrode spacing show that the effect of the loose sand at the top of the overburden highly affects the resistivity values measured at this point. The data obtained shows that the subsurface at this point is anisotropic just as the other points where the ground geophysical survey was done.

4.4.2 Schlumberger Sounding

The objective of the vertical electrode sounding (VES) is to deduce the variation of resistivity with depth below a given point on the ground surface and to correlate it with the available geological data to infer the depths and resistivities of the layers present. For this

University of Ghana http://ugspace.ug.edu.gh

survey the potential electrode spacing is 1 meter ($^{MN}/_{2} = 0.5\ m$). For the sounding, AB >MN, where AB is the current electrode spacing and MN is the potential electrode spacing.

Three VES surveys were carried out at each point with the first sounding done exactly on the general survey point while the other two are done 10 meters north and south of the first survey point and labeled "a" and "b" respectively. The data from the three sounding points were integrated to generate a pseudo-section.

A four-layer model of the subsurface was inferred from the data from point KP3. The models from the three points generally show relatively high apparent resistivity values at for the first layer and then a significant drop in magnitude in the second and third layer. The fourth layer in all three models show very high apparent resistivity values which can be attributed to the bedrock. The VES curves (Figures 27, 28 and 29) show a drop in apparent resistivity for the three sounding points at KP3 up to the current electrode spacing of 2.5m from which it tends to rise steeply. The curves types shown by the VES curves for the apparent resistivity data from all three points (KP3, KP3a and KP3b) is the "HA" curve since the apparent resistivity for the first layer of the four-layer model generated is greater than the apparent resistivity of the second layer which is less than that of the third with the third layer being of a lower apparent resistivity than the fourth layer ($\rho 1 > \rho 2 < \rho 3 < \rho 4$). The average depth to the bedrock given by the three curves is 1.24 meters.

The sounding done 10 meters north of the point KP3 (KP3a) also gives a three-layer model with a depth to bedrock of 1.25 meters. The depth to bedrock given by the curve for survey point KP3b also gives a three-layer model with a depth to bedrock of 1.25 meters. The pseudo-section of the data from the three points KP3a, KP3 and KP3b (Figure 30) indicates a thin layer of relatively average apparent resistivity at the top of the section followed by a drop to very low apparent resistivity with increasing depth. The changes in the electrical

University of Ghana http://ugspace.ug.edu.gh

properties of the subsurface rocks remain uniform for all three points making up the pseudo-section. The transition from the low apparent resistivity to high apparent resistivity is gradual as shown in Figure 30.

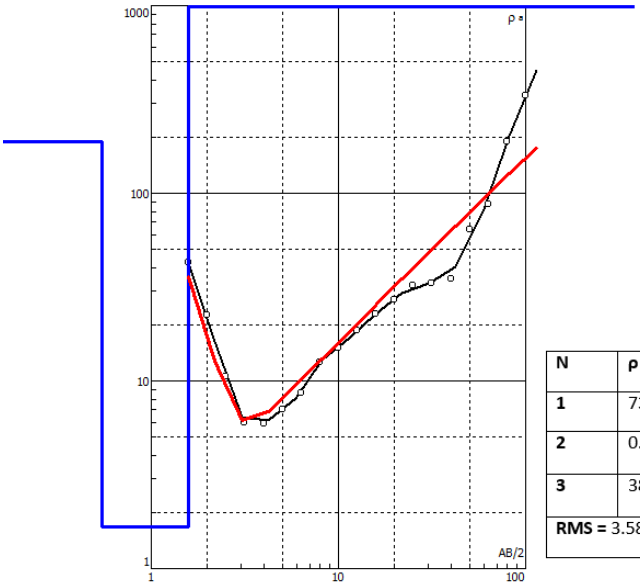

N	ρ (Ohm.m)	H (meters)	d (meters)	Altitude (meters)
1	73.6	0.79	0.79	-0.79
2	0.685	0.44	1.23	-1.23
3	3854			
RMS = 3.58%				

Figure 27: VES curve of schlumberger sounding data from Survey Point KP3

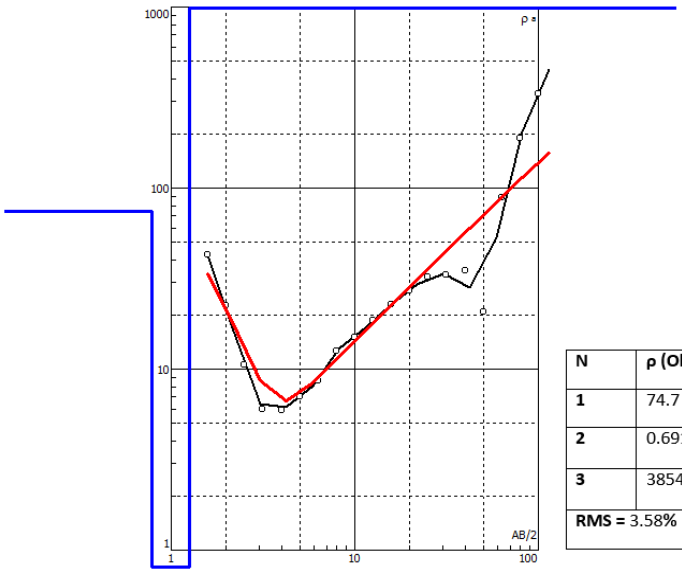

N	ρ (Ohm.m)	H (meters)	d (meters)	Altitude (meters)
1	74.7	0.79	0.79	-0.79
2	0.691	0.475	1.26	-1.26
3	3854			
RMS = 3.58%				

Figure 28: VES curve of Schlumberger data taken at point KP3a, 10 meters north of point KP3

University of Ghana http://ugspace.ug.edu.gh

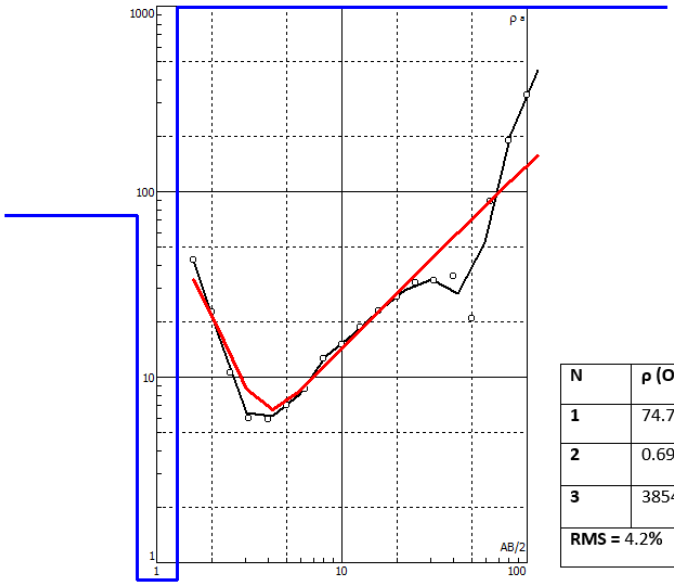

N	ρ (Ohm.m)	H (meters)	d (meters)	Altitude (meters)
1	74.7	0.79	0.79	-0.79
2	0.691	0.475	1.26	-1.265
3	3854			
RMS = 4.2%				

Figure 29: VES curve of Schlumberger data taken at point KP3b, 10 meters south of survey point KP3

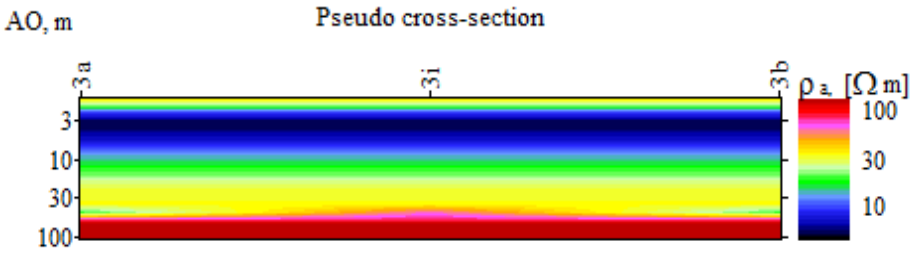

Figure 30: Pseudo-section of points KP3a, KP3 and KP3b

The relatively high apparent resistivity at the top of the section can be attributed to compaction of the ground through anthropogenic activities. The trends in the VES curves for the measured apparent resistivity values at point KP3 are similar to the trends seen in the VES curves and the pseudo-sections generated from the data from points KP1 and KP2 (Appendix 2b). A thin layer of averagely low apparent resistivity overlies the region of relatively low apparent resistivity in the pseudo-section (Figure 30) that is generated from the integration of the data from the three sounding points at KP3. The apparent resistivity gradually rises from the middle of the section to the bottoms.

University of Ghana http://ugspace.ug.edu.gh

Data from point KP5 along with point KP5a (10 m north) and KP5b (10 m south) all produced three-layer subsurface models. The VES curve produced from the data from point KP5 gives a curve that shows a steep drop till about the 7.94 m current electrode spacing before it starts to rise sharply (Figure 31). Similar plots (shown in the appendix 2a) are obtained for the survey points KP4, KP10 and KP14. The average depth to bedrock given by the three VES curves is 9.76 m. The VES curve for point KP5a and KP5b (Figures 32 and 33) showed similar trends to the curve for point KP5 with the depths to bedrock given as 12.1, 9.65 and 7.53 m respectively. All three curves showed a drop in the apparent resistivity values from the start of the sounding up to the 6.3 m current electrode expansion after which it starts to rise up to the end of the expansion (100 m current electrode spacing). The curve type formed by the data from each of the three points at this location is the "H" type curve as the apparent resistivity for the first layer is greater than the apparent resistivity for the second layer which is also less that the apparent resistivity for the third layer ($\rho 1 > \rho 2 < \rho 3$).

The pseudo-section (Figure 34) generated from the data from the three sounding points shows the occurrence of relatively high apparent resistivity which drops gradually from the top of the section to relatively low apparent resistivity in the middle of the section. There is a rise in the apparent resistivity from the middle of the section towards the bottom. A distinct column of low apparent resistivity is seen to be sandwiched between high apparent resistivity in the pseudo-section.

University of Ghana http://ugspace.ug.edu.gh

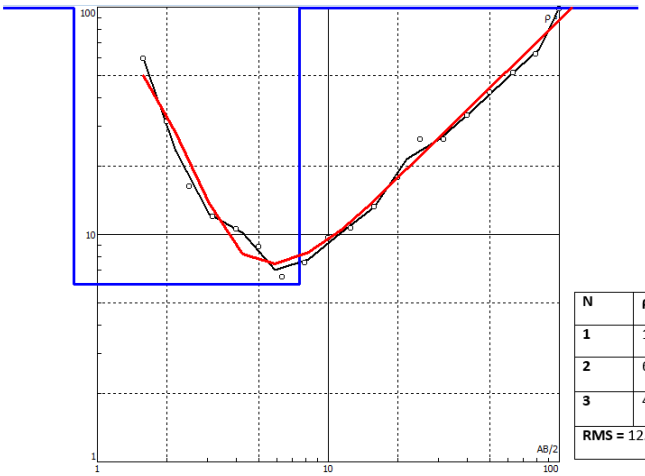

N	ρ (Ohm.m)	H (meters)	d (meters)	Altitude (meters)
1	104	0.79	0.79	-0.79
2	6.04	6.74	7.53	-7.53
3	4731			
RMS = 12.8%				

Figure 31: VES curve of the Schlumberger sounding data taken from survey point KP5

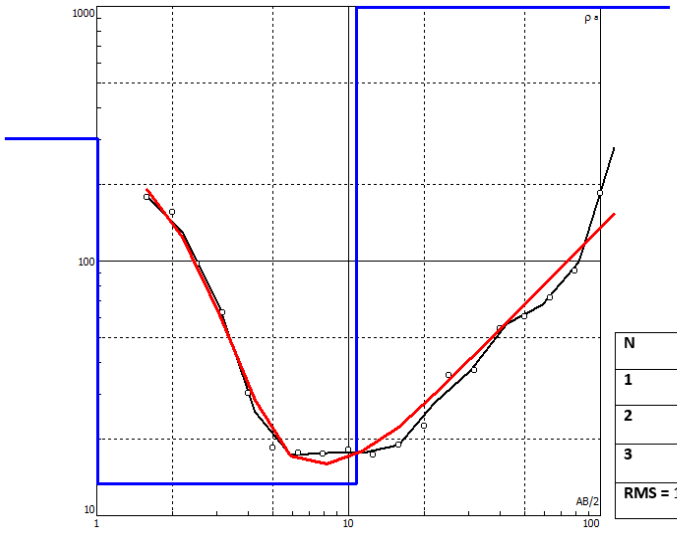

N	ρ (Ohm.m)	H (meters)	d (meters)	Altitude (meters)
1	302	1.01	1.01	-1.01
2	13.3	9.76	10.8	-10.77
3	16068			
RMS = 12.8%				

Figure 32: VES curve of Schlumberger data taken at point KP5a, 10 meters north of survey point KP5

University of Ghana http://ugspace.ug.edu.gh

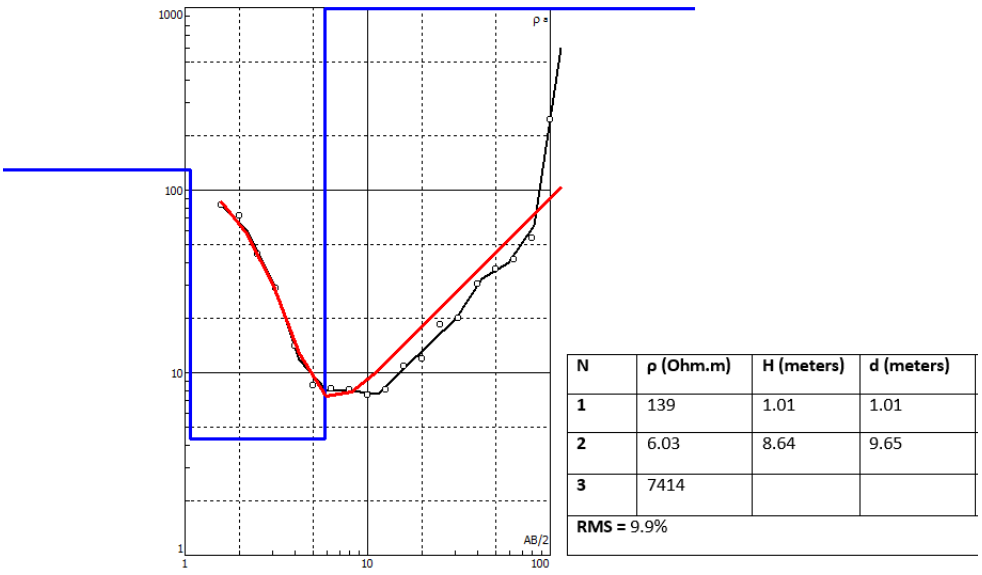

N	ρ (Ohm.m)	H (meters)	d (meters)
1	139	1.01	1.01
2	6.03	8.64	9.65
3	7414		

RMS = 9.9%

Figure 33: VES curve of Schlumberger data taken at point KP5b, 10 meters south of survey point KP5

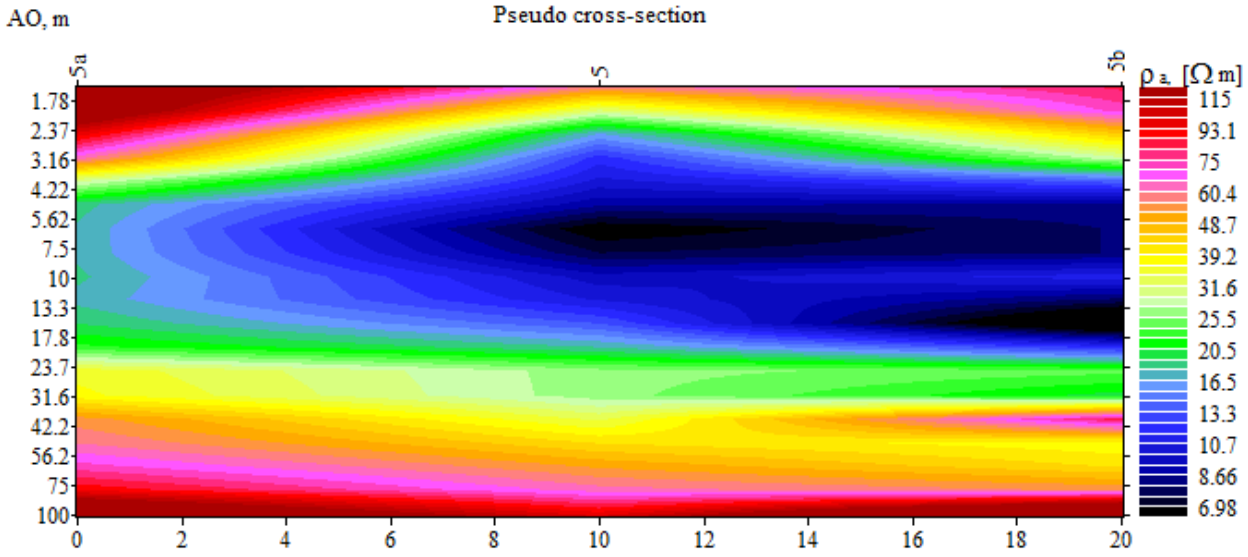

Figure 34: Pseudo section of points KP5a, KP5 and KP5b

The occurrence of relatively high apparent resistivity at the top part of the section is likely to due to the competent or well compacted top layers of the soil. The drop in high apparent resistivity from the top of the section to the low resistivity in the middle of the section is

University of Ghana http://ugspace.ug.edu.gh

gradual while the rise in apparent resistivity from the low apparent to relatively high apparent resistivity regions is more gradual.

The VES curve obtained from the data taken at point KP6 also produced a three layered subsurface models just like the points KP6a (10 meters north) and KP6b (10 meters south). The depths to the bedrock for the points KP6, KP6a and KP6b are 2.44 m, 3.81 m and 1.48 m (Figures 35, 36 and 37). The sounding curves the three points drop from high apparent resistivity to low apparent resistivity up to the 7.94 m current electrode spacing. The pseudo-section produced from the data from the three points show a middle region of relatively low apparent resistivity bounded by a relatively high apparent resistivity as shown in figure 38. The curve types derived from the VES plots shown in Figures 35, 36 and 37 are “H”, “HA” and “H” respectively.

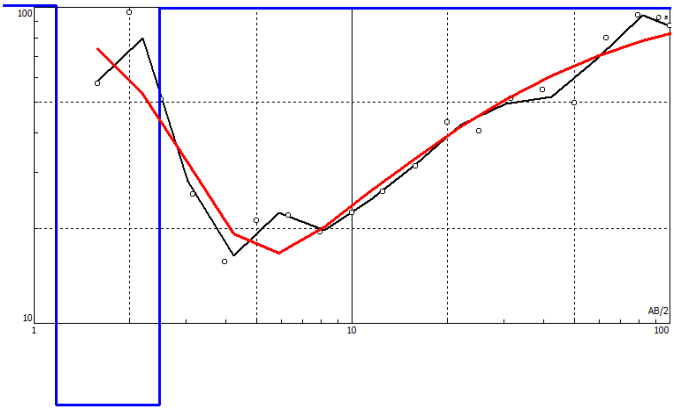

N	ρ (Ohm.m)	H (meters)	d (meters)	Altitude (meters)
1	102	1.17	1.17	-1.17
2	4.06	1.31	2.48	-2.48
3	100			
RMS = 20%				

Figure 35: VES curve of the Schlumberger sounding data taken from survey point KP6

University of Ghana http://ugspace.ug.edu.gh

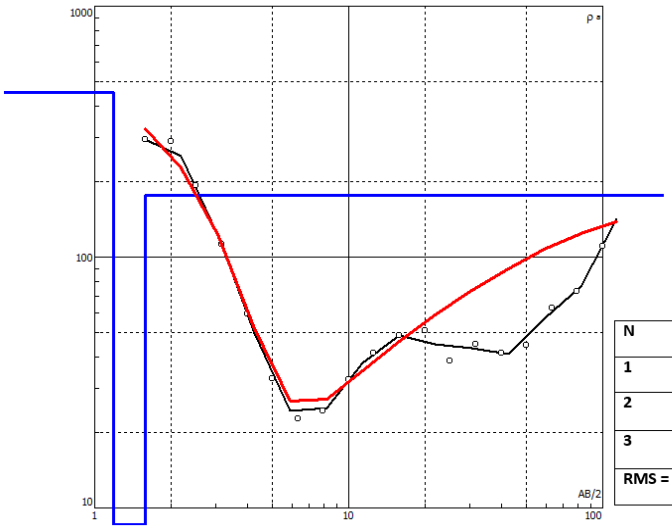

N	ρ (Ohm.m)	H (meters)	d (meters)	Altitude (meters)
1	454	1.19	1.19	-1.19
2	1.51	0.397	1.59	-1.59
3	177			
RMS = 19.8%				

Figure 36: VES curve of Schlumberger data taken at point KP6b, 10 meters north of survey point KP6

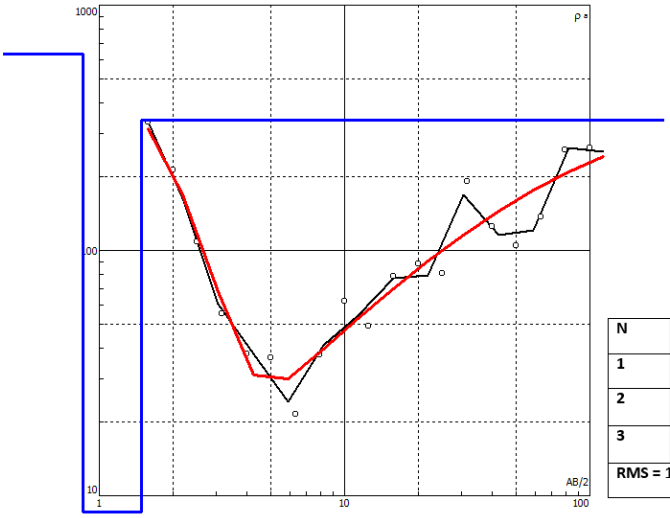

N	ρ (Ohm.m)	H (meters)	d (meters)	Altitude (meters)
1	633	0.856	0.856	-0.56
2	3.43	0.632	1.49	-1.49
3	339			
RMS = 19.3%				

Figure 37: VES curve of Schlumberger data taken at point KP6b, 10 meters south of survey point KP6

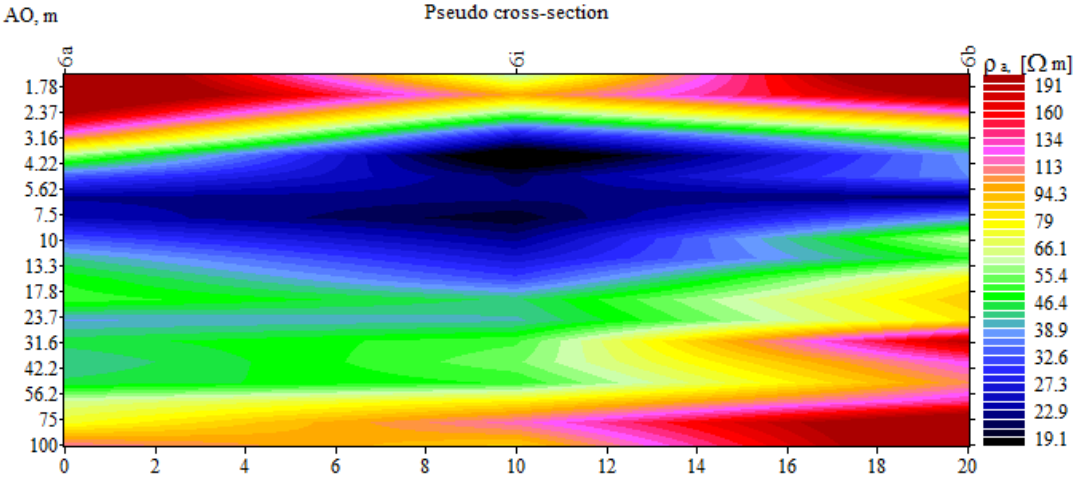

Figure 38: Pseudo section of points KP6a, KP6 and KP6b

University of Ghana http://ugspace.ug.edu.gh

The “H” curves are described by a high apparent resistivity in the first layer of the three layer model followed by a low apparent resistivity second layer and a third layer of high apparent resistivity (ρ1 > ρ2 <ρ3). The “HA” describes a four layer model with the first layer having a higher apparent resistivity than the second layer with the second layer having a lower apparent resistivity than the third layer and the fourth layer (ρ1 > ρ2 < ρ3< ρ4).

The relatively high apparent resistivity at the upper limits of the pseudo-section can be as a result of either high amount compaction thus reducing the amount of soil fluids present to conduct current. It can also be as a result of the presence of very loose overburden thus increasing the amount of airspaces occupied by air in the ground. The region of low resistivity thickens at the point KP6 while it thins out towards points KP6a and KP6b. the increase in apparent resistivity with increasing depth is gradual after the low apparent resistivity region. The VES plots for the three sounding points at KP15 (Appendix 2b) has similar trends to the curves from the KP6 soundings.

The three sounding points at KP7 produced distinct three layer subsurface model. The three curves for points KP7, KP7a and KP7b (figures 39, 40 and 41) illustrate a rise in the apparent resistivity with increasing electrode spacing. The depths to bedrock from the point KP7 is given as 18.6 m while the depth to bedrock of the points KP7a and P7b are 6.25 m and 34.7 m respectively. The VES curve for point KP7 is the “A” type whereas the cures for points KP7a and KP7b were the “K” and “A” type respectively. The “K” curve type are defined by a three-layer model with the first layer having a lower apparent resistivity value than the second layer which also has higher apparent resistivity value as compared to the third layer (ρ1<ρ2> ρ3). The “A” type curve is also describes a three-

University of Ghana http://ugspace.ug.edu.gh

layer earth model with the apparent resistivity of the first layer being lower than the second layer which is also lower than the third (ρ1< ρ2 < ρ3). The graduation from the low apparent resistivity from the top of the pseudo-section (Figure 42) into the high apparent resistivity at the bottom of the section is gradual with the low resistivity region thinning out towards the KP7b point. Comparatively, the VES curves for the apparent resistivity data recorded at KP7 shows similar trends to the VES curves for points KP9 and KP12 (Appendix 2b)

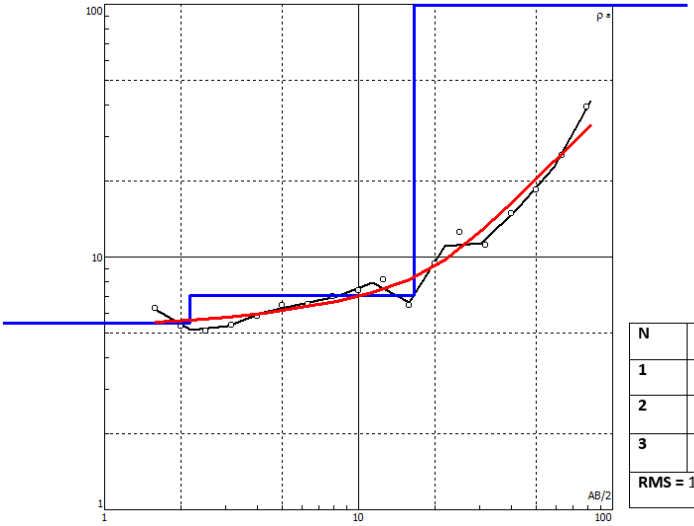

N	ρ (Ohm.m)	H (meters)	d (meters)	Altitude (meters)
1	5.49	2.16	2.16	-2.16
2	7.03	14.4	16.6	-16.56
3	2516			
RMS = 11.7%				

Figure 39: VES curve of the Schlumberger sounding data taken from survey point KP7

University of Ghana http://ugspace.ug.edu.gh

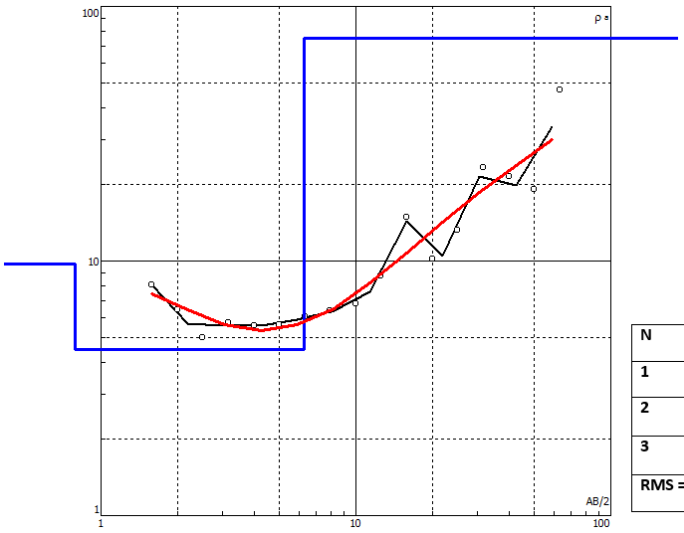

N	ρ (Ohm.m)	H (meters)	d (meters)	Altitude (meters)
1	9.77	0.79	0.79	-0.79
2	4.51	5.46	6.25	-6.25
3	75			
RMS = 11.7%				

Figure 40: VES curve of Schlumberger data taken at point KP7a, 10 meters north of survey point KP7

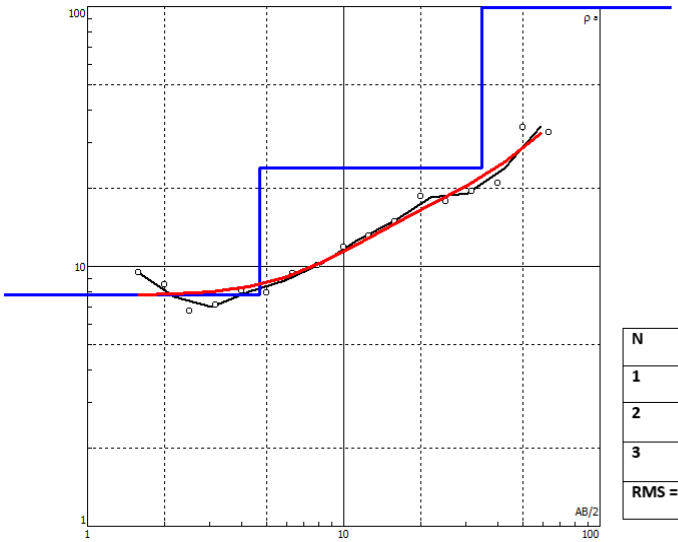

N	ρ (Ohm.m)	H (meters)	d (meters)	Altitude (meters)
1	7.76	4.7	4.7	-4.7
2	23.9	30	34.7	-34.7
3	3810			
RMS = 8.15%				

Figure 41: VES curve of Schlumberger data taken at point KP7b, 10 meters south of survey point KP7

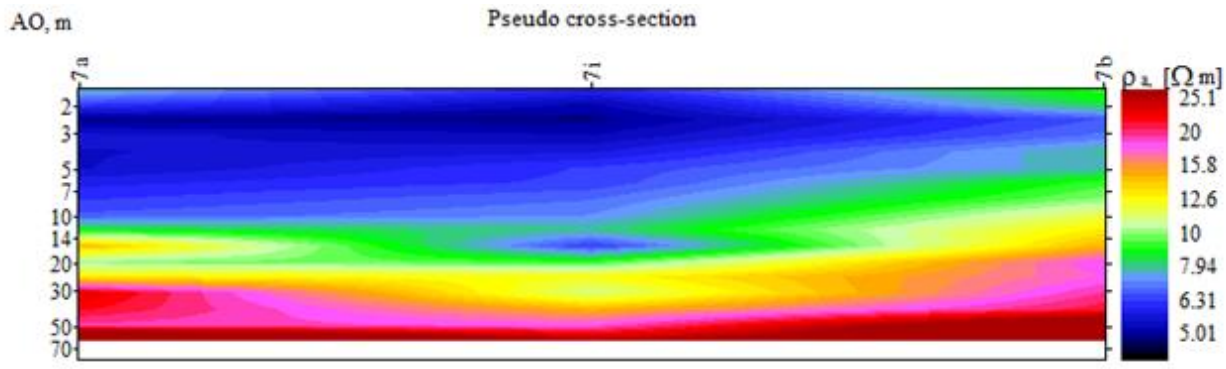

Figure 42: Pseudo section of points KP7a, KP7 and KP7b

University of Ghana http://ugspace.ug.edu.gh

All the schlumberger sounding done at the points KP8, KP8a and KP8b all produced three layer models of the earth subsurface from their VES curves. The VES curve for point KP8 (Figure 43) indicates a sharp drop in apparent resistivity from the starting electrode of the survey up to the 7.74 m current electrode spacing before it starts to rise sharply. Similar trends are seen in the curves for point KP8a and KP8b although the drop and rise in the curves for point KP8a and KP8b are much gentler (Figures 44 and 45 respectively). The depths to bedrock for point KP8 is given as 5.33 m while that of points KP8a and KP8b are 3.37 m and 7.03 m respectively. The pseudo-section generated (Figure 46) shows a portion of the top of the section having a relatively high apparent resistivity and the other portion being on the northern side (KP8a) and southern side (KP8b) having a very low apparent resistivity. The VES curves from the data at all three points at KP8 show the "H" type curve where the first layer of a three-layer model is of a higher apparent resistivity than the second layer which also has a lower apparent resistivity than the third layer ($\rho 1 > \rho 2 < \rho 3$). The relatively high apparent resistivity is attributed to anthropogenic activities leading to the compaction of the overburden. The survey point KP8a is closer to the sea whereas the point KP8b is close to a waterbody within the community thus explaining the low apparent resistivity values measures as shown in Figure 43. Similar plots are obtained for the survey point KP13.

University of Ghana http://ugspace.ug.edu.gh

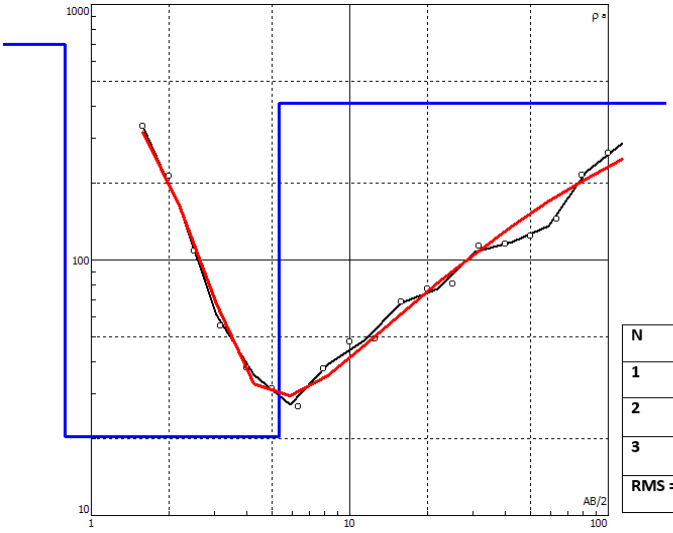

N	ρ (Ohm.m)	H (meters)	d (meters)	Altitude (meters)
1	695	0.79	0.79	-0.79
2	20.4	4.54	5.33	-5.3
3	411			
RMS = 10.3%				

Figure 43: VES curve of the Schlumberger sounding data taken from survey point KP8

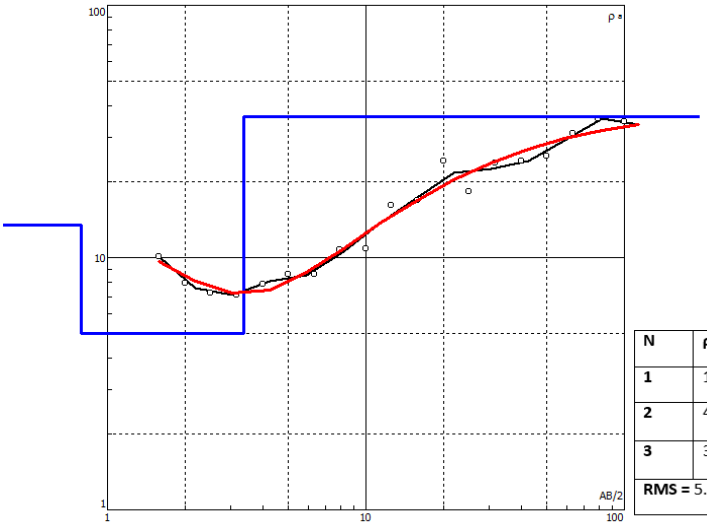

N	ρ (Ohm.m)	H (meters)	d (meters)	Altitude (meters)
1	13.4	0.79	0.79	-0.79
2	4.99	2.58	3.37	-3.37
3	36.3			
RMS = 5.83%				

Figure 44: VES curve of Schlumberger data taken at point KP8a, 10 meters north of survey point KP8

University of Ghana http://ugspace.ug.edu.gh

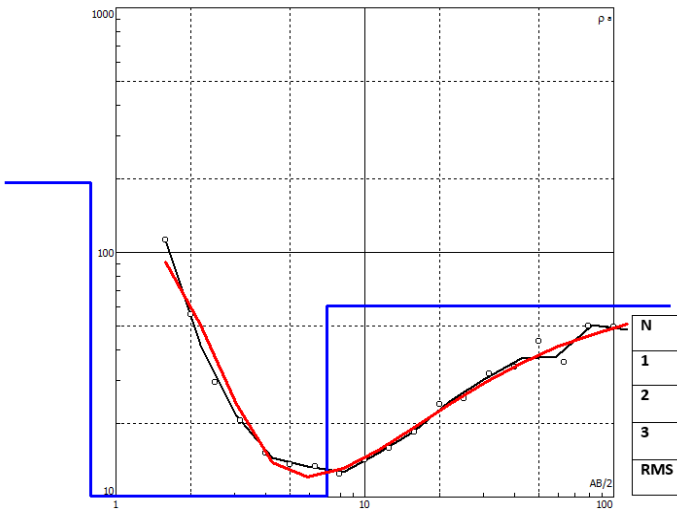

N	ρ (Ohm.m)	H (meters)	d (meters)	Altitude (meters)
1	192	0.79	0.79	-0.79
2	10.1	6.24	7.03	-7.03
3	60.7			
RMS = 9.61%				

Figure 45: VES curve of Schlumberger data taken at point KP8b, 10 meters south of survey point KP8

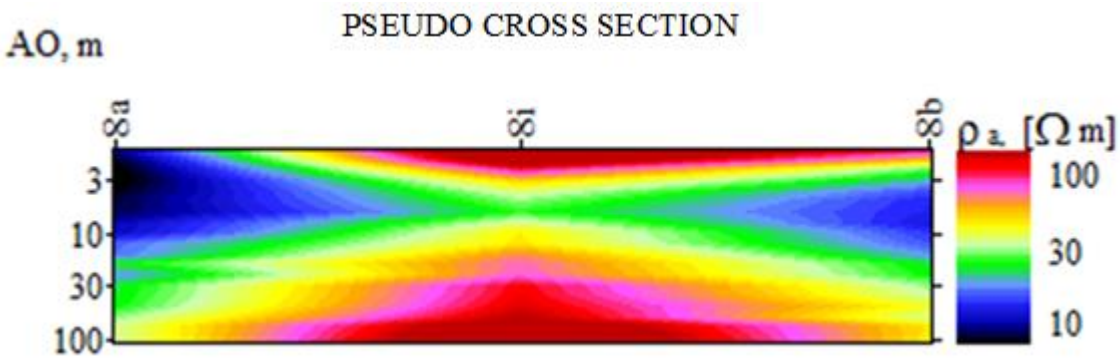

Figure 46: Pseudo section of points KP8a, KP8 and KP8b

Survey point KP11 is located along the Kokrobite beach while the adjacent points KP11a and KP11b were sited 10 m north and south respectively. The survey point KP11b is just about 70 m away from the coastline.

University of Ghana http://ugspace.ug.edu.gh

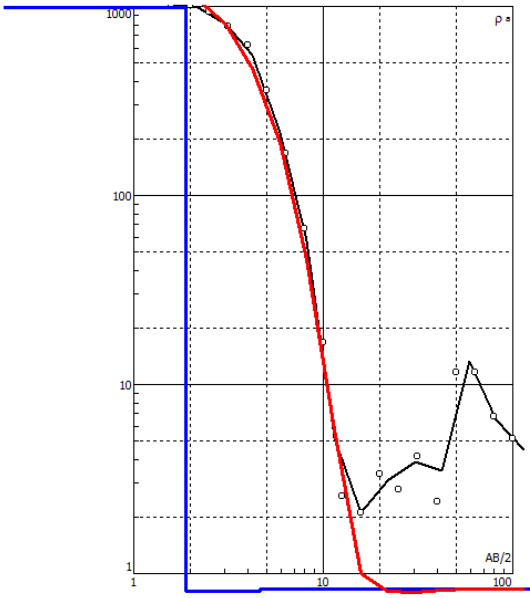

N	ρ (Ohm.m)	H (meters)	d (meters)	Altitude (meters)
1	1406	1.87	1.87	-1.87
2	0.409	1.47	3.34	-3.34
3	7.08			
RMS = 19%				

Figure 47: VES curve of the Schlumberger sounding data taken from survey point KP11

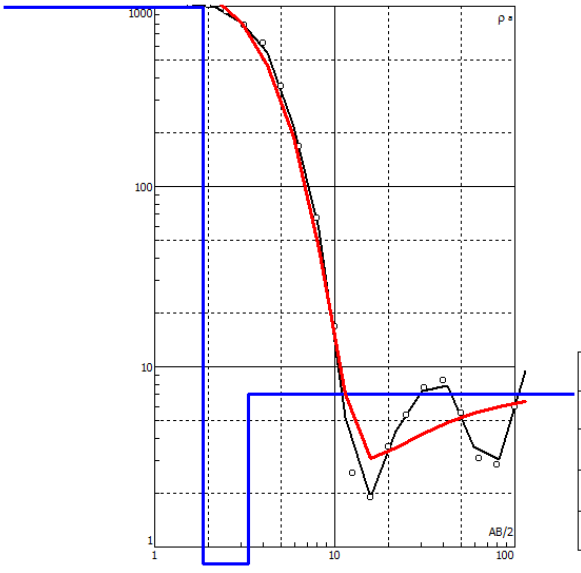

N	ρ (Ohm.m)	H (meters)	d (meters)	Altitude (meters)
1	1406	1.87	1.87	-1.87
2	0.409	1.47	3.34	-3.34
3	7.08			
RMS = 19%				

Figure 48: VES curve of Schlumberger data taken at point KP11a, 10 meters north of survey point KP11

University of Ghana http://ugspace.ug.edu.gh

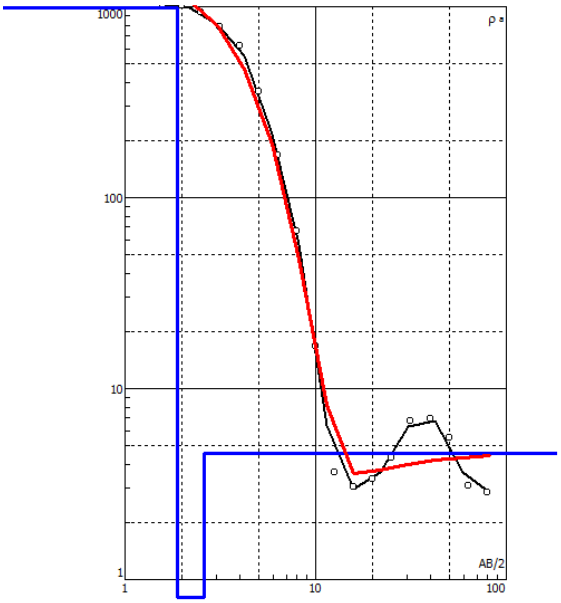

N	ρ (Ohm.m)	H (meters)	d (meters)	Altitude (meters)
1	1367	1.89	1.89	-1.89
2	0.4	0.718	2.16	-2.608
3	4.56			
RMS = 19%				

Figure 49: VES curve of Schlumberger data taken point KP11b, 10 meters south of survey point KP11

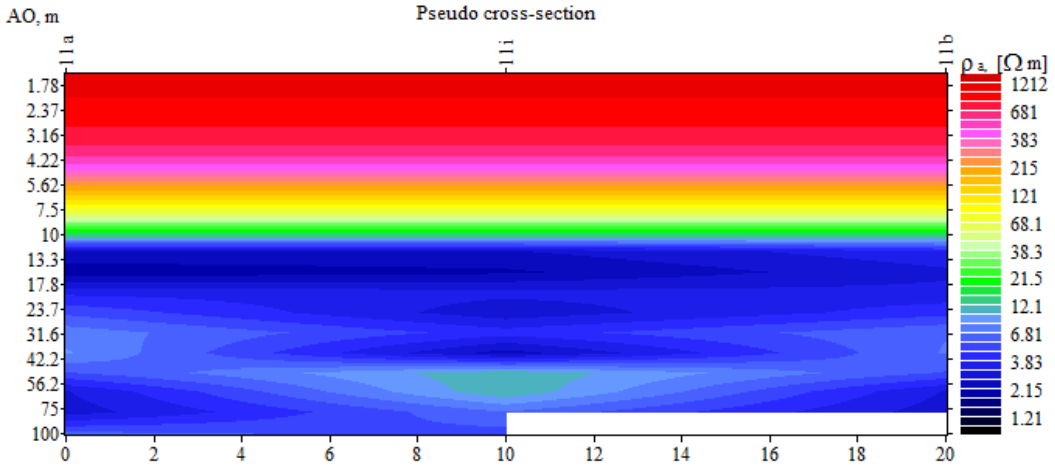

Figure 50: Pseudo section of points KP11a, KP11 and KP11b

The VES curves produces from these points all gave four-layer representations of the subsurface as shown in Figures 47, 48 and 49. The VES curve for point KP11, just like the curves for KP11a and KP11b showed a steep drop in from high apparent resistivity to low apparent resistivity with increasing current electrode spacing. After the 15.1 m current

University of Ghana http://ugspace.ug.edu.gh

electrode spacing, the curve starts to rise gently. The depth to bedrock for point KP11 is given as 3.72 m whereas that of points KP11a and KP11b are 4.08 m and 12.6 m respectively. The "HA" curve type characterizes the VES curve for the apparent resistivity for KP11 and the KP11a. The curves show a four-layer subsurface model with the first layer having a higher apparent resistivity than the second layer which also has a lower apparent resistivity value than the third and fourth layer ($\rho1 > \rho2 < \rho3 < \rho4$). The VES curve for the data from point KP11b illustrates an "HK" curve type which is characterized by a four-layer subsurface model with the first layer having a higher apparent resistivity than the second and the third layers and the third layer having a lower apparent resistivity than the fourth layer ($\rho1 > \rho2 < \rho3 > \rho4$). The pseudo-section shown in Figure 50 affirms the occurrence of high apparent resistivity at the upper portions of the section. This can be attributed to the presence of very loose beach sand which cannot conduct current well as a result of too much airspaces in its grains. The apparent resistivity reduces with depth as the beach sand overlies more compact and conductive soil material.

In all, various curve types were obtained from the VES curves plotted from all the sounding points were juxtaposed on the geological map of the area (Figure 51). The dominant curve types are the "H" and the "HA" type which is observed in almost the whole of the study area except for the southern parts, closer to the coastline that are characterized by the "A" and "K" curve types.

University of Ghana http://ugspace.ug.edu.gh

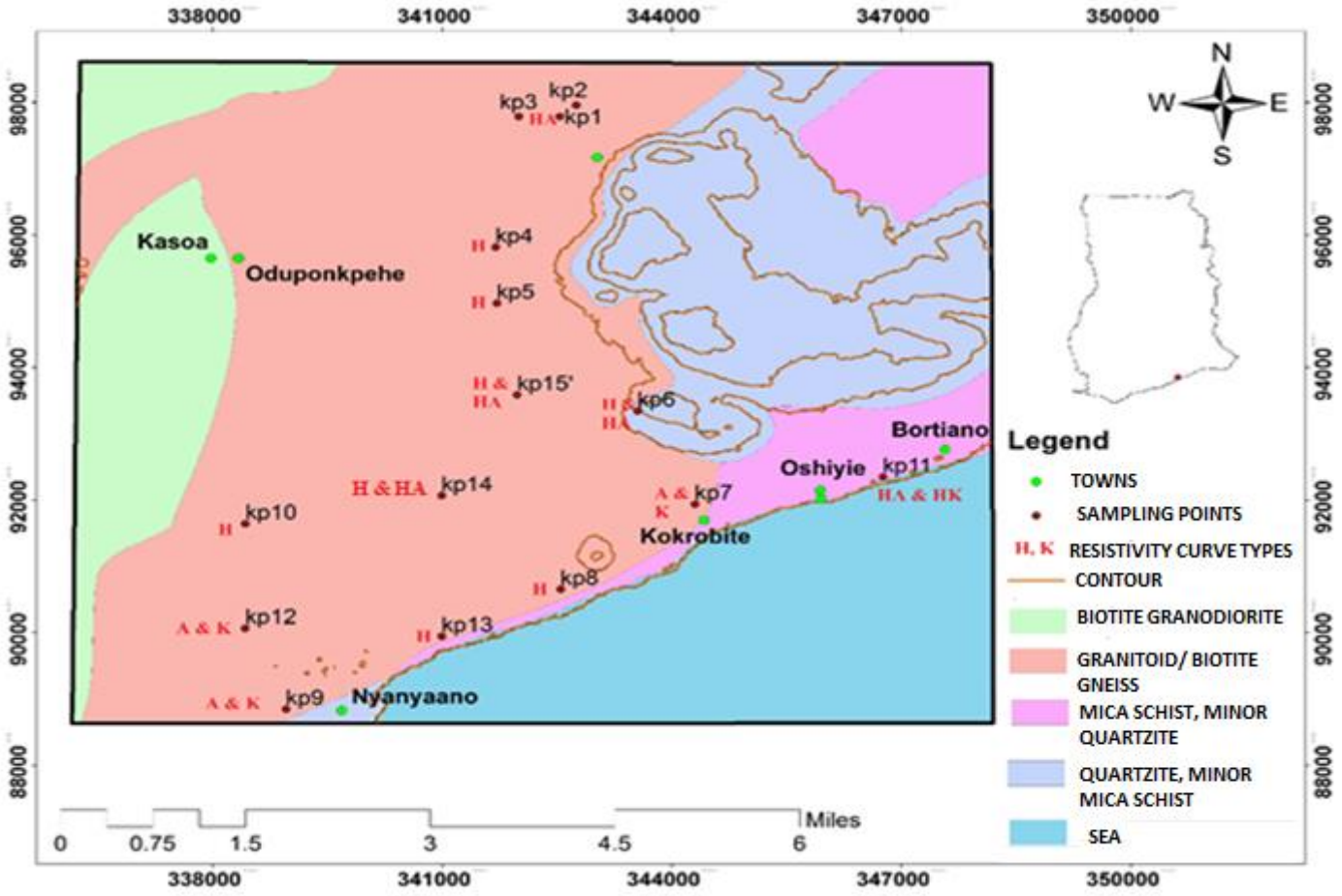

Figure 51: Proposed Geological map of the study area showing the various resistivity curve types recorded at the various survey points

University of Ghana http://ugspace.ug.edu.gh

4.4.3 Azimuthal Sounding

The data for the wenner azimuthal array showed a variety of figures ranging from ellipses to ovals and circles. The types of shape formed showed the response of the earth to the current that was introduced into it. The lobes formed from the plots of the data indicate the directions of the fractures present.

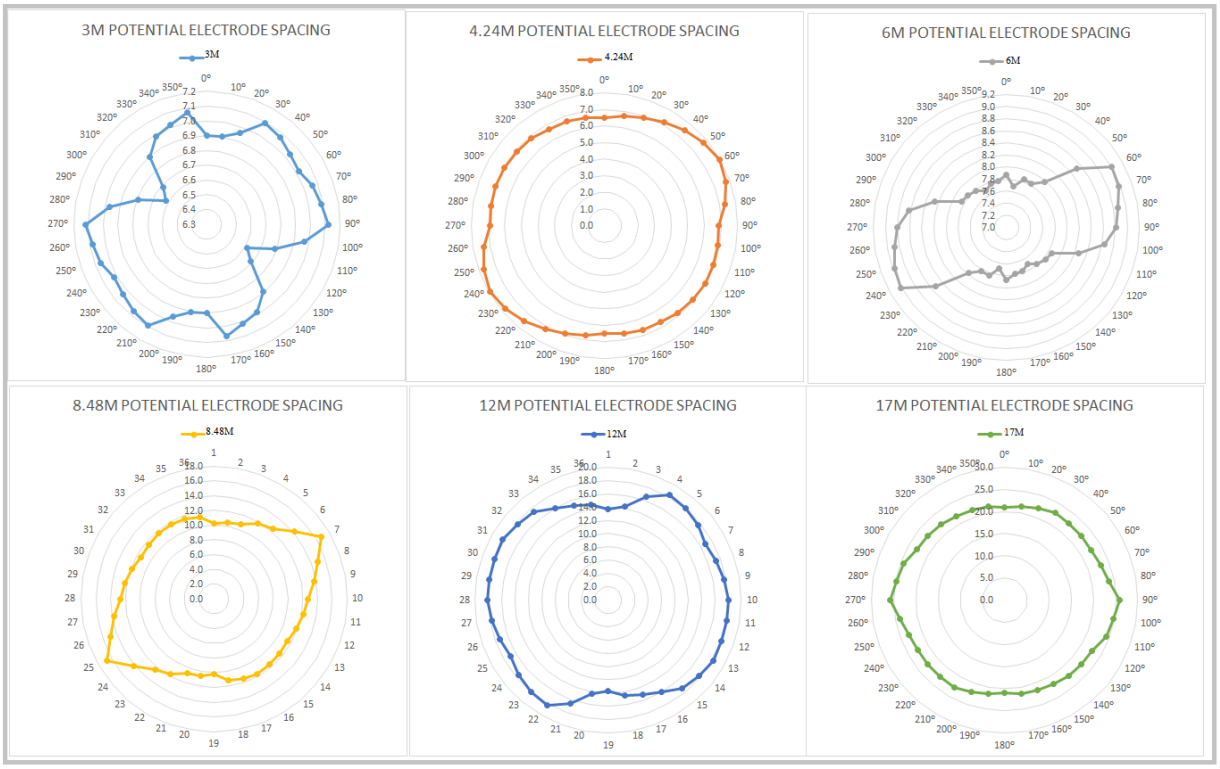

Figure 52: Plots of Wenner Azimuthal resistivity sounding at survey point KP3

The polar plots from the survey point KP3 for six different potential electrode spacing (as shown in Figure 52) showed various forms of circular to ellipsoidal shapes. The individual plots of the resistivity at the various electrode spacing shown in Figure 52 illustrate a form that is more or less one lobbed for the electrode spacing 3 m, 6 m and 8.48 m. The plots for the electrode spacing 4.24 m and 17 m are almost circular. The 12 m electrode spacing also gives a plot that is almost circular but however shows some northeast-southwest

University of Ghana http://ugspace.ug.edu.gh

trending peaks. From the visual inspection of the plots from this survey point, it is seen that there is one fracture set present and it trends in the northeast-southwest direction. Polar plots for the data at KP1 and KP2 (Appendix 2c) give similar trends as compared to the plot for the survey point KP3.

Survey points KP5 has its composite plot (Figure 53) showing a general east-west pointing single lobes. The individual plots of the various electrode spacing show a single lobbed east-west directed ellipse best illustrated by the plots of electrode spacing 17 m, 24 m and 67 m.

University of Ghana http://ugspace.ug.edu.gh

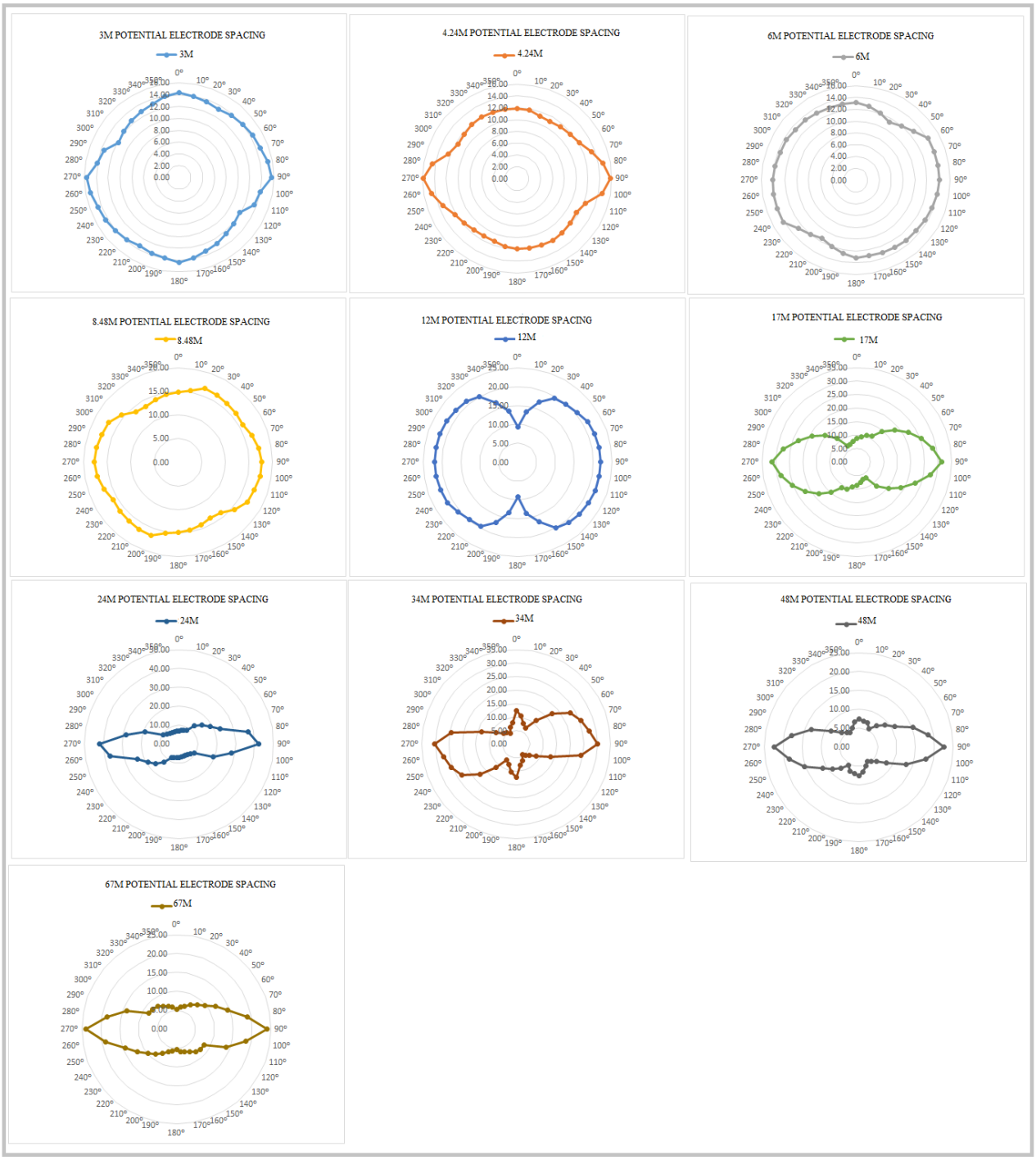

Figure 53: Plots of Wenner Azimuthal resistivity sounding at survey point KP5

The 4.24 m electrode spacing plot shows a lobe that is not too well defined in the east-west direction but however, the 3 m, 6 m and the 8.48 m electrode spacing plots show almost circular plots with indications of an east-west directed peak as shown in Figure 53.

University of Ghana http://ugspace.ug.edu.gh

The plots for the 34 m and the 48 m electrode spacing showed two lobes with the principal one being in the east-west direction while the minor lobe is in the northeast-southwest direction. The plots obtained for the survey points are similar to the plots for survey point KP4 (shown in the Appendix 2c). The plots indicate that there are two fracture sets present in the area of the survey point KP5 with the principal fracture set being in the east-west direction whereas the minor one is in the northeast-southwest direction.

Survey point KP6 showed single lobes in seven out of nine plots for the various electrode spacing as seen in Figure 54. Of these, four of the ellipses drawn were in the northeast-southwest directions and three were in the northwest-southeast directions. The plot for the 4.24 m electrode spacing however showed two lobe with the dominant lobe being in the northeast-southwest direction. The 48 m electrode spacing also produced two lobes although both seemed to be of similar magnitude in the northeast-southwest and the northwest-southeast directions. The plot for survey point KP15 (Appendix 2c) shows similar trends as compared to the plot for survey point KP6.

University of Ghana http://ugspace.ug.edu.gh

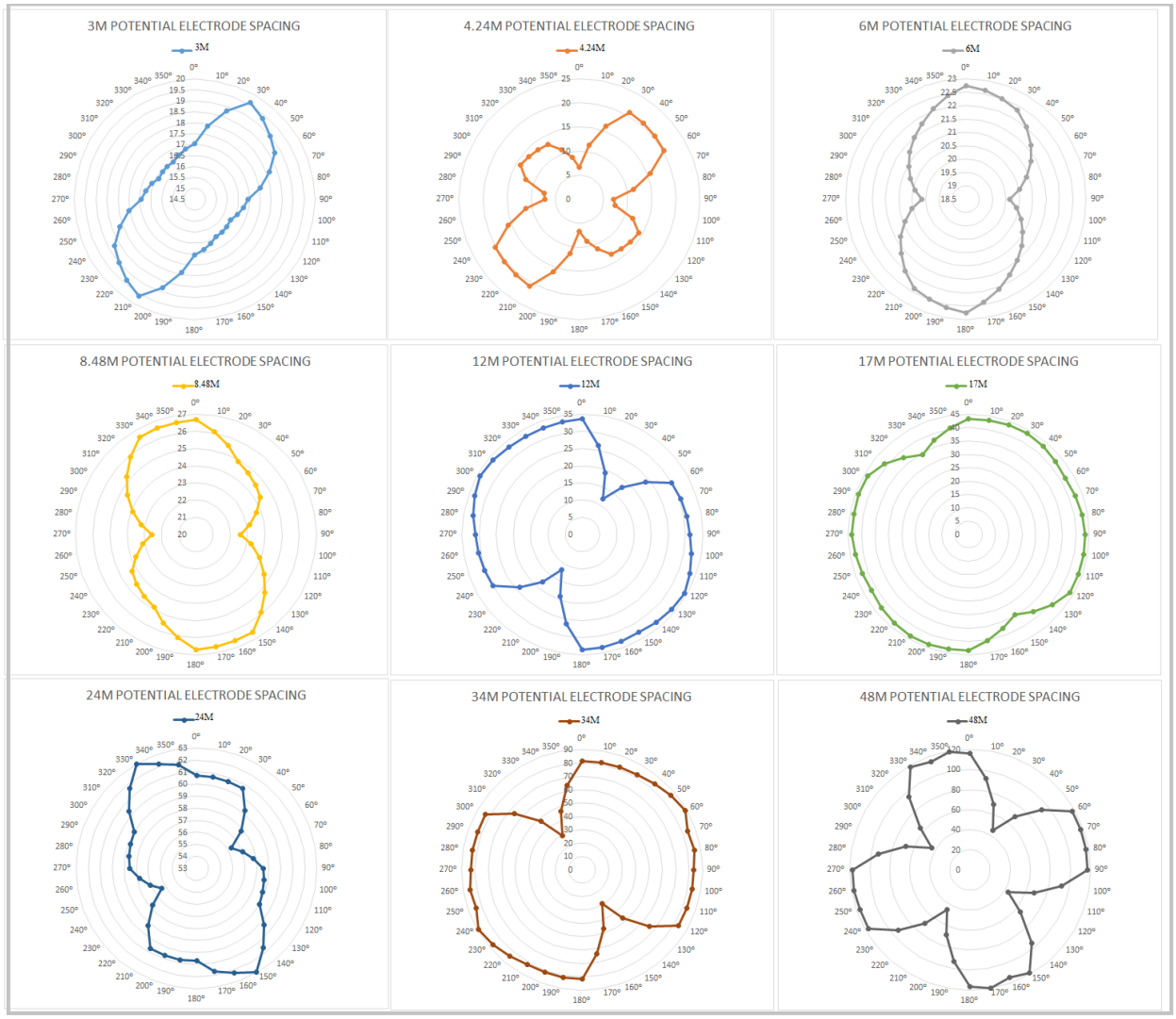

Figure 54: Plots of Wenner Azimuthal resistivity sounding at survey point KP6

From the plots above, it is deduced that there are two fracture sets present with a northeast-southeast and a northwest-southeast trend.

Electrode spacing 6 m and 17 m at the survey point KP7 showed almost circular plots although they gave indications of a northeast-southwest trend of a fracture set present. The electrode spacing of 34 m had its plot showing a figure that cannot be described as a circular plot but however not clearly defining a north-south trending fracture set. Two

University of Ghana http://ugspace.ug.edu.gh

distinct lobes (Figure 55) and a third minor lobe characterized the plot for the 12 m electrode spacing. For this plot, the principal lobes are in the northeast-southwest and the north-northwest - south-southeast directions while the minor lobe is in the northeast-southwest direction. Similar trends are seen in the plots for the survey point KP9 and KP12 shown in the appendix.

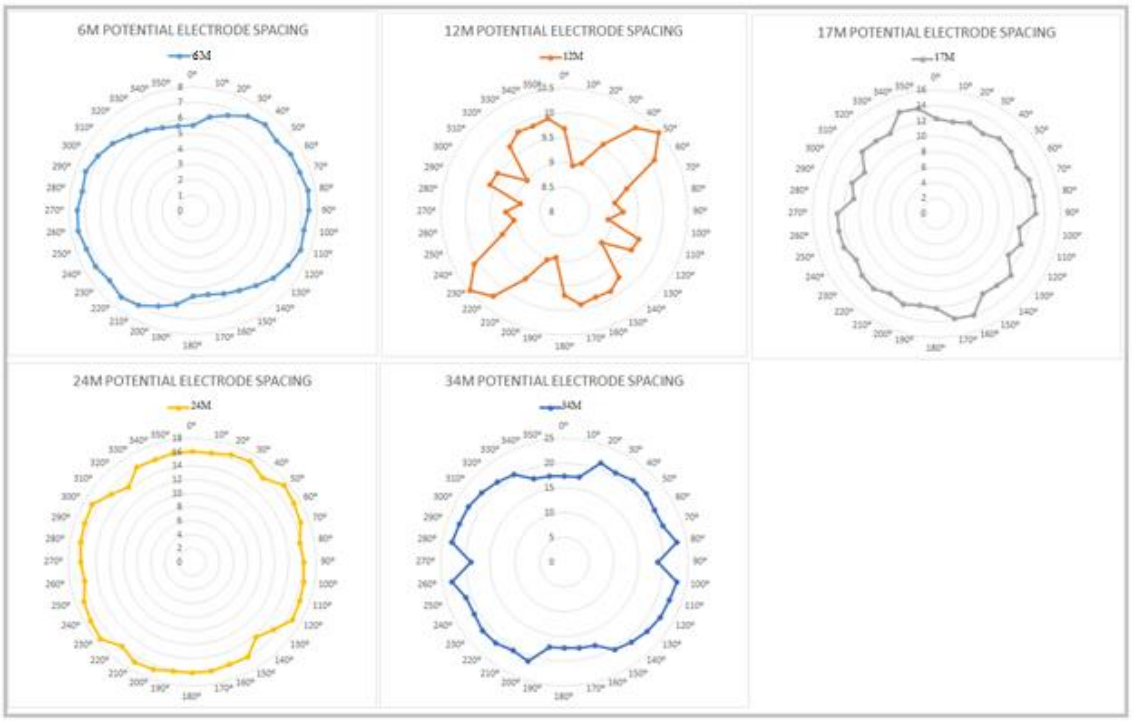

Figure 55: Plots of Wenner Azimuthal resistivity sounding at survey point KP7

Polar plots for the wenner azimuthal array data from point KP10 and KP14 show similar trends as compared to the plots for survey point KP7 although there are some differences in the individual azimuthal plots.

University of Ghana http://ugspace.ug.edu.gh

The 17 m electrode spacing at survey point KP8 (Figure 56) showed almost circular plot with a minor peaks in the northeast-southwest portions. The plots for the 12m and the 24 m electrode spacing showed a single lobe in the northeast-southwest direction while the 6 m and the 34 m electrode plots show multiple lobes with the principal peaks being in the northwest-southeast direction and the minor peaks in the north-south, east-west and the northeast-southwest directions (Figure 56). The plots for survey point KP8 are similar to the plots for survey point KP13 shown in Appendix 2c.

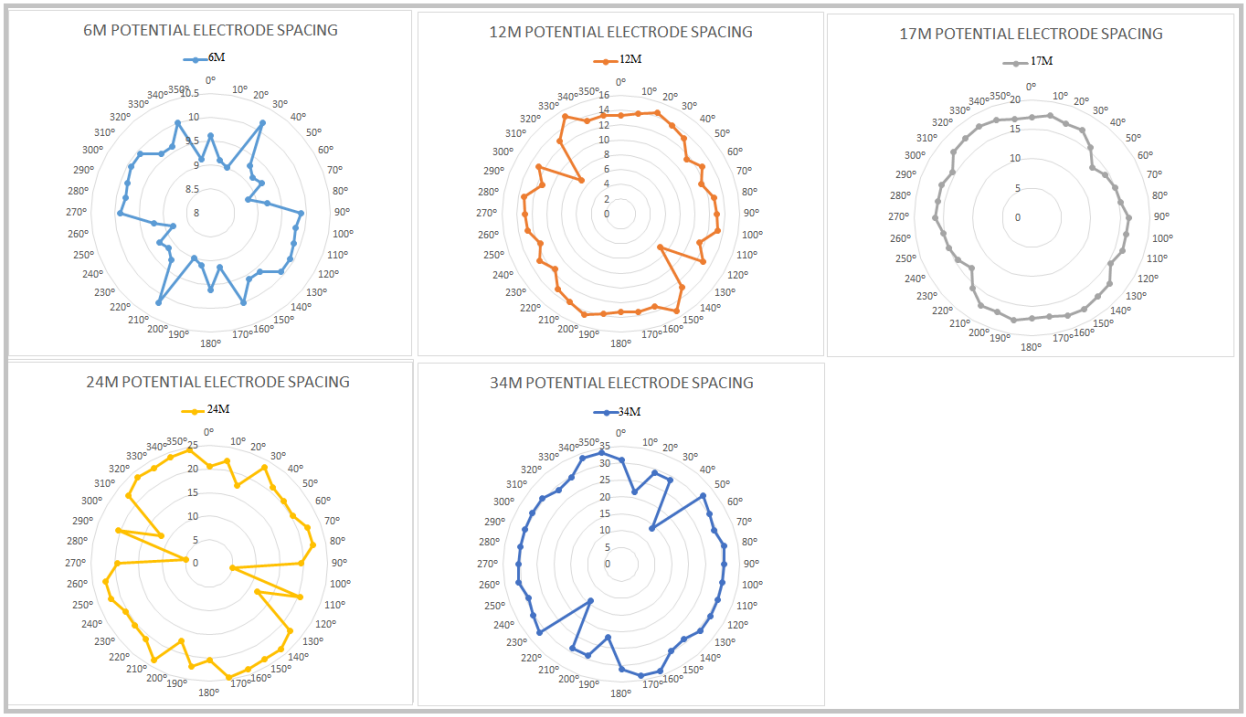

Figure 56: Plots of Wenner Azimuthal resistivity sounding at survey point KP8

Readings that were taken for the electrode spacing 6 m, 12 m, 17 m and 24 m at survey point KP11 showed to principal lobes in the composite form (Figure 57). The polar plot for the 6 m electrode spacing showed one principal lobe in the northeast-southwest directions while the minor peaks are in the north-south, northwest-southeast and the east west direction. The plot for the 12 m and the 17 m electrode spacing one lobe in the

University of Ghana http://ugspace.ug.edu.gh

northeast-southwest direction whereas the plot for the 24 m electrode spacing show two main principal lobes in the north-south and east-west directions as shown in Figure 57. From the plots, it is deduced that there are two principal fracture sets that are present at this location.

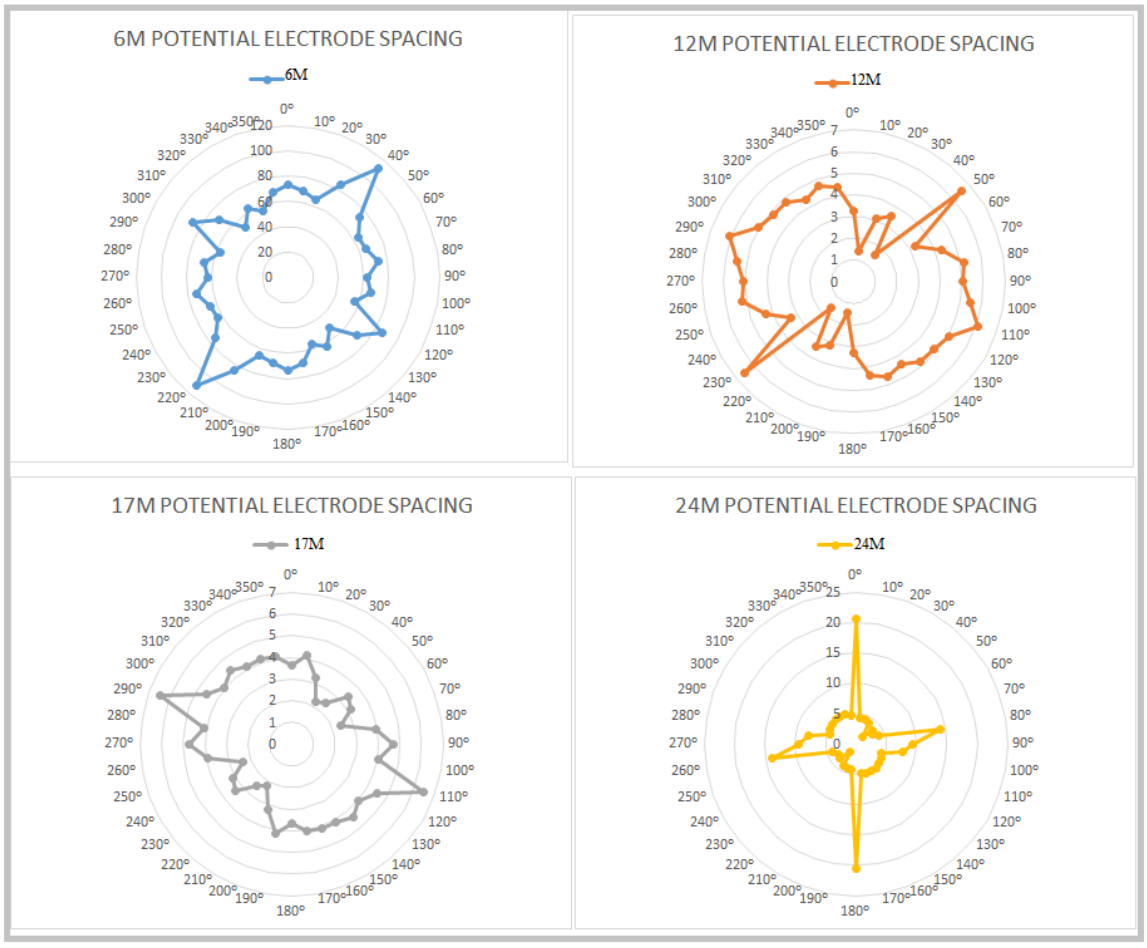

Figure 57: Plots of Wenner Azimuthal resistivity sounding at survey point KP11

Details from all the azimuthal plots were put on a geological map of the area to indicate the various directions of the fractures while also characterizing their relation to each other within the area (as shown in Figure 58).

University of Ghana http://ugspace.ug.edu.gh

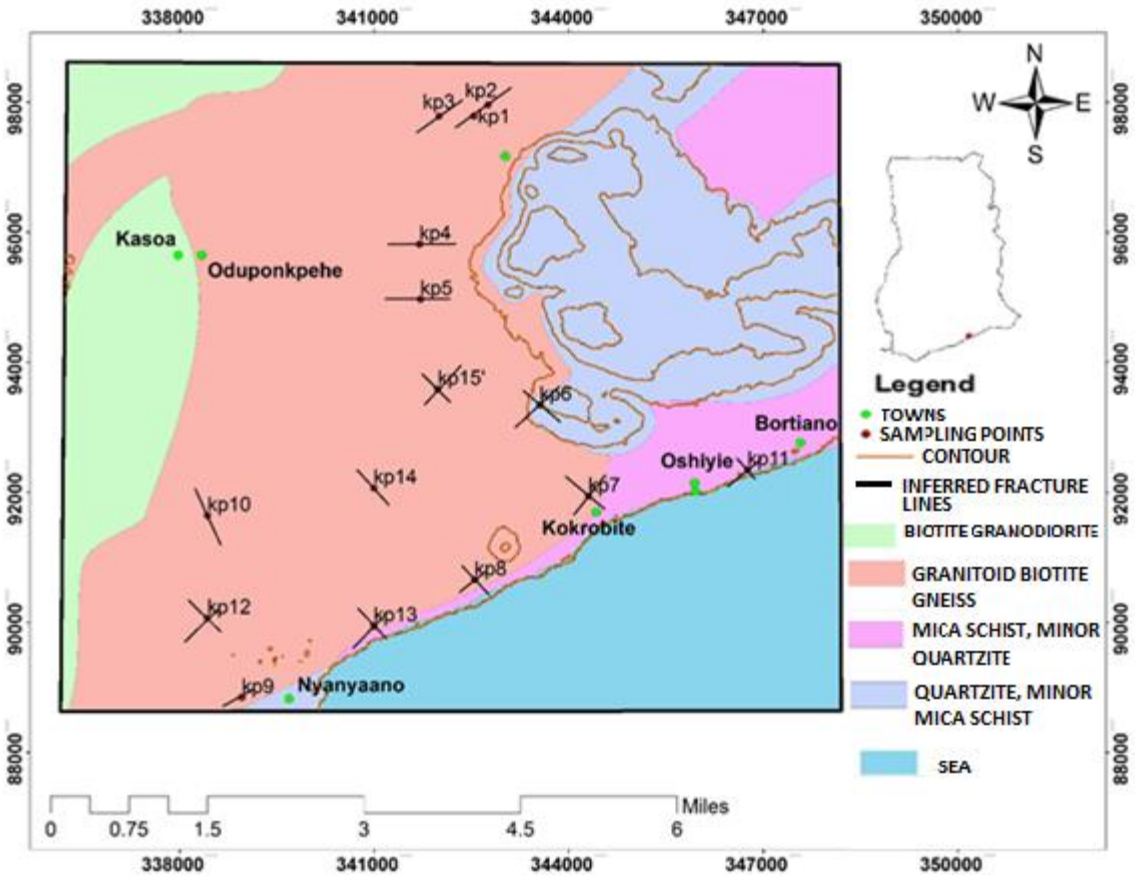

Figure 58: A proposed geological map of the area showing the inferred fracture lines deduced from the azimuthal geophysical survey

The grids from the aero magnetic geophysical data showed some trends which were investigated using ground geophysical survey methods. The methods chosen are specialized to pick up certain features within the subsurface. The grid produced from the uranium measurements from the radiometric data indicated the high amounts of uranium present in the area which leads to the presence of high amounts of radon; a gas associated with faults and fractures within the subsurface. From the various ground geophysical surveys carried out, a trend of low resistivity regions within the subsurface was seen throughout at all the survey points. From the pseudo-sections produced for the various survey points, the region of low resistivity was clearly seen below the top of the section except in a few areas where it starts from the top of the section. The square array

University of Ghana http://ugspace.ug.edu.gh

measurements done at the survey points indicate the anisotropic properties of the subsurface while the wenner azimuthal array showed the fractures present and their trends graphically in the polar plots. Based on the records for the azimuthal plots, it is reasonable to say that there is the occurrence of faults and fractures within the area with the northeast-southwest direction being the principal direction while the northwest-southeast and the east-west directions are the minor directions. The low apparent resistivity regions correspond to the depths at which the fractures were detected using the azimuthal plots. The depths to bedrock varied within the area are mainly due to different levels of tectonic activity as well as environmental conditions present. With the terrain mostly vastly made up of lowlands with the southwestern part of the Akwapim-Togo range and the Dampa hill standing out as the main highlands, outcrops are scarce within the area. The few outcrops seen on the hills and along the beach showed multiple joints thus indicating the occurrence of high energy tectonic activities within the area.

University of Ghana http://ugspace.ug.edu.gh

4.5 Comparism of the Geophysical Electrical Resistivity Methods Used

The rock mass underlying the study area is anisotropic. This is highlighted by the square array plots as well as the azimuthal plots obtained. The anisotropy of the subsurface can arise as a result of various geological processes.

For this study, the square array and the azimuthal plots gave indications on the occurrence of fractures within the subsurface as well as the attributes of those fracture sets with regards to direction and orientation. The degree of anisotropy is clearly defined by the square array method. The square array and the schlumberger sounding give indications of the depth to bedrock at the various sample points within the area. Although different depths to bedrock are given by the two arrays (square array and schlumberger array), similar trends are observed in the VES curves done for the same station. The azimuthal array dove over the various stations show the various fracture sets as well as their orientations. The azimuthal plots show the occurrence of variation in apparent resistivity with depth. The lobes present on the plots generated from the drawn curves illustrate both the directions of high resistivity variation and also the trends of the fracture sets within the ground. A general northeast-southwest and a northwest-southeast trend is picked out from the plots made. The number of lobes present indicate the number of fracture sets present at each survey point.

The VES plots from the schlumberger soundings data illustrate the number of layers present while giving the depths to the bedrock at each of the various survey points. The average number of layers at given at the various survey points. For all the pseudo – sections, regions of very low apparent resistivity run through the sections at various depths from the surface of the earth.

University of Ghana http://ugspace.ug.edu.gh

The square array is generally thought to be more sensitive to a given rock anisotropy than the Schlumberger or the Wenner arrays (Habberjam, 1979). For anisotropic conditions, it is less likely to be obscured by inhomogeneity within the rock mass, relief, electrode positioning noise and other forms of noise. The square array ha a potential electrode spacing to current electrode spacing ratio of 1:1 unlike the wenner array which is 1:3 or the schlumberger array which is 1:10. With this ratio, the square array tends to have the largest electrode spacing thus being good for fracture detection. From the results obtained, it is noticed that the square array has a relatively higher depths of penetration than the schlumberger array for similar electrode spacing.

With regards to space requirements for the survey, the square array required the least space followed by the schlumberger array and the wenner azimuthal array. The comparative depth reached were in the same order.

In the course of the survey, the following disadvantages of the resistivity surveys were noted;

i. The interpretations of the data are ambiguous thus geological controls are required to make accurate interpretations.
ii. The interpretations made are limited to simple structural configurations.
iii. The signatures of deep seated variations are masked by the effects of topography and near surface features.
iv. The accuracy of depth determination is however relatively lower as compared to other survey methods with the depth of penetration being hindered by the maximum power that can be introduced into the ground and by the practical difficulties of laying the cables.

University of Ghana http://ugspace.ug.edu.gh

CHAPTER FIVE

CONCLUSION AND RECOMMENDATIONS

5.1 Conclusion

The area studied gave various indications that showed the presence of faults and fractures. Trends of tectonic activity were observed in the aero magnetic grids that were produced. The uranium concentration grid produced from the radiometric data showed the presence of a high amount of uranium occurring within the area. The ground investigation carried out within the area at the 15 selected survey pints showed the occurrence of fractures within the subsurface in the area. A geological map with the inferred faults and fracture lines plotted on it as shown in figure 57, is produced from the ground geophysical data acquired. Based on all the data obtained from the various surveys carried out in the area, it is reasonable to say that there is the occurrence of the western boundary fault as its minor associated faults occurring in the area. The principal directions of the fractures noticed is the northeast-southwest and northwest-southeast, thus concordant with the already known trend of the Western Boundary fault. A few other fractures occurred in the east-west and the north-south directions and those are assigned to the minor faults associated to the Western Boundary fault. The principal fault/fracture directions are concordant with the inferred fault/fractures from the regional mapping carried out within the area by other researchers.

From the surveys carried out, it is noticed that most of the areas had well compacted top surfaces. Also, some buildings close to the beaches in the areas of Kokrobite, Langma and Nyanyano showed various degrees of cracks in their walls. Residents in the area attested to the frequent experiences of different degrees of vibration of the earth especially in the late hours of the day. The rose plots of the joints occurring in the rocks within the area indicate the occurrence of different stress and strain directions thus accounting for the

University of Ghana http://ugspace.ug.edu.gh

cracks in the walls of buildings. Different depth to bed rock within the area as observed from the geophysical survey was confirmed by the different depths of the few boreholes located in the area.

The square array provides very good readings for apparent resistivity, apparent anisotropy and strike for concealed anisotropic formations. From the interpretation of different field curves, it is possible to estimate values for the mean, longitudinal and transversal resistivities, as well as depth, apparent anisotropy, and strike of concealed formations. If a complete study is to be conducted over anisotropic ground, the square array is the more economic field strategy, as the alternative is to carry out linear soundings in at least four different orientations. However, major disadvantages occur in rough and densely vegetated ground. The Schlumberger array together with the square array worked best in giving the depth to bedrock at the various survey points while the azimuthal array clearly showed the fractures present in the area.

5.2 Recommendation

Further work must be done on the other parts of the Akwapim-Togo range to identify the minor faults present in order to inculcate them into the development planning of the areas where it occurs. Also the carrying out of seismic geophysical surveys, most preferably seismic sounding, along the fault one will provide a measure to which other geophysical data on the area can be compared and deductions made to accurately map out the main fault lines and the minor fault lines. The seismic geophysical survey measure a different physical property of the earth materials from which the data obtained can be used to characterize the subsurface. Future projects with better funding can undertake this in order

University of Ghana http://ugspace.ug.edu.gh

to obtain data using another aspect of geophysics which will be a supporting data to the one in this work.

There should be proper planning and enforcement of strict building and construction laws to ensure the quality and standards of the buildings put up in the area as well as the materials used since the area is faulted and as such prone to earthquakes and tremors due to its proximity to the epicenter of the major earthquakes that have occurred in Ghana.

University of Ghana http://ugspace.ug.edu.gh

REFERENCES

Ahmed, S. M., Blay, P. K., Castor, S. B., Coakley, G. J. (1977). Geology of Field Sheets 33, 59, 61 and 62. Winneba, NW Accra, SW, NW and NE respectively. Geological Survey Bulletin No. 32, pp. 1-48.

Akpati, B. N. (1978). Geological Structure and Evolution of the Keta Basin, Ghana West Africa. Geological Society of America Bulletin 89, 124 - 132

Amponsah, P. E. (2004). Seismic Activity in Ghana: past, present and futures. Annals of Geophysics, Vol. 47, N. 2/3

Amponsah, P. E. (2002). Seismic activity in relation to fault systems in southern Ghana, Journal of African Earth Sciences 35, 227- 234.

Antobreh, A. A., Faleide, J. T., Tsikalas, F., Planke, S. (2009). Rift-Shear architecture and tectonic development of the Ghana margin developed from multichannel seismic reflection and potential field data. Marine and petroleum Geology 26, 345 - 368

Asumadu-Sakyi, A.B., Fletcher, J.J., Oppon, O.C., Quashie, F.K., Wordson, D.A., Adjei, C.A., Amartey, E.O., Darko, E.O. and Amponsah P. E., (2011). Preliminary Studies on Geological Fault Location Using Solid State Nuclear Track Detection. Research Journal of Environmental and Earth Sciences 3(1): 24-31.

Attoh, K., Brown, L., 2008. Deep structures of the southeastern margin of the West African craton from seismic reflection data, offshore Ghana. In: Ennih, N., Liégeois, J.-P. (Eds.), The boundaries of the West African Craton, Geological Society, London, Spec. Pub., vol. 207, pp. 499–508.

Attoh, K., Brown, I., Haenlein, J., (2005). The role of Pan-African structures in intraplate seismicity near the termination of the Romanche fracture zone, West Africa, Journal of African Earth Sciences 43, 549 - 555

Attoh, K., Ekwueme, B, N. (1997). In: de Wit, M. J., Ashwall, L., (Eds), The West African Shield. Oxford University Press, Greenstone Belts, pp. 513 - 524

Bacon, B., Quaah, A. O. (1981). Earthquake activity in southeastern Ghana. Bulletin Seismological Society of America, 771-784.

University of Ghana http://ugspace.ug.edu.gh

Bilim F., Ates, A. (2003). Analytical signal inferred from reduced to the pole data. Journal of the Balkan Geophysical Society Vol. 6, No. 2. 66-74

Bolshakov D.K., Modin I.N., Pervago E.V. and Shevnin V.A. (1997). Separation of anisotropy and inhomogeneity influence by the spectral analysis of azimuthal resistivity diagrams. Proceedings of the 3rd EEGS±European Section Meeting, Aarhus, Denmark, pp. 147±150.

Busby, J. P. (2000). The effectiveness of azimuthal apparent – resistivity measurements as a method for determining fracture strike orientations. Geophysical Prospecting, 2000, 48, 677 – 695.

Blundell, D.B. (1976). Active Faults in West Africa. Earth and Planetary Science Letters, 31, p. 287-290

Blundell, D.J. (1976). Active faults in West Africa. Earth and Planetary Sciences Letters 31, 287 290 (Elsevier Scientific Publishing Company, Amsterdam)

Blundell, D.J. and Banson, J.K.A. (1975). Interpretation of seismic reflection survey across the Continental Shelf south of Accra and its bearing on Earthquakes in the area. Rep. Geology Survey, No. 75/1, Accra

Cardimona, S. (2002). Electrical resistivity techniques for subsurface investigation. Paper presented at the second annual conference on the application of geophysics and NDT methodology transformation facilities and infrastructure, Los Angeles, California. Abstract retrieved from http:/trid.trd.org/view.aspx

Carpenter, P. J., Kaufmann, R. S., and Price, B. (1990). Use of resistivity soundings to Determine landfill structure. Ground Water. Vol. 24, No. 4, pp. 446 – 452.

Cohn, M. E., Rudman A. J. (1995). Orientation of near-surface fractures from azimuthal measurements of apparent resistivity. SEG/Houston, Texas/95 Extended, pp. 372-374

Deltail, J. R., Valery, P., Montadert, C., Fondeur, C., Patriat, P., Mascle, J. (1974). Continental Margin in the northern part of the gulf of Guinea, In; Burk, C., Drake, C. L. (Eds.), Geology of the Continental Margin, Springer, New York, pp. 297-311

University of Ghana http://ugspace.ug.edu.gh

Edwards, R.A., R.B. Whitmarsh, R.A. Scrutton (1997). Synthesis of the Crustal Structure of the Transform Continental margin off Ghana, Northern Gulf of Guinea; Geo-Marine Letters, 17, pp. 12-20

Geological Survey Department of Ghana, (2010). Geological Map of Ghana

Geosoft Levelling System, Tutorial and User Guide, (2007). Chapter 6, p. 53-54.

Graham, K.M. (2013). Geological and structural interpretation of part of the Buem formation, Ghana using aerogeophysical data. College of Science, Kwame Nkrumah University of Science and Technology, Ghana [Unpublished]

Gunn, P. (1997). Quantitative methods of interpreting aeromagnetic data. AGSO Journal of Australian Geology and Geophysics, 17(2). 105-114

Habberjam, G.M. (1979). Apparent resistivity observations and the use of square array techniques. Geoexploration Monographs No. 9. Geopublication Associate, Berlin.

Habberjam, G.M. (1975). Apparent resistivity, anisotropy and strike measurements. Geophysical Prospecting 23, 211–247.

Habberjam, G.M., Watkins, G. E. (1967). The use of a square configuration in resistivity Prospecting: Geophysical Prospecting, volume 15, p. 221- 235

Hautaniemi, H., Kurimo, M., Multala, J., Levaniemi, H, Vironmaki, J. (2005). The “Three In One” aerogeophysical concept of GTK in 2004. Geological Survey of Finland, Special Paper 39, 21-74

Junner, N. R. (1935). Gold in the Coast. Geological Survey Memoir (4) 1-85.

Junner, N. R., Service, H. (1936). Geological notes on Volta River District and Togoland under British Mandate. Directors Annual Report 1935-1936, pp. 1-36.

Keller G.V. and Frischknecht F.C. 1966. Electrical Methods in Geophysical Prospecting. Pergamon Press, Inc.

Kesse, G. O., (1985).The mineral and rock resources of Ghana. A.A. Balkema, Rotterdam, 610 p.

University of Ghana http://ugspace.ug.edu.gh

Iddirisu, Y and Armah, K. E. T. (1997). Determination of Fracture Trends in Groundwater Exploration in the Dahomeyan Terrain, Ghana, using Azimuthal Resistivity Survey. Ghana Mining Journal, Vol. 3, Nos. 1 & 2. pp. 43-48

Lane Jr., J. W., Haeni, F. P., Watson, W. M. (1995). Use of a square array direct current resistivity method to detect fractures in crystalline bedrock in New Hampshire Ground Water 33, 476 – 485.

Lilian, S, and Niels, O. J. (199). Detection of Local Fracture Systems by Azimuthal Resistivity Surveys: Examples from South Norway. JOURNAL OF Applied Hydrogeology, pp. 27-33.

Macleod, I.N., Vierra, S., Chaves, A.C. (1993). Analytical signal and reduction-to-pole in the interpretation of total magnetic field data at low magnetic latitudes. Proceedings of the third international congress of the Brazilian society of geophysicist.

Mascle, J., Sibuet, J.C., 1974. New pole for early opening of South Atlantic. Nature 252, 464–465.

Ministry of Local Government and Rural Development, (2006). Annual Report for 2006.

Milligan, P., Gunn, P. (1997) Enhancement and presentation of airborne geophysical data. AGSO Journal of Australian Geology and Geophysics, 17 (2). 63-75

Muff R., Efa E. (2006). Explanatory Notes for the Geological Map for Urban Planning 1:50 000 of Greater Accra Metropolitan Area. Ghana–Germany Technical Cooperation Project: Environmental and Engineering Geology for Urban Planning in the Accra-Tema Area.

Nsiah-Akoto, I., Andam, A. B., Amponsah, P. E., Hood, C. O. (2013). The Radon Health Hazards Education in Ghana. Elixir Geoscience 56 (13399-13401)

Pickett, E.A. and S. Allerton (1998). Structural observations from the Côte d'Ivoire – Ghana Transform Margin. In: MASCLE, J., LOHMANN, G.P., and Moullade, M. n (Eds.) 1998, Proceedings of the Ocean Drilling Program, Scientific results, vol. 159, p. 3-11

University of Ghana http://ugspace.ug.edu.gh

Reeves, C. (2005). Aeromagnetic surveys: Principles, Practices and Interpretations. Geosoft.

Schmutz, M., Andrieux, P., Bobachev, A., Montoroi, J. P., Nasri S., (2006). Azimuthal sounding over a steeply dipping anisotropic formation: A case study in central Tunisia

Taylor, R. W., Fleming, A. H. (1988). Characterizing joint systems by azimuthal resistivity surveys. Ground Water 26, 464 - 474

Telford, W., Gelbert, I., Sheriff, R. (1990). Applied Geophysics (Second Ed). London, Cambridge University Press

University of Ghana http://ugspace.ug.edu.gh

APPENDIX 1A

AERO GEOPHYSICAL DATA

The aircraft used was a Cessna 404 Titan fixed wing (ZS-KRG) operated by Aircraft Operating Company, Johannesburg, South Africa. The aircraft was equipped with the following sensors and systems:

- Three Geometrics 822-A magnetometers (two wing pod and one stinger mounted)
- RMS AADCII compensator.
- Exploranium GR-820 spectrometer.
- Two 1024 cubic inch NaI (TI) crystal detector packages, each with an upward-looking crystal.
- A Hertz Totem-2A VLF system.
- Novatel 3951R twelve channel GPS receiver.
- Omnistar GPS system
- A King model KRA100 radar altimeter
- High Sense GFCS-II geophysical flight control system.

The ground monitoring was done using the Syntrex H8 cesium magnetometer with a M82 board Novatel 951 twelve channel GPS.

University of Ghana http://ugspace.ug.edu.gh

Survey parameters

Table 8: Table showing the survey parameters for the GTK aero geophysical survey

Nominal traverse line spacing	400 m (800 m for Area 4)
Nominal control line spacing	5000 m
Nominal terrain clearance	80 m
Traverse line direction approx.	315
Control line direction approx.	045
Airspeed (Nominal)	280-290 km/hr
Measurement interval, mag and VLF	0.1 s
Measurement interval, radiometrics	1 s
Measurement spacing, mag and VLF	8 m
Measurement spacing, radiometrics	80 m

Navigation and coordinate transformations

The navigational system yields a flight path expressed in WGS84 Latitude-Longitude coordinates. The Transformation to local Ghana National (War Office Spheroid) UTM coordinates used the following projection parameters:

University of Ghana http://ugspace.ug.edu.gh

Table 9: table showing the projection parameters in the aero geophysical data processing

Spheroid	Semi-major Axis (a)	Semi-minor axis (b)
WGS84	6378137.00	6356752.3132
Ghana National	6378306.0648	6356757.9242

Local datum shift applied:

Table 10: Table showing the local datum shift parameters

Delta X:	-199
Delta Y:	32
Delta Z:	322 UTM
Central meridian	1W
False Easting	274320
False Northing	-515883
Scaling Factor	0.99975

All data processing was carried out using the Geosoft Oasis Montaj General levelling system modules.

University of Ghana http://ugspace.ug.edu.gh

APPENDIX 2A

SQUARE ARRAY APPARENT RESISTIVITY MEASUREMENTS

1 = first position and

2 = second position

Apparent resistivity measurements are in Ohm.m.

Table 11: Apparent resistivity measurements taken at point KP1

ELECTRODE SPACING (m)	α1	α2	β1	β2	γ1	γ2	γ1/γ2	ρm1	ρm2
3	8.36	19.77	11.16	50.57	1.18	30.96	0.04	9.66	31.62
4.3	7.49	8.76	9.76	14.57	1.16	5.67	0.20	8.55	11.30
6	6.36	7.08	6.63	10.62	0.34	3.44	0.10	6.50	8.67
8.5	6.59	7.76	6.03	9.32	0.48	1.43	0.33	6.30	8.51
12	8.39	8.57	10.56	6.71	0.57	1.20	0.47	9.41	7.58
17	6.29	14.18	13.10	13.99	0.84	0.40	2.13	9.07	14.08
24	5.44	3.00	16.83	6.85	0.45	0.93	0.48	9.57	4.53
34	49.50	16.27	19.67	8.35	0.84	1.42	0.59	31.20	11.65
48	6.99	9.32	15.99	3.14	0.69	0.18	3.95	10.57	5.41
67	2.92	6.62	9.53	5.59	0.25	0.79	0.32	5.27	6.08
96	0.58	6.47	0.31	4.76	0.24	0.50	0.47	0.43	5.55

Table 12 : Apparent resistivity measurements taken at point KP2

ELECTRODE SPACING (m)	α1	α2	β1	β2	γ1	γ2	γ1/γ2	ρm1	ρm2
3	42.55	42.16	6.41	48.94	49.00	6.89	7.11	16.51	45.42
4.3	10.49	7.55	0.72	12.50	9.60	6.50	1.48	2.74	9.71
6	9.10	5.44	0.43	10.63	6.21	4.15	1.50	1.97	7.61
8.5	12.29	6.77	2.00	13.08	11.13	6.59	1.69	4.95	9.41
12	12.48	6.15	0.05	16.77	12.45	4.59	2.71	0.77	10.15
17	17.38	1.16	2.68	11.77	15.70	2.61	6.02	6.82	3.69
24	21.48	9.89	2.03	20.12	22.35	4.72	4.74	6.60	14.10
34	37.63	10.77	5.14	32.81	13.31	8.98	1.48	13.90	18.80
48	39.58	2.81	1.36	26.64	10.70	3.01	3.56	7.34	8.65
67	41.86	7.34	5.30	30.50	12.28	10.98	1.12	14.89	14.97

University of Ghana http://ugspace.ug.edu.gh

Table 13: Apparent resistivity measurements taken at point KP4

ELECTRODE SPACING (m)	α1	α2	β1	β2	γ1	γ2	γ1/γ2	ρm1	ρm2
3	3.25	2.79	2.66	2.98	0.72	0.32	2.24	0.48	2.88
4.25	3.58	2.70	2.32	2.85	1.05	0.11	9.74	0.34	2.77
6	4.24	2.96	3.58	3.66	1.31	0.90	1.46	1.09	3.29
8.48	4.64	2.98	3.86	3.92	0.58	0.05	10.96	0.18	3.42
12	3.47	5.07	2.93	4.99	0.31	0.46	0.66	0.38	5.03
17	4.98	0.98	2.63	3.35	0.20	0.19	1.09	0.19	1.81
24	1.30	1.12	1.22	1.92	0.24	0.55	0.43	0.36	1.46
34	5.28	0.71	2.73	2.08	0.11	0.52	0.21	0.23	1.22
48	2.63	1.78	1.74	11.36	0.72	0.52	1.37	0.61	4.50
67	1.35	0.91	1.05	2.40	0.67	0.86	0.78	0.76	1.47

Table 14: Apparent resistivity measurements taken at point KP9

ELECTRODE SPACING (m)	α1	α2	β1	β2	γ1	γ2	γ1/γ2	ρm1	ρm2
3	2.70	4.92	4.70	2.44	2.05	2.49	0.82	3.57	3.47
4.3	2.70	4.21	3.03	2.84	2.93	1.04	2.81	2.86	3.46
6	2.94	4.31	5.43	3.32	2.25	1.20	1.87	4.00	3.78
8.5	3.03	5.50	10.95	3.48	5.92	1.34	4.43	5.76	4.38
12	3.29	6.46	9.02	4.34	4.90	2.21	2.22	5.45	5.29
17	4.50	9.00	10.97	5.42	5.12	2.58	1.98	7.03	6.99
24	6.39	10.00	12.67	8.25	6.71	3.75	1.79	9.00	9.08
34	9.41	14.50	14.71	13.96	7.62	1.39	5.48	11.76	14.23
48	12.74	6.46	8.45	15.58	4.31	1.15	3.74	10.37	10.03
67	15.51	12.18	7.96	24.09	3.91	1.13	3.47	11.11	17.13
96	24.92	8.60	5.95	17.61	4.72	4.64	1.02	12.17	12.30

Table 15: Apparent resistivity measurements taken at point KP10

ELECTRODE SPACING (m)	α1	α2	β1	β2	γ1	γ2	γ1/γ2	ρm1	ρm2
3	10.27	11.14	10.77	8.63	0.56	2.37	0.24	10.52	9.80
4.3	6.88	8.27	7.09	5.93	0.30	2.46	0.12	6.98	7.00
6	6.89	8.87	7.22	5.24	0.43	3.21	0.13	7.06	6.82
8.5	8.15	10.80	8.60	6.83	0.81	3.07	0.26	8.37	8.59
12	2.83	10.26	11.40	6.69	2.74	2.54	1.08	5.67	8.29
17	7.11	17.74	10.52	10.74	3.12	3.47	0.90	8.65	13.80
24	5.62	5.18	11.75	12.86	1.39	1.55	0.90	8.12	8.16
34	10.00	6.83	10.69	6.36	2.30	1.33	1.73	10.34	6.59
48	1.44	7.60	9.88	9.14	2.97	0.64	4.64	3.77	8.33
67	5.25	9.40	22.83	3.09	1.42	1.15	1.24	10.95	5.39
96	4.51	6.30	7.28	5.71	4.91	1.30	3.78	5.73	5.99

University of Ghana http://ugspace.ug.edu.gh

Table 16: Apparent resistivity measurements taken at point KP11

ELECTRODE SPACING (m)	α1	α2	β1	β2	γ1	γ2	γ1/γ2	ρm1	ρm2
3	313.20	464.10	484.40	272.00	91.01	209.10	0.44	389.50	355.30
4.3	183.70	198.10	203.50	130.60	16.66	68.15	0.24	193.35	160.85
6	41.69	69.87	78.51	31.77	37.45	37.37	1.00	57.21	47.11
8.5	7.77	17.70	21.40	8.60	12.45	9.74	1.28	12.89	12.33
12	1.61	4.24	3.96	3.30	2.14	2.12	1.01	2.53	3.74
17	3.31	2.18	2.51	2.37	0.46	1.53	0.30	2.88	2.27
24	0.96	4.34	1.66	5.57	0.61	6.05	0.10	1.27	4.91
34	3.92	3.61	2.65	3.56	1.10	0.81	1.36	3.22	3.58
48	2.64	3.43	3.71	6.07	2.05	0.95	2.16	3.13	4.57
67	3.33	9.60	6.09	12.21	4.42	0.23	19.06	4.50	10.83

Table 17: Apparent resistivity measurements taken at point KP12

ELECTRODE SPACING (m)	α1	α2	β1	β2	γ1	γ2	γ1/γ2	ρm1	ρm2
3	2.25	3.18	5.06	3.58	2.54	0.35	7.22	3.37	1.59
4.3	2.67	3.66	5.36	3.73	2.97	0.16	18.94	3.79	1.72
6	3.00	4.16	5.36	4.56	2.51	0.28	8.98	4.01	1.59
8.5	3.58	5.28	5.54	4.56	3.91	0.14	27.74	4.45	1.98
12	3.33	5.24	8.09	5.74	4.14	0.32	12.92	5.19	2.03
17	4.44	7.54	9.76	6.36	5.58	0.01	398.86	6.58	2.36
24	5.45	7.94	11.69	9.72	5.59	0.68	8.18	7.98	2.36
34	8.66	11.15	15.73	9.80	9.11	1.66	5.50	11.67	3.02
48	9.19	14.99	21.40	17.97	12.37	2.07	5.97	14.02	3.52
67	12.15	16.65	27.79	22.33	17.97	2.04	8.81	18.38	4.24

Table 18: Apparent resistivity measurements taken at point KP13

ELECTRODE SPACING (m)	α1	α2	β1	β2	γ1	γ2	γ1/γ2	ρm1	ρm2
3	4.63	4.61	4.78	4.28	0.49	1.97	0.25	4.70	4.44
4.3	4.62	4.52	3.91	3.84	0.73	0.78	0.94	4.25	4.16
6	4.45	4.54	5.33	4.33	0.90	0.64	1.41	4.87	4.43
8.5	5.32	4.93	5.91	4.22	0.62	0.85	0.73	5.61	4.56
12	3.98	5.98	7.26	6.15	0.23	1.76	0.13	5.38	6.06
17	8.03	8.40	9.13	7.26	0.71	2.07	0.34	8.56	7.81
24	10.39	10.53	11.75	10.91	0.74	3.53	0.21	11.05	10.72
34	14.34	15.09	13.51	14.10	0.83	5.40	0.15	13.92	14.58
48	29.28	11.66	23.16	17.92	3.19	3.68	0.87	26.04	14.46
67	28.14	18.14	25.94	21.60	7.37	4.13	1.78	27.02	19.79
96	43.45	18.98	25.10	20.11	2.40	8.86	0.27	33.02	19.53

University of Ghana http://ugspace.ug.edu.gh

Table 19: Apparent resistivity measurements taken at point KP14

ELECTRODE SPACING (m)	α1	α2	β1	β2	γ1	γ2	γ1/γ2	ρm1	ρm2
3	10.27	11.14	10.77	8.63	0.56	2.37	0.24	10.52	9.80
4.3	6.88	8.27	7.09	5.93	0.30	2.46	0.12	6.98	7.00
6	6.89	8.87	7.22	5.24	0.43	3.21	0.13	7.06	6.82
8.5	8.15	10.80	8.60	6.83	0.81	3.07	0.26	8.37	8.59
12	2.83	10.26	11.40	6.69	2.74	2.54	1.08	5.67	8.29
17	7.11	17.74	10.52	10.74	3.12	3.47	0.90	8.65	13.80
24	5.62	5.18	11.75	12.86	1.39	1.55	0.90	8.12	8.16
34	10.00	6.83	10.69	6.36	2.30	1.33	1.73	10.34	6.59
48	1.44	7.60	9.88	9.14	2.97	0.64	4.64	3.77	8.33
67	5.25	9.40	22.83	3.09	1.42	1.15	1.24	10.95	5.39
96	4.51	6.30	7.28	5.71	4.91	1.30	3.78	5.73	5.99

Table 20: Apparent resistivity measurements taken at point KP15

ELECTRODE SPACING (m)	α1	α2	β1	β2	γ1	γ2	γ1/γ2	ρm1	ρm2
3	16.66	16.23	19.96	13.15	1.33	9.19	0.14	18.24	14.61
4.3	11.94	11.79	10.59	9.92	1.30	1.89	0.69	11.24	10.81
6	13.17	13.02	11.41	7.77	1.64	0.91	1.79	12.26	10.06
8.5	14.78	14.63	13.98	7.54	0.75	0.78	0.95	14.37	10.50
12	6.75	6.60	7.25	6.50	0.41	0.63	0.65	7.00	6.55
17	6.46	6.31	3.74	4.29	0.26	0.43	0.61	4.92	5.20
24	6.79	6.64	3.85	5.67	0.63	0.53	1.17	5.11	6.14
34	6.88	6.73	1.83	1.79	0.52	1.42	0.37	3.55	3.47
48	2.71	2.56	6.73	2.20	0.78	0.35	2.22	4.27	2.37
67	5.35	5.20	1.83	1.63	0.25	0.34	0.74	3.13	2.91
96	2.86	2.71	9.37	2.71	0.23	0.47	0.48	5.18	2.71

University of Ghana http://ugspace.ug.edu.gh

APPENDIX 2B

VES CURVES FOR THE SCHLUMBERGER SOUNDINGS

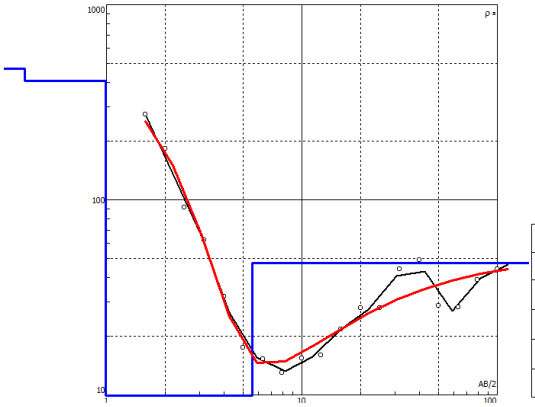

N	ρ (Ohm.m)	H (meters)	d (meters)	Altitude (meters)
1	468	0.381	0.381	-0.381
2	406	0.608	0.989	-0.989
3	9.92	4.58	4.57	-5.569
4	47.6			
RMS = 15.1%				

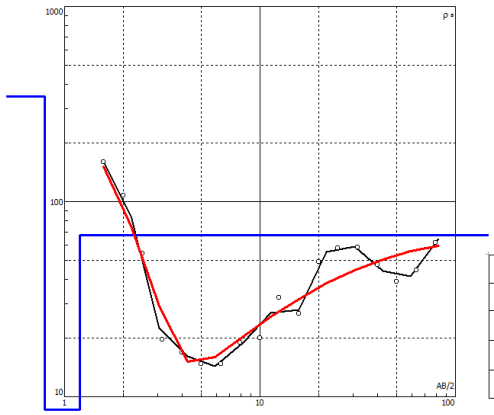

N	ρ (Ohm.m)	H (meters)	d (meters)	Altitude (meters)
1	346	0.79	0.79	-0.79
2	1.37	0.405	1.2	-1.195
3	67.1			
RMS = 18.5%				

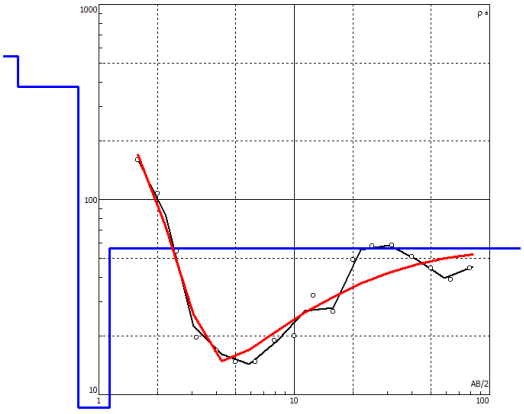

N	ρ (Ohm.m)	H (meters)	d (meters)	Altitude (meters)
1	541	0.387	0.387	-0.387
2	379	0.396	0.783	-0.783
3	1.35	0.348	1.13	-1.131
4	56.4			
RMS = 18.5%				

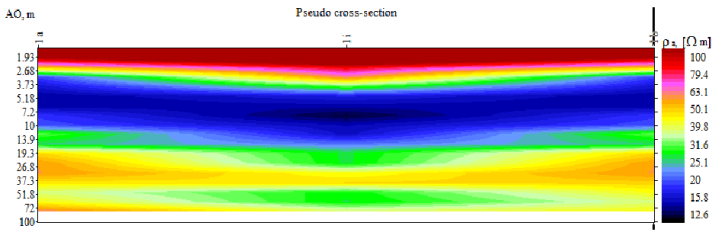

Figure 59: VES curves and pseudo-section for KP1a, KP1 and KP1b

University of Ghana http://ugspace.ug.edu.gh

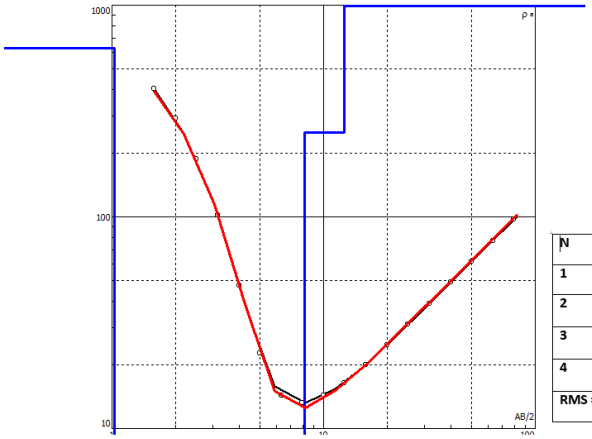

N	ρ (Ohm.m)	H (meters)	d (meters)	Altitude (meters)
1	624	1.03	1.03	-1.03
2	9.17	7.13	8.16	-8.16
3	251	4.4	12.6	-12.56
4	8440			
RMS = 2.44%				

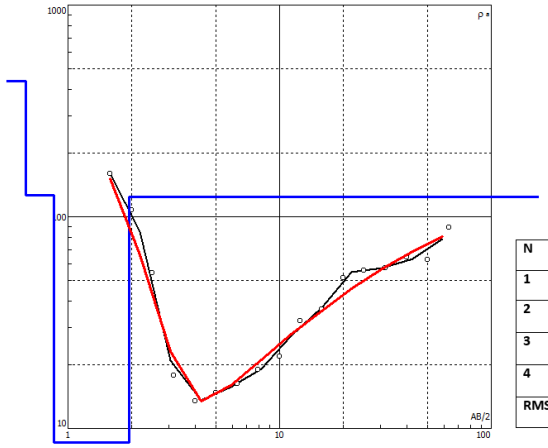

N	ρ (Ohm.m)	H (meters)	d (meters)	Altitude (meters)
1	439	0.631	0.631	-0.631
2	126	0.229	0.86	-0.86
3	3.32	1.08	1.94	-1.94
4	124			
RMS = 10.4%				

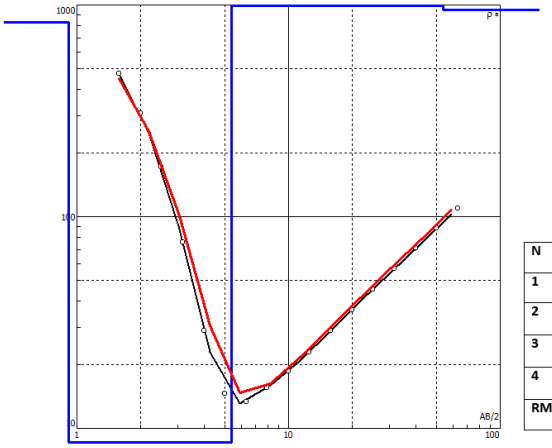

N	ρ (Ohm.m)	H (meters)	d (meters)	Altitude (meters)
1	828	0914	0.914	-0.914
2	8.58	4.46	5.37	-5.37
3	2828	48.3	53.7	-53.7
4	947			
RMS = 10.5%				

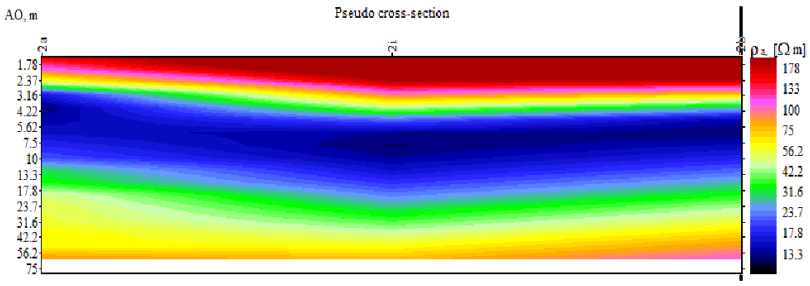

Figure 60: VES curves and pseudo-section for KP2, KP2a and KP2b

University of Ghana http://ugspace.ug.edu.gh

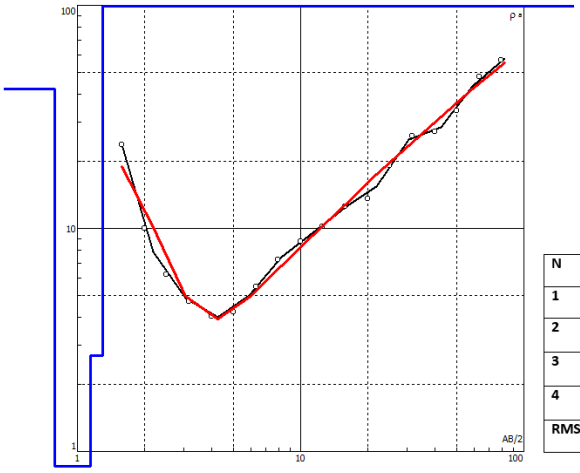

N	ρ (Ohm.m)	H (meters)	d (meters)	Altitude (meters)
1	42.2	0.79	0.79	-0.79
2	0.321	0.353	1014	-1.143
3	2.68	0.151	1.29	-1.29
4	240			
RMS = 11%				

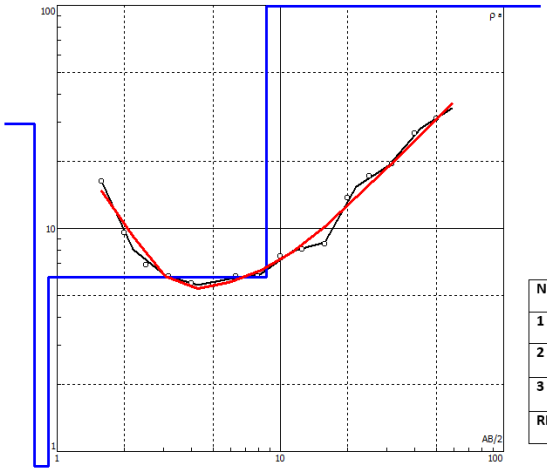

N	ρ (Ohm.m)	H (meters)	d (meters)	Altitude (meters)
1	29.5	0.79	0.79	-0.79
2	0.44	0.121	0.91	-0.91
3	6.03	7.72	8.63	-8.63
RMS = 7.99%				

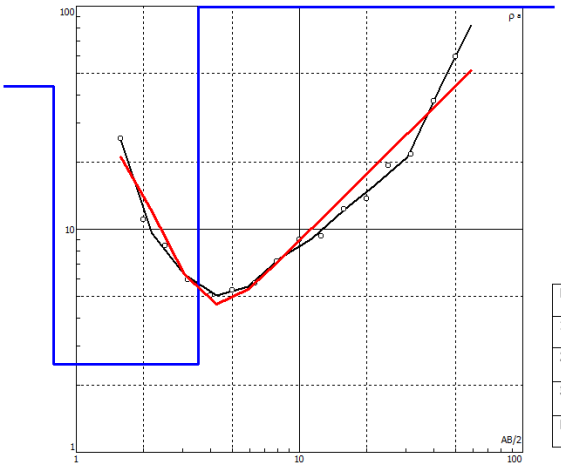

N	ρ (Ohm.m)	H (meters)	d (meters)	Altitude (meters)
1	43.9	0.79	0.79	-0.79
2	2.47	2.73	3.52	-3.52
3	2289			
RMS = 19.6%				

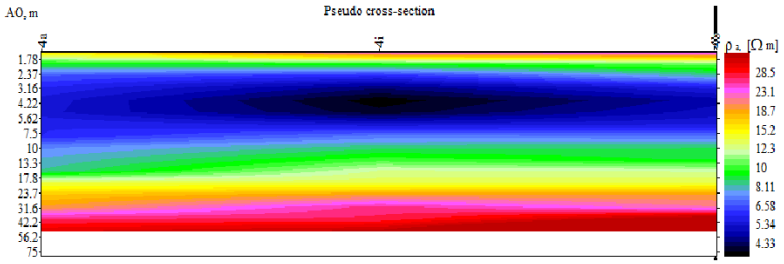

Figure 61: VES curves and pseudo-section for point KP4, KP4a and KP4b

University of Ghana http://ugspace.ug.edu.gh

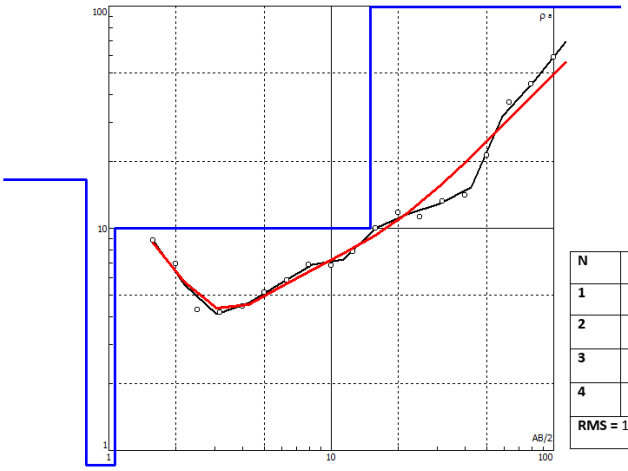

N	ρ (Ohm.m)	H (meters)	d (meters)	Altitude (meters)
1	16.6	0.79	0.79	-0.79
2	0.483	0.277	1.07	-1.067
3	9.97	13.9	15	-15
4	3559			
RMS = 12.7%				

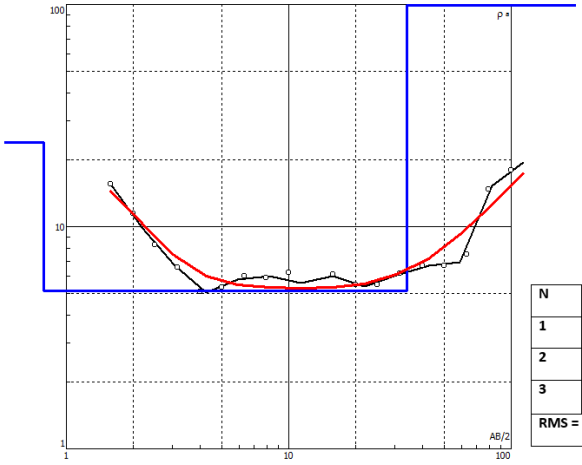

N	ρ (Ohm.m)	H (meters)	d (meters)	Altitude (meters)
1	23.9	0.79	0.79	-0.79
2	5.15	33.2	34	-33.99
3	1398			
RMS = 12.5%				

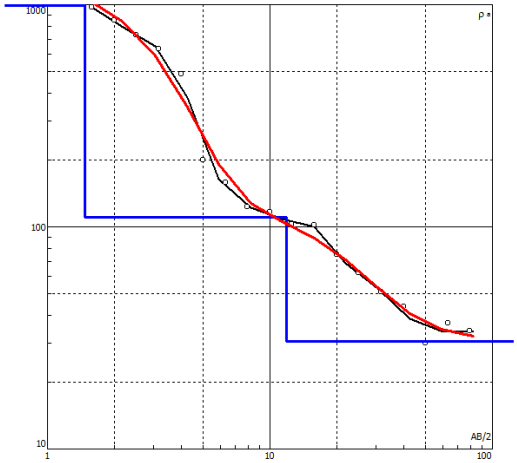

N	ρ (Ohm.m)	H (meters)	d (meters)	Altitude (meters)
1	1215	1.47	1.47	-147
2	110	10.4	11.9	-11.87
3	30.4			
RMS = 7.52%				

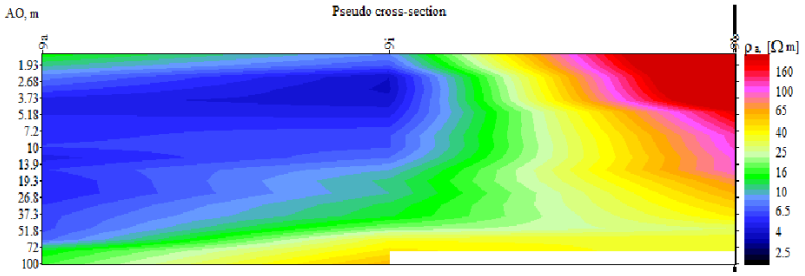

Figure 62: VES curves and pseudo-section for the point KP9, KP9a and KP9b

University of Ghana http://ugspace.ug.edu.gh

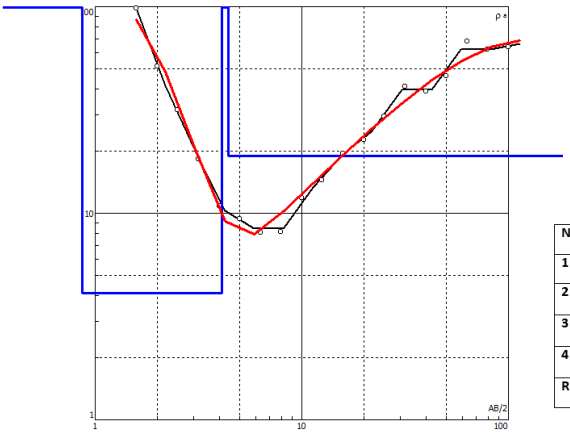

N	ρ (Ohm.m)	H (meters)	d (meters)	Altitude (meters)
1	169	0.863	0.863	-0.863
2	4.113	3.24	4.1	-4.103
3	2564	0.302	4.41	-4.405
4	18.9			
RMS = 9%				

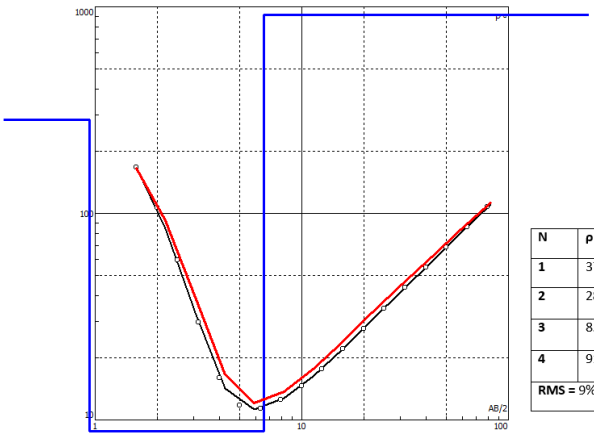

N	ρ (Ohm.m)	H (meters)	d (meters)	Altitude (meters)
1	377	0.316	0.316	-0.316
2	284	0.619	0.935	-0.935
3	8.8	5.63	6.57	-6.57
4	912			
RMS = 9%				

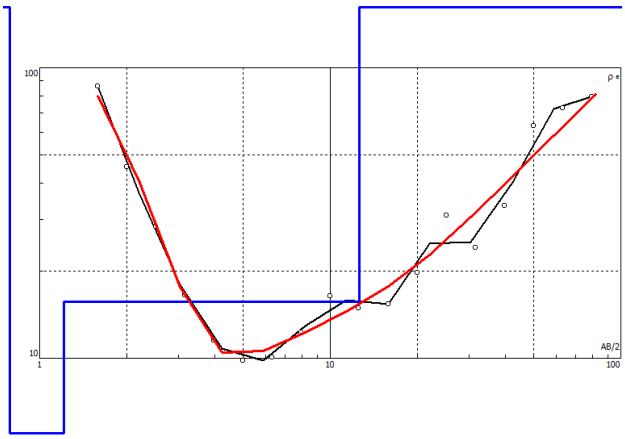

N	ρ (Ohm.m)	H (meters)	d (meters)	Altitude (meters)
1	179	0.79	0.79	-0.79
2	1.59	0.418	1.21	-1.21
3	15.6	11.4	12.6	-12.61
4	6754			
RMS = 9%				

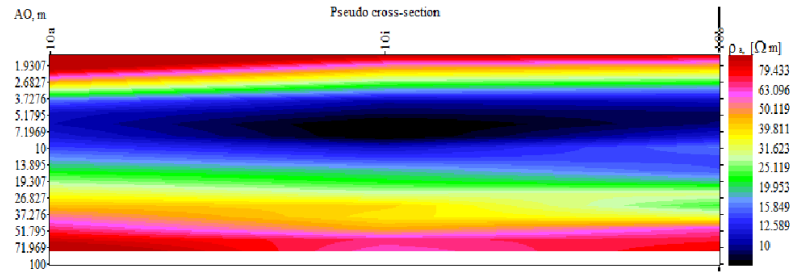

Figure 63: VES curves and pseudo-section for schlumberger sounding at KP10, KP10a and KP10b

University of Ghana http://ugspace.ug.edu.gh

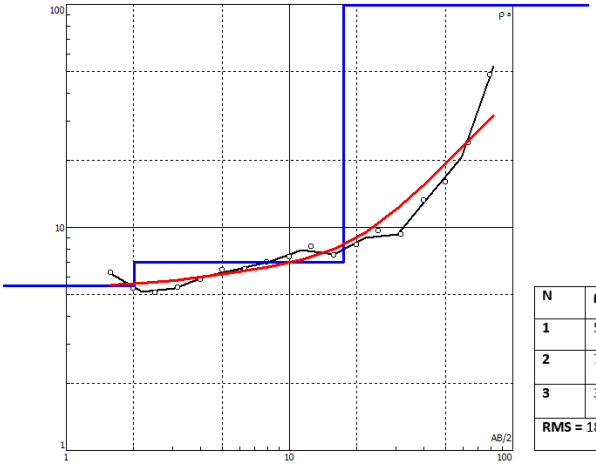

N	ρ (Ohm.m)	H (meters)	d (meters)	Altitude (meters)
1	5.47	2.02	2.02	-2.02
2	7.01	15.4	17.4	-17.42
3	3149			
RMS = 18.1%				

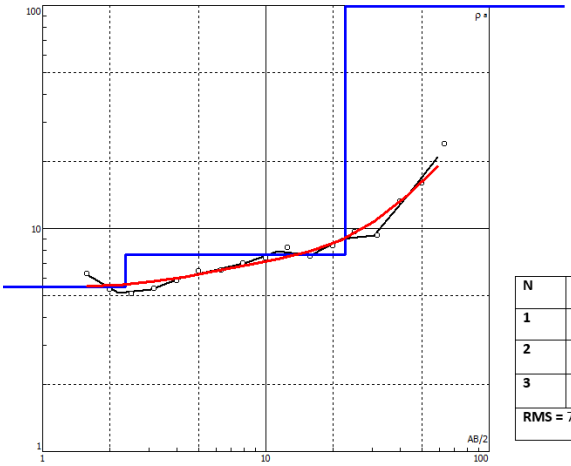

N	ρ (Ohm.m)	H (meters)	d (meters)	Altitude (meters)
1	5.45	2.34	2.34	-2.34
2	7.65	20.3	22.6	22.64
3	3149			
RMS = 7.43%				

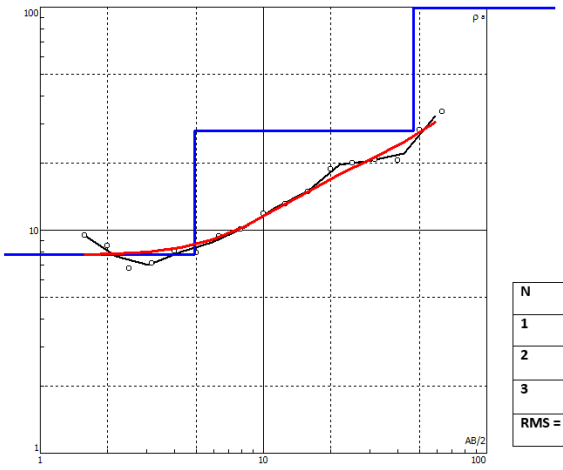

N	ρ (Ohm.m)	H (meters)	d (meters)	Altitude (meters)
1	7.75	4.93	4.93	-4.93
2	27.8	41.9	46.8	-46.83
3	3708			
RMS = 8.7%				

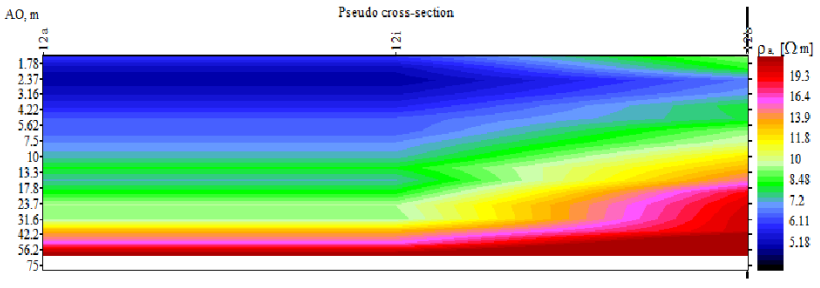

Figure 64: VES plots and pseudo-section of schlumberger sounding at KP12, KP12a and KP12b

University of Ghana http://ugspace.ug.edu.gh

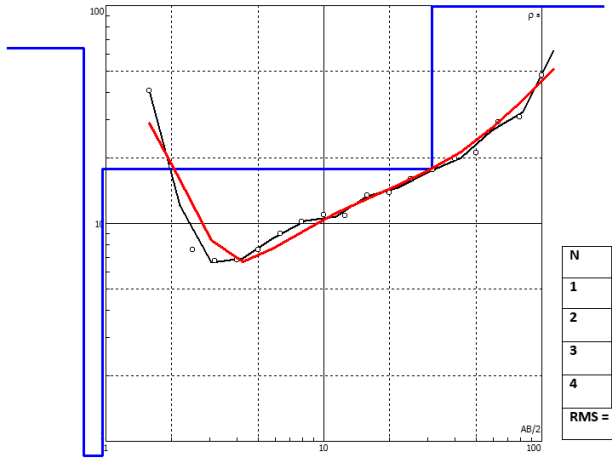

N	ρ (Ohm.m)	H (meters)	d (meters)	Altitude (meters)
1	63.5	0.79	0.79	-0.79
2	0.357	0.172	0.962	-0.962
3	17.8	30.4	31.4	-31.36
4	3665			
RMS = 15.4%				

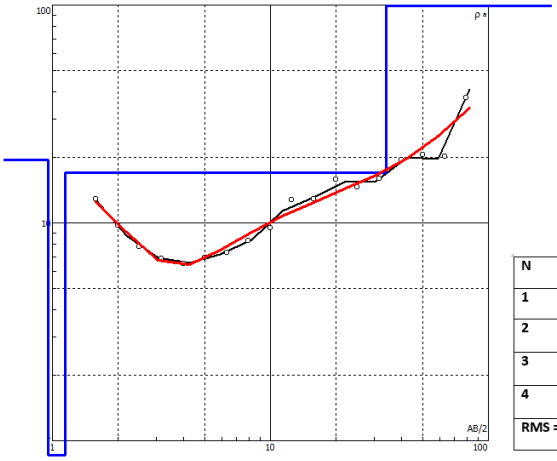

N	ρ (Ohm.m)	H (meters)	d (meters)	Altitude (meters)
1	19.5	0.956	0.956	-0.96
2	0.42	0.193	1.15	-1.15
3	17	32.8	33.9	-33.95
4	3665			
RMS = 9.97%				

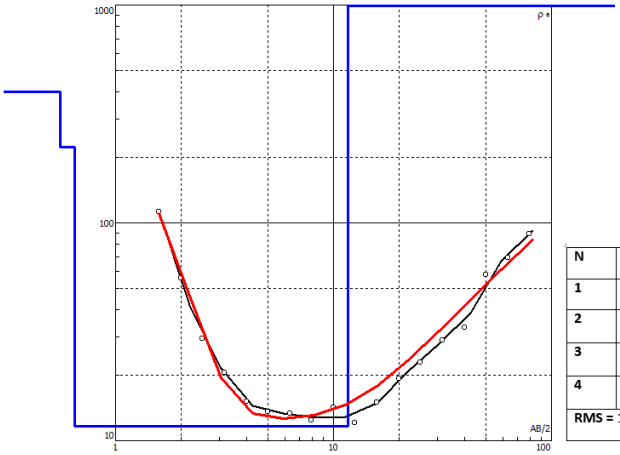

N	ρ (Ohm.m)	H (meters)	d (meters)	Altitude (meters)
1	400	0.557	0.557	-0.557
2	233	0.092	0.649	-0.649
3	11.7	11	11.6	-11.65
4	2266			
RMS = 10.8%				

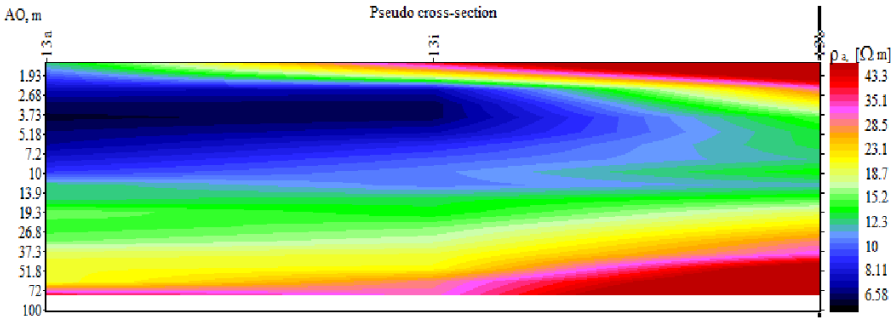

Figure 65: VES plots and pseudo-section of schlumberger sounding at KP13, KP13a and KP13b

University of Ghana http://ugspace.ug.edu.gh

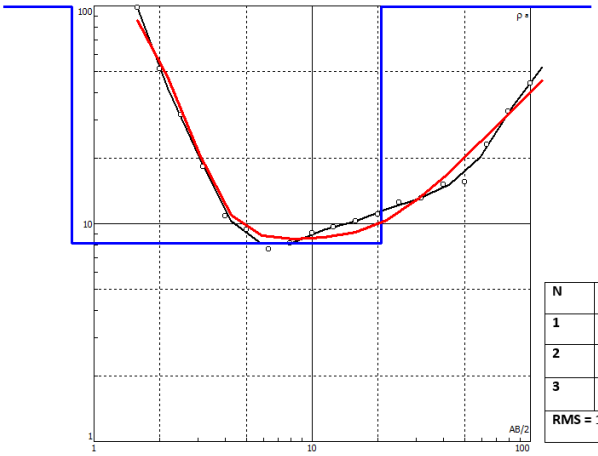

N	ρ (Ohm.m)	H (meters)	d (meters)	Altitude (meters)
1	184	0.79	0.79	-0.79
2	8.11	20	20.8	-20.79
3	3665			
RMS = 10.1%				

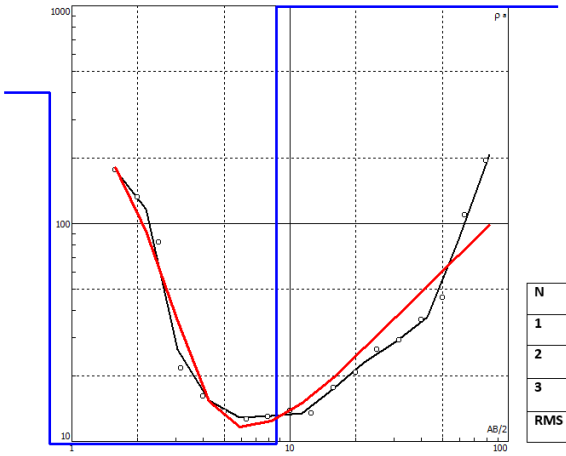

N	ρ (Ohm.m)	H (meters)	d (meters)	Altitude (meters)
1	401	0.79	0.79	-0.79
2	9.76	7.88	8.67	-8.67
3	3555			
RMS = 17.3%				

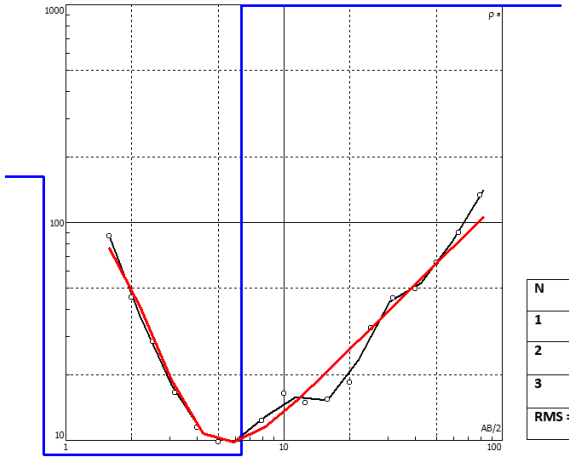

N	ρ (Ohm.m)	H (meters)	d (meters)	Altitude (meters)
1	162	0.79	0.79	-0.79
2	7.4	5.61	6.4	-6.4
3	7785			
RMS = 14.5%				

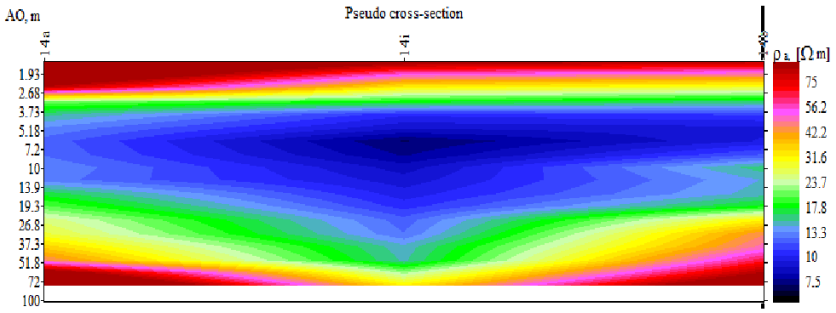

Figure 66: VES plots and pseudo-section of schlumberger sounding at KP14, KP14a and KP14b

University of Ghana http://ugspace.ug.edu.gh

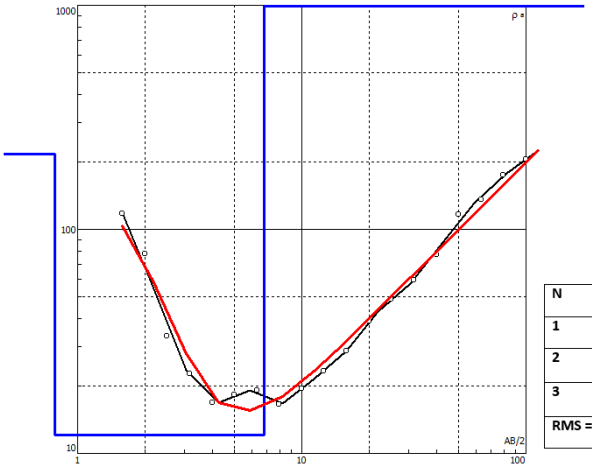

N	ρ (Ohm.m)	H (meters)	d (meters)	Altitude (meters)
1	216	0.79	0.79	-0.79
2	12.1	6	6.79	-6.79
3	1642			
RMS = 9.99%				

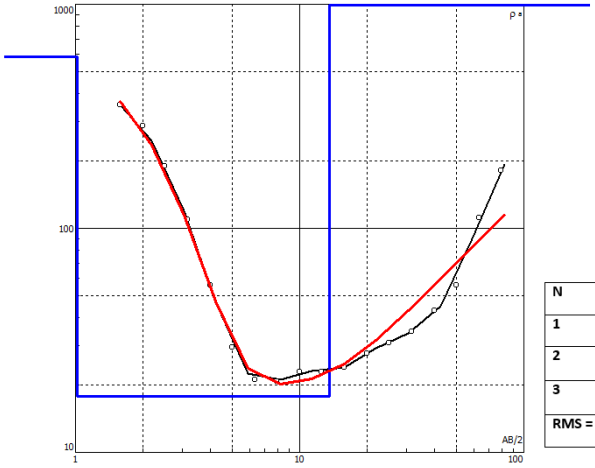

N	ρ (Ohm.m)	H (meters)	d (meters)	Altitude (meters)
1	583	1.02	1.02	-1.02
2	17.8	12.6	13.6	-13.62
3	1642			
RMS = 18.1%				

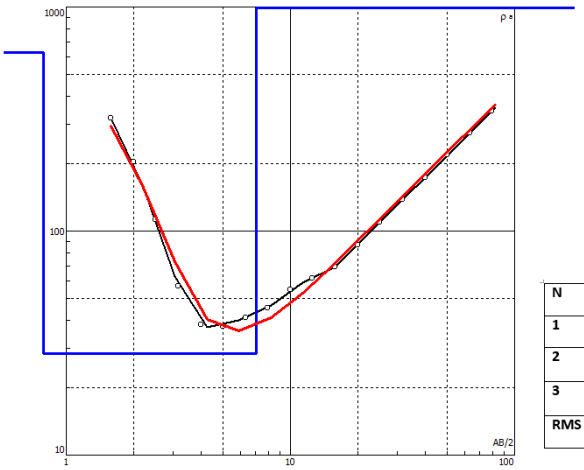

N	ρ (Ohm.m)	H (meters)	d (meters)	Altitude (meters)
1	628	0.79	0.79	-0.79
2	28.4	6.24	7.03	-7.03
3	3835			
RMS = 7.89%				

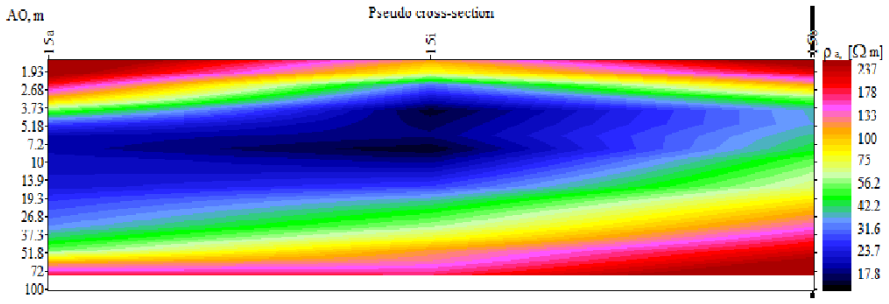

Figure 67: VES plots and pseudo-section of schlumberger sounding at KP15, KP15a and KP15b

University of Ghana http://ugspace.ug.edu.gh

APPENDIX 2C

POLAR PLOTS FOR THE WENNER AZIMUTHAL ARRAY DATA

Figure 68: Wenner Azimuthal array plots for KP1

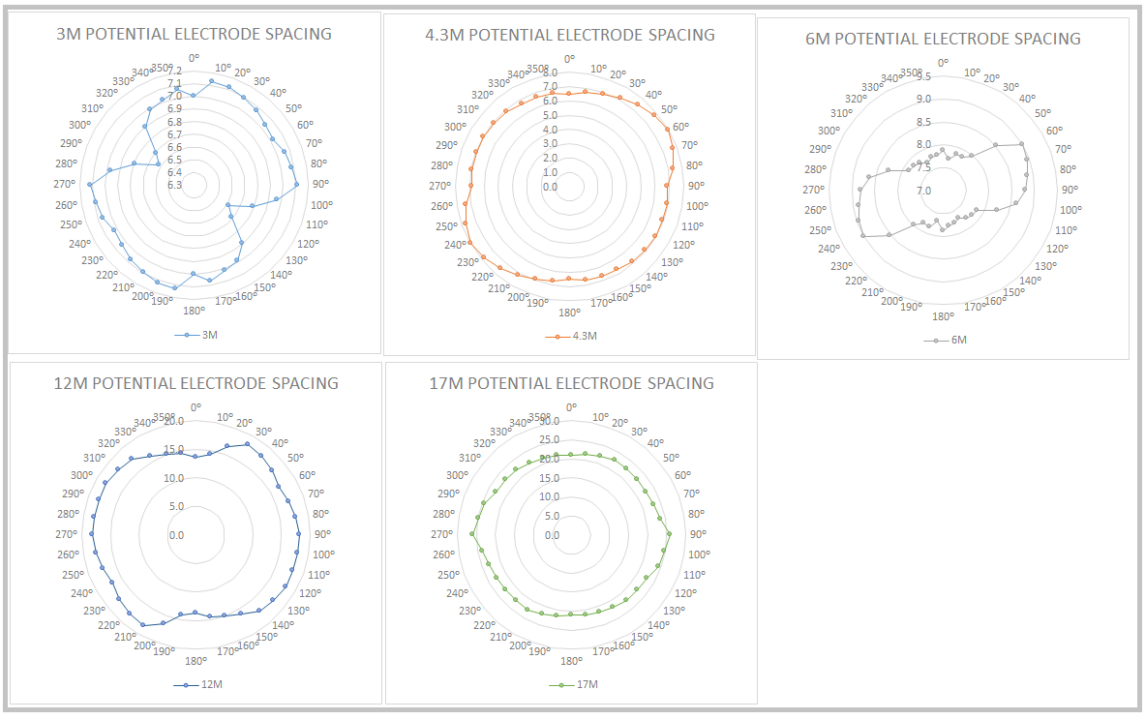

Figure 69: Wenner Azimuthal array plots for KP2

University of Ghana http://ugspace.ug.edu.gh

Figure 70: Wenner Azimuthal array plots for KP4

University of Ghana http://ugspace.ug.edu.gh

Figure 71: Wenner Azimuthal array plots for KP9

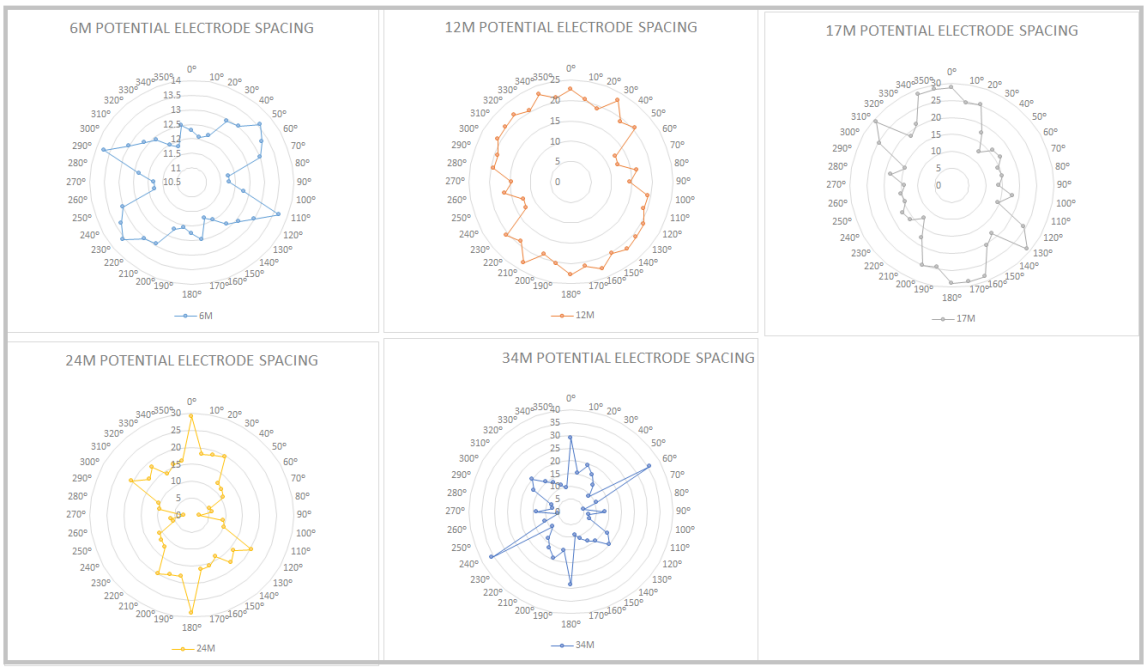

Figure 72: Wenner Azimuthal array plots for KP10

University of Ghana http://ugspace.ug.edu.gh

Figure 73: Wenner Azimuthal array plots for KP12

Figure 74: Wenner Azimuthal array plots for KP13

University of Ghana http://ugspace.ug.edu.gh

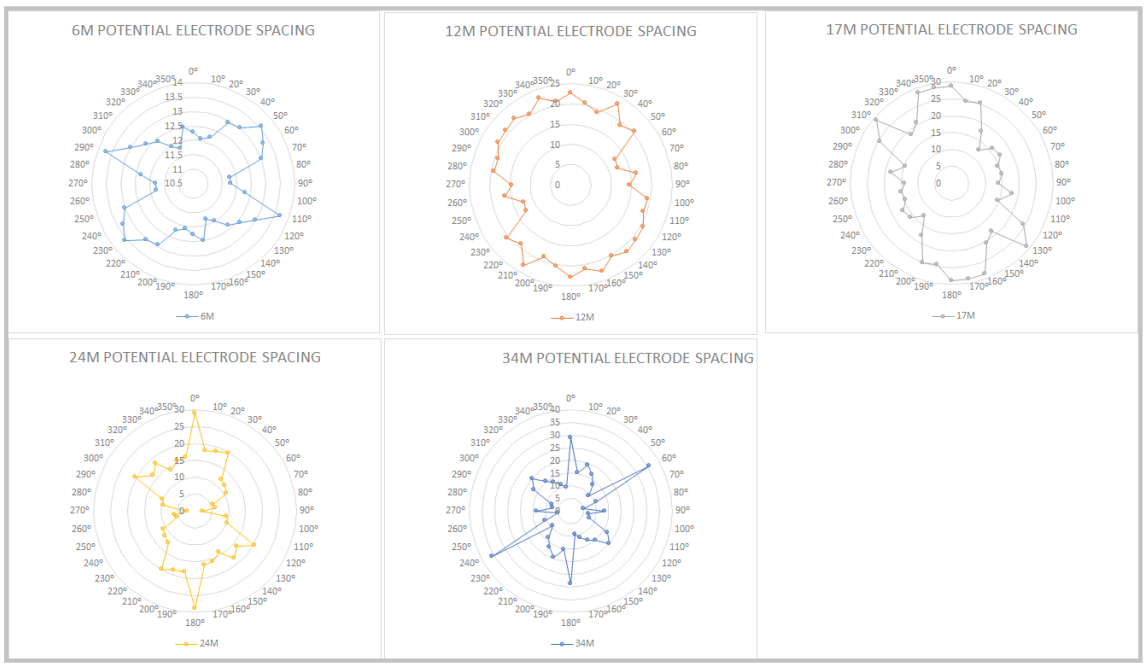

Figure 75: Wenner Azimuthal array plots for KP14

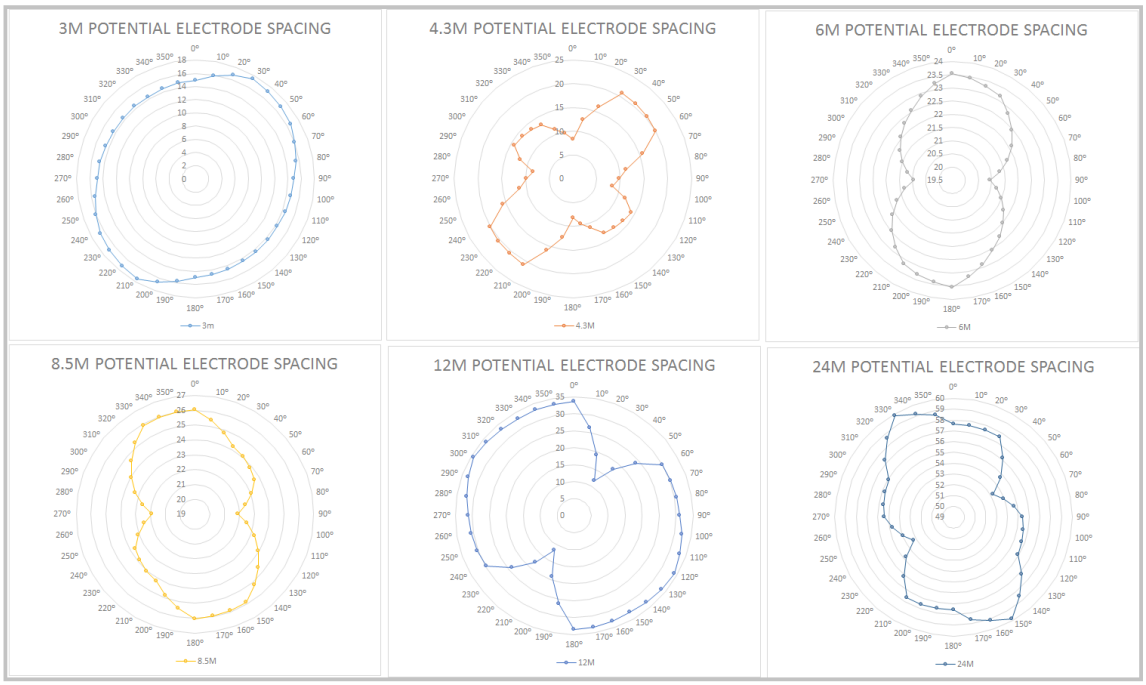

Figure 76: Wenner Azimuthal array plots for KP15